

Hard Exclusive Reactions and the Structure of Hadrons

K. Goeke^a, M.V. Polyakov^{a,b}, M. Vanderhaeghen^c

^a *Institut für Theoretische Physik II, Ruhr-Universität Bochum, D-44780 Bochum, Germany*

^b *Petersburg Nuclear Physics Institute, 188350, Gatchina, Russia*

^c *Institut für Kernphysik, Johannes Gutenberg-Universität, D-55099 Mainz, Germany*

Abstract

We outline in detail the properties of generalized parton distributions (GPDs), which contain new information on the structure of hadrons and which enter the description of hard exclusive reactions. We highlight the physics content of the GPDs and discuss the quark GPDs in the large N_c limit and within the context of the chiral quark-soliton model. Guided by this physics, we then present a general parametrization for these GPDs. Subsequently we discuss how these GPDs enter in a wide variety of hard electroproduction processes and how they can be accessed from them. We consider in detail deeply virtual Compton scattering and the hard electroproduction of mesons. We identify a list of key observables which are sensitive to the various hadron structure aspects contained in the GPDs and which can be addressed by present and future experiments.

Contents

1	INTRODUCTION	3
2	GENERALIZED PARTON DISTRIBUTIONS (GPDs)	9
2.1	Definitions, link with ordinary parton distributions and nucleon form factors	9
2.2	Polynomial conditions, D-term	11
2.3	Angular momentum sum rule	14
2.4	Chiral properties of GPDs	16
2.4.1	Spontaneously broken chiral symmetry and the D-term	16
2.4.2	Pion pole contribution to the GPD $\tilde{E}(x, \xi, t)$	17
2.5	Twist-3 GPDs	18
2.5.1	General properties of the twist-3 GPDs	19
2.5.2	Wandzura-Wilczek approximation for the twist-3 GPDs	22
2.6	GPDs for $N \rightarrow \Lambda, \Sigma$ transitions : SU(3) relations and beyond	26
2.7	GPDs for $N \rightarrow \Delta$ transition	29
2.8	Further generalizations: GPDs for $N \rightarrow \pi N$ transitions	32
3	GPDs IN THE LARGE N_c LIMIT	34
3.1	Generalized parton distributions at large N_c : general properties	34
3.1.1	GPDs for octet to decuplet transition in the large N_c limit	37
3.2	GPDs in the chiral-quark soliton model	37
3.2.1	Results for \tilde{H} and \tilde{E}	40
3.2.2	Results for \tilde{H} and \tilde{E}	45
4	GPDs FROM HARD ELECTROPRODUCTION REACTIONS	49
4.1	Introduction	49
4.2	Phenomenological parametrization of GPDs	49
4.2.1	Parametrization of the GPD H^q	49
4.2.2	Parametrization of the D-term	54
4.2.3	Parametrization of the GPD E^q and quark contribution to the proton spin	56
4.2.4	Parametrization of the GPD \tilde{H}^q	65
4.2.5	Parametrization of the GPD \tilde{E}^q	66
4.3	Deeply virtual Compton scattering (DVCS)	67
4.3.1	Kinematical variables of the DVCS process	67
4.3.2	Twist-2 DVCS tensor	68
4.3.3	Twist-3 DVCS tensor	69
4.3.4	DVCS cross section and charge asymmetry	71
4.3.5	Electron single spin asymmetry (SSA)	75
4.4	DVCS with $N \rightarrow \Delta$ transition	81
4.5	Hard meson electroproduction (HMP)	84
4.5.1	Hard electroproduction of vector mesons	85
4.5.2	Hard electroproduction of pions	94
4.5.3	Hard electroproduction of strangeness	98
4.5.4	Hard electroproduction of $\pi\Delta$ final states	101
5	CONCLUSIONS, PERSPECTIVES AND KEY EXPERIMENTS	103

1 INTRODUCTION

The famous Lagrangian of Quantum Chromodynamics (QCD):

$$L = -\frac{1}{4} G_{\mu\nu}^a G^{a\mu\nu} + \sum_f \bar{\psi}_f \left(i\not{D} + g\not{A} - m_f \right) \psi_f, \quad (1)$$

contains, in principle, all phenomena of hadronic and nuclear physics ranging from the physics of pions to the properties of heavy nuclei. The main difficulty and challenge in the derivation of strong interaction phenomena from the QCD Lagrangian (1) is that the theory is formulated in terms of quark and gluon degrees of freedom whereas phenomenologically one deals with hadronic degrees of freedom. Understanding of how colorless hadrons are built out of colored degrees of freedom (quarks and gluons) would allow us to make predictions for strong interaction phenomena directly from the Lagrangian (1). The physics of hadronization of quarks and gluons is governed by such phenomena as confinement and spontaneous chiral symmetry breaking which are in turn related to the non-trivial structure of the QCD vacuum. It implies that the studies of hadronization processes provide us with valuable information on the fundamental questions of the vacuum structure of non-abelian gauge theories.

The quark and gluon structure of hadrons can be best revealed with the help of weakly interacting probes, such as (provided by Nature) photons and W , Z bosons. One needs probes which are weakly coupled to quarks in order to “select” a well defined QCD operator expressed in terms of quark and gluon degrees of freedom of the Lagrangian (1). By measuring the reaction of a hadron to such a probe, one measures the matrix element of the well-defined quark-gluon operator over the hadron state revealing the quark-gluon structure of the hadron.

Historically the famous experiment of Otto Stern *et al.* [Fri33] measuring the anomalous magnetic moment of the proton revealed for the first time the non-trivial (now we say quark-gluon) structure of the proton. In modern language we can say that in this experiment with the help of the low energy photon probe (weakly interacting to quarks) one selects the QCD operator $\sum_q e_q \bar{q} \gamma^\mu q$, then one couples it to the proton, $\langle p | \sum_q e_q \bar{q} \gamma^\mu q | p \rangle$, and extracts the structural information encoded in the values of hadron form factors. The experimental observation of a large Pauli form factor $F_2(0)$ ¹ of the proton [Fri33] has created the physics of hadrons as strongly interacting many body systems.

Are we limited to explore the structure of hadrons by QCD operators created by photons and W , Z bosons? Can we find other weak coupling mechanism to select more sophisticated QCD operators to explore the structure of hadrons? Actually weak interactions as such are an inherent property of QCD due to the phenomenon of asymptotic freedom meaning that at short distances the interactions between quarks and gluons become weak. This implies that if one manages to create a small size configuration of quarks and gluons it can be used as a new probe of hadronic structure. The possibility to create small size configurations of quarks and gluons is provided by hard reactions, such as deep inelastic scattering (DIS), semi-inclusive DIS, Drell-Yan processes, hard exclusive reactions, etc.

¹ The irony is that this form factor carries the name of W. Pauli who tried to talk out O. Stern of his experiment, because for all theoreticians at that time there were no doubts that the proton is a point like particle. See the nice historical overview in Ref. [Dre00].

The common important feature of hard reactions is the possibility to separate clearly the perturbative and nonperturbative stages of the interactions, this is the so-called factorization property. Qualitatively speaking, the presence of a hard probe allows us to create small size quark, antiquark and gluon configurations whose interactions are described by means of perturbation theory due to the asymptotic freedom of QCD. The non-perturbative stage of such a reaction describes how a given hadron reacts to this configuration, or how this probe is transformed into hadrons.

In the present work we deal with hard exclusive reactions of the type:

$$\gamma^*(q) + T(p) \rightarrow \gamma(q') + T'(p'), \quad \gamma_L^*(q) + T(p) \rightarrow M(q') + T'(p'), \quad (2)$$

in which a photon γ^* with high energy and large virtuality $-q^2 = Q^2 > 0$ scatters off the hadronic target T and produces a meson M (or a low mass mesonic cluster) or a real photon γ , and a low-mass hadronic state T' (where the mass is small compared to Q^2). The all order factorization theorems for such kind of reactions have been proven in Ref. [Col97] (meson production) Refs. [Ji98a, Col99, Rad98] (real photon production). These theorems assert that the amplitude of the reactions (2) can be written in the form (we show this for the case of hard meson production [Col97]):

$$\sum_{i,j} \int_0^1 dz \int dx_1 f_{i/p}(x_1, x_1 - x_B; t, \mu) H_{ij}(Q^2 x_1/x_B, Q^2, z, \mu) \phi_j(z, \mu) \\ + \text{power-suppressed corrections}, \quad (3)$$

where $f_{i/p}$ is a generalized parton distribution (GPD), [Bar82, Dit88, Mul94, Ji97b, Rad97, Col97] (see details in Sec. 2), x_1 is the fraction of the target momentum carried by the interacting parton, ϕ_j is the distribution amplitude (DA) of the meson, and H_{ij} is a hard-scattering coefficient, computable as a power series in the strong coupling constant $\alpha_s(Q)$. The amplitude depends also on the Bjorken variable $x_B = Q^2/2(pq)$, and on the momentum transfer squared $t = (p - p')^2$ which is assumed to be much smaller than the hard scale Q^2 . In Eq. (3) the GPDs $f_{i/p}$ and the meson DAs ϕ_j contain the non-perturbative physics and H_{ij} the perturbative one. The proof of cancellation of the soft gluon interactions in the processes (2) is intimately related to the fact that the final meson arises from a quark-antiquark (gluon) pair generated by the hard interaction. Thus the pair starts as a small size configuration and only substantially later grows to a normal hadronic size, i.e. into a meson.

Qualitatively one can say that the reactions (2) allow one to perform a “microsurgery” of a nucleon by removing in a controlled way a quark of one flavor and spin and implanting instead another quark (in general with a different flavor and spin). It is illustrated in Fig. 1 for the case of the deeply virtual Compton scattering (DVCS) and in Fig. 2 for hard exclusive meson production (HMP). The lower blobs in both figures correspond to GPDs. It is important that according to the QCD factorization theorem in both types of processes the same *universal* distribution functions enter. This allows us to relate various hard processes to each other. Additionally the detected final state can be used as a filter for the spin, flavor, C-parity, etc. of the removed and implanted quarks.

In the processes as in Eq. (2) the short distance stage of the reaction described by H_{ij} in Eq. (3) corresponds to the interaction of a parton with a highly virtual photon. This stage is described by perturbative QCD. The corresponding hard scattering coefficients have been computed to the NLO order in Refs. [Ji98a, Bel98b, Man98b] for DVCS and

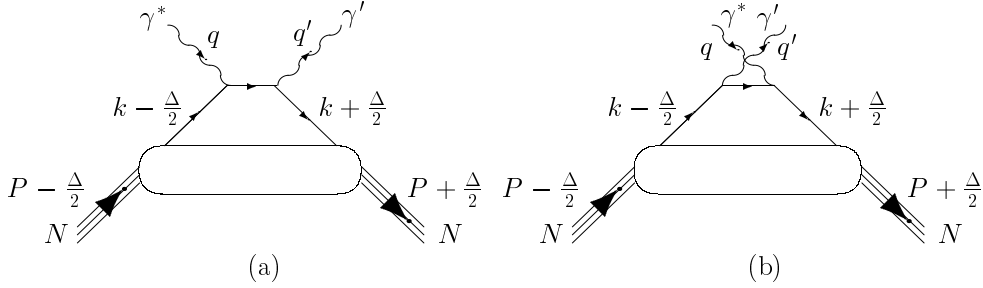


Figure 1: “Handbag” diagrams for DVCS.

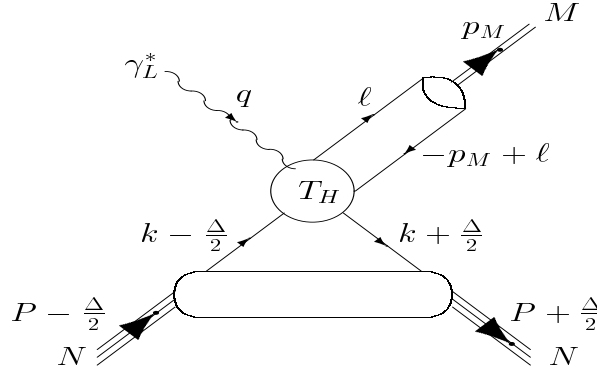


Figure 2: Factorization for the leading order hard meson electroproduction amplitude.

recently in Ref. [Bel01c] for the hard pion production. Also the perturbative evolution of generalized parton distributions is elaborated to the NLO order [Bel99, Bel00d, Bel00e]. This shows that the perturbative QCD calculations of the hard scattering coefficients and evolution kernels are under theoretical control. In this work we shall not review the corresponding perturbative calculations, for a review see Refs. [Ji98b, Rad01b], and for our analysis we will always stick to the LO expressions.

We can say that the hard scattering part (“handbag part” of Fig. 1 and the part denoted as T_H in Fig. 2) of the process “creates” a well-defined QCD operator which is “placed” into the target nucleon and the outgoing meson. We concentrate in present work mostly on studies of such non-perturbative objects entering the factorization theorem (3). They can be generically described by the following matrix elements:

$$\langle B | \bar{\psi}_\alpha(0) \text{Pe}^{ig \int_0^z dx_\mu A^\mu} \psi_\beta(z) | A \rangle, \quad \langle B | G_{\alpha\beta}^a(0) \left[\text{Pe}^{ig \int_0^z dx_\mu A^\mu} \right]^{ab} G_{\mu\nu}^b(z) | A \rangle, \quad (4)$$

where the operators are on the light-cone, i.e. $z^2 = 0$. Depending on the initial and the final states A and B , the following nomenclature of the non-perturbative matrix elements exists:

- $A = B = \text{one particle state}$ – parton distributions in the hadron A . These objects enter the description of hard inclusive and semi-inclusive reactions.
- $B = \text{vacuum}, A = \text{one particle state}$ – distribution amplitudes or light-cone wave functions of a hadron A . They enter the description of, say, hadronic form factors at large momentum transfer as well as hard exclusive production of mesons.
- Both A and B are one particle states with different momenta, i.e. $p(A) \neq p(B)$ – generalized parton distributions. They enter the description of hard exclusive production of mesons and deeply virtual Compton scattering.
- $B = \text{vacuum}, A = \text{many particle state}$ – generalized distribution amplitudes. They enter the description of hard exclusive multi-meson production or transition form factors between multi-meson states at large momentum transfer.
- $A = \text{one particle state}, B = \text{many particle state}$, e.g. $B = \pi N, KN$, etc. – can be called many body generalized parton distributions. They enter the description of semi-exclusive production of mesons and semi-exclusive DVCS.
- $A = B = \text{many particle state}$ – can be called interference parton distributions. An interesting object which has not yet been considered in the literature.

Although all these objects have different physical meaning, their unifying feature is that they describe the response of hadronic states to quark-gluon configurations with small transverse size, which have an extension along the light-cone direction. This can also be rephrased by saying that one probes the transition from one hadronic state to another by low-energy extended objects–“QCD string operators” (4). From such a point of view, the studies of hard exclusive reactions allow us to extend considerably the number of low-energy fundamental probes that can be used to study hadrons. An advantage of hard exclusive reactions is that in this case the number of probes with different quantum numbers is very large and also that these reactions probe non-diagonal transitions in flavor and spin spaces. To great extent, the properties of these new probes have not been studied, especially such aspects as chiral perturbation theory for these probes², the large N_c limit, the influence of spontaneous breaking of the chiral symmetry, etc. In the present work we attempt to address these questions.

	0^{-+}	0^{++}	1^{--}	1^{+-}	1^{++}	2^{++}
	$\eta(\eta')$	f_0	$\omega(\phi)$	h_1	f_1	f_2
$e_f(q_f - \bar{q}_f)$		\times				\times
$e_f(q_f + \bar{q}_f) + \frac{3}{4}G$			\times			
$e_f(\Delta q_f - \Delta \bar{q}_f)$	\times				\times	
$e_f(\Delta q_f + \Delta \bar{q}_f)$				\times		

Table 1: Combinations of parton distributions entering the amplitude for the production of a meson cluster with quantum numbers indicated in the first row (J^{PC}) and with zero isospin. In the second row we give typical meson representatives for these quantum numbers.

²See however works in this direction [Pol99a, Leh01, Tho00, Pob01, Che01, Arn01] which we do not review here.

As an illustration of the wider scope of hard exclusive reactions for studies of hadronic structure we give here a qualitative discussion to what type of usual parton distributions these reactions are sensitive. We shall see that the hard exclusive reactions allow us (leaving aside truly non-forward effects) to probe flavor and C-parity combinations of usual parton distributions which are not accessible in inclusive measurements. The amplitude of a hard exclusive meson production on the nucleon depends on the nucleon generalized parton distributions. In the limiting case of zero “skewedness” (i.e. when the momentum transfer $\Delta \rightarrow 0$ in Figs. 1,2) the latter are reduced to usual parton distributions in the nucleon. In this sense it holds that the hard exclusive meson production is, among other things, sensitive to the usual parton distributions in the nucleon. In Tables 1-3 [Fra01] we give examples of hard exclusive production processes of mesons with various quantum numbers on a proton target and list the corresponding parton distributions to which the amplitudes are sensitive. In these tables the non empty entries mean that the given combination of parton distributions can be probed in the production of a mesonic system with the given quantum numbers. The physics content of the GPDs is of course not reduced to the

	0^{-+}	0^{++}	1^{--}	1^{+-}	1^{++}	2^{++}
	π^0	a_0	ρ^0	b_1	a_1	a_2
$2(u - \bar{u}) + (d - \bar{d})$		\times				\times
$2(u + \bar{u}) + (d + \bar{d}) + \frac{3}{4}G$			\times			
$2(\Delta u - \Delta \bar{u}) + (\Delta d - \Delta \bar{d})$	\times				\times	
$2(\Delta u + \Delta \bar{u}) + (\Delta d + \Delta \bar{d})$				\times		

Table 2: Combinations of parton distributions entering the amplitude for the production amplitude of a meson cluster with the quantum numbers indicated in the first row (J^{PC}) and with isospin one and zero charge. In the second row we give typical meson representatives for these quantum numbers.

	0^{--}	0^{++}	1^{-+}	1^{++}	1^{+-}	2^{++}
	π^+	a_0	ρ^+	b_1	a_1	a_2
$(2u - \bar{u}) - (2d - \bar{d})$		\times				\times
$(2u + \bar{u}) - (2d + \bar{d})$			\times			
$(2\Delta u - \Delta \bar{u}) - (2\Delta d - \Delta \bar{d})$	\times				\times	
$(2\Delta u + \Delta \bar{u}) - (2\Delta d + \Delta \bar{d})$				\times		

Table 3: Combinations of parton distributions entering the amplitude for the production amplitude of a meson cluster with the quantum numbers indicated in the first row (J^{PG} , instead of C -parity we indicate the G -parity) and with charge +1. In the second row we give typical meson representatives for these quantum numbers.

forward quark distributions. In fact, the “truly non-forward” effects play a crucial role in the physics of hard exclusive processes (2), i.e. HMP as well as DVCS. These effects also contain new information about the structure of mesons and baryons which is not accessible by standard hard inclusive reactions.

The paper is organized as follows. In section 2 we review the formalism of generalized parton distributions. We concentrate on such properties of quark GPDs which are related

to the structure of the nucleon leaving aside a discussion of the perturbative evolution which has been extensively reviewed in Refs. [Ji98b, Rad01b]. Section 3 is devoted to studies of quark GPDs in the limit of a large number of colors N_c . In this chapter we also review and present new calculations of GPDs in the chiral quark-soliton model. The basic structures of GPDs discussed in the sections 2 and 3 are then used in chapter 4 in order to construct a phenomenological parametrization of the GPDs. These parametrizations are then used to make predictions for a wide variety of hard electroproduction processes. Since our main objective is to investigate how to reveal the basic features of the nucleon structure in these reactions we restrict ourselves in the calculation of the hard interaction kernels to the leading perturbative order for observables. Studies of the NLO effects on observables can be found in Refs. [Bel98a, Bel00a, Bel01c]³. In particular, we perform detailed studies for DVCS observables in Sec. 4.3 at twist-2 and twist-3 level. We demonstrate how various DVCS observables are sensitive to parameters of GPDs, e.g. to the quark total angular momentum contribution to the nucleon spin. In Sec. 4.5 we study hard meson production discussing in detail for each specific process the information about nucleon structure one accesses. In all calculations we restrict ourselves to the region of not too small x_B (valence region), where one is mainly sensitive to the quark GPDs. Discussions of various aspects of hard exclusive meson production at small x_B can be found e.g. in Refs. [Bro94, Fra96, Abr97, Mar98b, Iva98, Iva99, Shu99, Cle00] and of DVCS at small x_B in Ref. [Fra98b, Fra99a]. We note that in the hard exclusive processes at small x_B the GPDs can be related to the usual parton distributions in a model independent way.

The GPDs have also been discussed within the context of wide angle Compton scattering [Rad98, Die99] where the GPDs are related to soft overlap contributions to elastic and generalized form factors (for a review of such processes see Ref. [Rad01b]). Additionally the GPDs enter the description of the diffractive photoproduction of heavy quarkonia, see e.g. Refs. [Rys97, Fra98c, Fra99c, Mar99], as well as in diffractive $\gamma \rightarrow 2\text{jets}$ [Gol98] and in $\pi \rightarrow 2\text{jets}$ processes [Fra93, Fra00b, Bra01, Cher01]. We do not review these applications in the present work.

Finally, we summarize our main findings in section 5 and list a number of key experiments to access the GPDs and to extract their physics content.

³In these papers it was found that for some of observables the NLO corrections can be rather large. This implies that more detail studies of the NLO effects are needed.

2 GENERALIZED PARTON DISTRIBUTIONS (GPDs)

In this section we consider basic properties of the generalized parton distributions (GPDs). We shall pay special attention to such properties of GPDs which are related to the non-perturbative structure of hadrons and the QCD vacuum. We shall not discuss the perturbative evolution of the GPDs, as this issue is excellently reviewed in [Ji98b, Rad01b]. Our aim will be to cover topics which are complementary to the ones discussed in those reviews [Ji98b, Rad01b].

2.1 Definitions, link with ordinary parton distributions and nucleon form factors

The factorization theorem for hard exclusive reactions allows us to describe the wide class of such reactions in terms of *universal* generalized parton distributions. This nucleon structure information can be parametrized, at leading twist-2 level, in terms of four (quark chirality conserving) generalized structure functions. These functions are the GPDs denoted by $H, \tilde{H}, E, \tilde{E}$ (we do not consider chirally odd GPDs, which are discussed in Refs. [Hoo98, Die01b]) which depend upon three variables : x, ξ and t . The light-cone momentum ⁴ fraction x is defined (see Figs. 1 and 2) by $k^+ = x\bar{P}^+$, where k is the quark loop momentum and \bar{P} is the average nucleon momentum ($\bar{P} = (p + p')/2$, where $p(p')$ are the initial (final) nucleon four-momenta respectively). The skewedness variable ξ is defined by $\Delta^+ = -2\xi\bar{P}^+$, where $\Delta = p' - p$ is the overall momentum transfer in the process, and where $2\xi \rightarrow x_B/(1 - x_B/2)$ in the Bjorken limit. Furthermore, the third variable entering the GPDs is given by the Mandelstam invariant $t = \Delta^2$, being the total squared momentum transfer to the nucleon. ⁵ In a frame where the virtual photon momentum q^μ and the average nucleon momentum \bar{P}^μ are collinear along the z -axis and in opposite direction, one can parametrize the non-perturbative object in the lower blobs of Figs. 1 and 2 as (we follow Ref. [Ji97b]) ⁶:

$$\begin{aligned} & \frac{\bar{P}^+}{2\pi} \int dy^- e^{ix\bar{P}^+y^-} \langle p' | \bar{\psi}_\beta(-y/2) \psi_\alpha(y/2) | p \rangle \Big|_{y^+ = \bar{y}_\perp = 0} \\ &= \frac{1}{4} \left\{ (\gamma^-)_{\alpha\beta} \left[H^q(x, \xi, t) \bar{N}(p') \gamma^+ N(p) \right. \right. \\ & \quad \left. \left. + E^q(x, \xi, t) \bar{N}(p') i\sigma^{+\kappa} \frac{\Delta_\kappa}{2m_N} N(p) \right] \right. \\ & \quad \left. + (\gamma_5 \gamma^-)_{\alpha\beta} \left[\tilde{H}^q(x, \xi, t) \bar{N}(p') \gamma^+ \gamma_5 N(p) \right. \right. \\ & \quad \left. \left. + \tilde{E}^q(x, \xi, t) \bar{N}(p') \gamma_5 \frac{\Delta^+}{2m_N} N(p) \right] \right\}, \end{aligned} \quad (5)$$

where ψ is the quark field of flavor q , N the nucleon spinor and m_N the nucleon mass. The *lhs* of Eq. (5) can be interpreted as a Fourier integral along the light-cone distance y^- of

⁴using the definition $a^\pm \equiv 1/\sqrt{2}(a^0 \pm a^3)$ for the light-cone components

⁵In what follows we shall omit the t -dependence of GPDs if the corresponding quantity is assumed to be defined at $t = 0$.

⁶In all non-local expressions we always assume the gauge link $P \exp(ig \int dx^\mu A_\mu)$ ensuring the color gauge invariance of expressions.

a quark-quark correlation function, representing the process where a quark is taken out of the initial nucleon (having momentum p) at the space-time point $y/2$, and is put back in the final nucleon (having momentum p') at the space-time point $-y/2$. This process takes place at equal light-cone time ($y^+ = 0$) and at zero transverse separation ($\vec{y}_\perp = 0$) between the quarks. The resulting one-dimensional Fourier integral along the light-cone distance y^- is with respect to the quark light-cone momentum $x\bar{P}^+$. The *rhs* of Eq. (5) parametrizes this non-perturbative object in terms of four GPDs, according to whether they correspond to a vector operator $(\gamma^-)_{\alpha\beta}$ or an axial-vector operator $(\gamma_5\gamma^-)_{\alpha\beta}$ at the quark level. The vector operator corresponds at the nucleon side to a vector transition (parametrized by the function H^q , for a quark of flavor q) and a tensor transition (parametrized by the function E^q). The axial-vector operator corresponds at the nucleon side to an axial-vector transition (function \tilde{H}^q) and a pseudoscalar transition (function \tilde{E}^q).

In Fig. 1, the variable x runs from -1 to 1 . Therefore, the momentum fractions ($x + \xi$ or $x - \xi$) of the active quarks can either be positive or negative. Since positive (negative) momentum fractions correspond to quarks (antiquarks), it has been noted in [Rad96a] that in this way, one can identify two regions for the GPDs : when $x > \xi$ both partons represent quarks, whereas for $x < -\xi$ both partons represent antiquarks. In these regions, the GPDs are the generalizations of the usual parton distributions from DIS. Actually, in the forward direction, the GPDs H and \tilde{H} reduce to the quark density distribution $q(x)$ and quark helicity distribution $\Delta q(x)$ respectively, obtained from DIS :

$$H^q(x, 0, 0) = \begin{cases} q(x), & x > 0, \\ -\bar{q}(-x), & x < 0. \end{cases} \quad (6)$$

$$\tilde{H}^q(x, 0, 0) = \begin{cases} \Delta q(x), & x > 0, \\ \Delta \bar{q}(-x), & x < 0. \end{cases} \quad (7)$$

The functions E and \tilde{E} are not measurable through DIS because the associated tensors in Eq. (5) vanish in the forward limit ($\Delta \rightarrow 0$). Therefore, E and \tilde{E} are new leading twist functions, which are accessible through the hard exclusive electroproduction reactions, discussed in the following.

In the region $-\xi < x < \xi$, one parton connected to the lower blob in Fig. 1 represents a quark and the other one an antiquark. In this region, the GPDs behave like a meson distribution amplitude and contain completely new information about nucleon structure, because the region $-\xi < x < \xi$ is absent in DIS, which corresponds to the limit $\xi \rightarrow 0$.

Besides coinciding with the quark distributions at vanishing momentum transfer, the generalized parton distributions have interesting links with other nucleon structure quantities. The first moments of the GPDs are related to the elastic form factors of the nucleon through model independent sum rules. By integrating Eq. (5) over x , one obtains for any ξ the following relations for a particular quark flavor [Ji97b] :

$$\int_{-1}^{+1} dx H^q(x, \xi, t) = F_1^q(t), \quad (8)$$

$$\int_{-1}^{+1} dx E^q(x, \xi, t) = F_2^q(t), \quad (9)$$

$$\int_{-1}^{+1} dx \tilde{H}^q(x, \xi, t) = g_A^q(t), \quad (10)$$

$$\int_{-1}^{+1} dx \tilde{E}^q(x, \xi, t) = h_A^q(t). \quad (11)$$

where $F_1^q(t)$ represents the elastic Dirac form factor for the quark flavor q in the nucleon. When referring to the quark form factors in the following, we understand them in our notation to be for the proton, e.g. $F_1^u(t) \equiv F_1^{u/p}(t)$. In this notation, the u -quark form factor is normalized at $t = 0$ as $F_1^u(0) = 2$ so as to yield the normalization of 2 for the u -quark distribution in the proton, whereas the d -quark form factor is normalized at $t = 0$ as $F_1^d(0) = 1$ so as to yield the normalization of 1 for the d -quark distribution in the proton. These elastic form factors for one quark flavor in the proton, are then related to the physical nucleon form factors (restricting oneself to the u, d and s quark flavors), using $SU(2)$ isospin symmetry, as :

$$\begin{aligned} F_1^{u/p} &= 2 F_1^p + F_1^n + F_1^s, \\ F_1^{d/p} &= 2 F_1^n + F_1^p + F_1^s, \end{aligned} \quad (12)$$

where F_1^p and F_1^n are the proton and neutron electromagnetic form factors respectively, with $F_1^p(0) = 1$ and $F_1^n(0) = 0$. In Eq. (12) F_1^s is the strangeness form factor of the nucleon. Relations similar to Eq. (12) hold for the Pauli form factors F_2^q . For the axial vector form factors one uses the isospin decomposition :

$$g_A^u = \frac{1}{2}g_A + \frac{1}{2}g_A^0, \quad g_A^d = -\frac{1}{2}g_A + \frac{1}{2}g_A^0, \quad (13)$$

where $g_A(g_A^0)$ are the isovector (isoscalar) axial form factors of the nucleon respectively. Similar relations exist for h_A . The isovector axial form factor g_A is known from experiment, with $g_A(0) \approx 1.267$. The induced pseudoscalar form factor h_A contains an important pion pole contribution, through the partial conservation of the axial current (PCAC), as will be discussed in more details below.

An interesting connection of GPDs to light-cone wave functions of the nucleon was considered in Refs. [Die01a, Bro01]. In these papers an exact representation of generalized parton distributions for unpolarised and polarized quarks and gluons as an overlap of the nucleon light-cone wave functions has been constructed. Using such an overlap representation of the GPDs model calculations have been presented in Ref. [Cho01, Tib01, Burk01].

2.2 Polynomial conditions, D-term

One of the non-trivial properties of the generalized parton distributions is the polynomiality of their Mellin moments which follows from the Lorentz invariance of nucleon matrix elements [Ji97b]. Indeed the $(N + 1)$ -th Mellin moment of GPDs corresponds to the nucleon matrix element of the twist-2, spin- $(N + 1)$ *local* operator. Lorentz invariance then dictates that the Mellin moments of GPDs should be polynomials maximally of the order $N + 1$, *i.e.* the polynomiality property implies that [Ji97b]⁷:

$$\int_{-1}^1 dx x^N H^q(x, \xi) = h_0^{q(N)} + h_2^{q(N)} \xi^2 + \dots + h_{N+1}^{q(N)} \xi^{N+1}, \quad (14)$$

⁷The general method for counting of generalized form factors of twist-2 operators can be found in Ref. [Ji01]

$$\int_{-1}^1 dx x^N E^q(x, \xi) = e_0^{q(N)} + e_2^{q(N)} \xi^2 + \dots + e_{N+1}^{q(N)} \xi^{N+1}.$$

Note that the corresponding polynomials contain only even powers of the skewedness parameter ξ . This follows from the time reversal invariance, see Ref. [Man98a, Ji98b]. This fact implies that the highest power of ξ is $N + 1$ for odd N (singlet GPDs) and N for even N (nonsinglet GPDs). Furthermore due to the fact that the nucleon has spin $1/2$, the coefficients in front of the highest power of ξ for the singlet functions H^q and E^q are related to each other [Ji97b, Ji98b]:

$$e_{N+1}^{q(N)} = -h_{N+1}^{q(N)}. \quad (15)$$

The polynomiality conditions (14) strongly restrict the class of functions of two variables $H^q(x, \xi)$ and $E^q(x, \xi)$. For example the conditions (14) imply that GPDs should satisfy the following integral constraints:

$$\begin{aligned} \int_{-1}^1 \frac{dx}{x} \left[H^q(x, \xi + xz) - H^q(x, \xi) \right] &= - \int_{-1}^1 \frac{dx}{x} \left[E^q(x, \xi + xz) - E^q(x, \xi) \right] \\ &= z \sum_{n=0}^{\infty} h_{n+1}^{q(n)} z^n. \end{aligned} \quad (16)$$

Note that the skewedness parameter ξ enters the *lhs* of this equation, whereas the *rhs* of the equation is ξ -independent. Therefore this ξ -independence of the above integrals is a criterion of whether the functions $H^q(x, \xi)$, $E^q(x, \xi)$ satisfy the polynomiality conditions (14). Simultaneously these integrals are generating functions for the highest coefficients $h_{N+1}^{(N)}$. In addition, the condition (16) shows that there are nontrivial functional relations between the functions $H^q(x, \xi)$ and $E^q(x, \xi)$.

An elegant possibility to implement the polynomiality conditions (14) for the GPDs is to use the double distributions [Mul94, Rad96a, Rad97]. A detailed discussion of the double distributions has been given in the review of Ref. [Rad01b]. In this case the generalized distributions are obtained as a one-dimensional section of the two-variable double distributions $F^q(\beta, \alpha)$, $K^q(\beta, \alpha)$ (Recently in Refs. [Bel00c, Ter01] the inversion formula has been discussed):

$$H_{DD}^q(x, \xi) = \int_{-1}^1 d\beta \int_{-1+|\beta|}^{1-|\beta|} d\alpha \delta(x - \beta - \alpha\xi) F^q(\beta, \alpha), \quad (17)$$

and an analogous formula for the GPD $E^q(x, \xi)$:

$$E_{DD}^q(x, \xi) = \int_{-1}^1 d\beta \int_{-1+|\beta|}^{1-|\beta|} d\alpha \delta(x - \beta - \alpha\xi) K^q(\beta, \alpha). \quad (18)$$

Obviously, the double distribution function $F^q(\beta, \alpha)$ should satisfy the condition:

$$\int_{-1+|x|}^{1-|x|} d\alpha F^q(x, \alpha) = q(x), \quad (19)$$

in order to reproduce the forward limit (6) for the GPD $H^q(x, \xi)$. It is easy to check that the GPDs obtained by reduction from the double distributions satisfy the polynomiality conditions (14) but always lead to $h_{N+1}^{q(N)} = e_{N+1}^{q(N)} = 0$, *i.e.* the highest power of ξ for the singlet GPDs is absent. In other words the parametrization of the singlet GPDs in terms of double distributions is not complete. It can be completed by adding the so-called D-term to Eq. (17) [Pol99b]:

$$\begin{aligned} H^q(x, \xi) &= \int_{-1}^1 d\beta \int_{-1+|\beta|}^{1-|\beta|} d\alpha \delta(x - \beta - \alpha\xi) F^q(\beta, \alpha) + \theta \left[1 - \frac{x^2}{\xi^2} \right] D^q \left(\frac{x}{\xi} \right), \\ E^q(x, \xi) &= \int_{-1}^1 d\beta \int_{-1+|\beta|}^{1-|\beta|} d\alpha \delta(x - \beta - \alpha\xi) K^q(\beta, \alpha) - \theta \left[1 - \frac{x^2}{\xi^2} \right] D^q \left(\frac{x}{\xi} \right). \end{aligned} \quad (20)$$

Here $D^q(z)$ is an odd function (as it contributes only to the singlet GPDs) having a support $-1 \leq z \leq 1$. In the Mellin moments, the D-term generates the highest power of ξ :

$$h_{N+1}^{q(N)} = -e_{N+1}^{q(N)} = \int_{-1}^1 dz z^N D^q(z). \quad (21)$$

Note that for both GPDs $H^q(x, \xi)$ and $E^q(x, \xi)$ the absolute value of the D-term is the same, it contributes to both functions with opposite sign. The latter feature follows from the relation (15). We shall see in the section 3.2 that estimates of the D-term in the chiral quark–soliton model gives $D^u(z) \approx D^d(z)$. Therefore in the calculations below we shall assume that:

$$D^q(z) = \frac{1}{N_f} D(z), \quad (22)$$

where N_f is the number of active flavors and $D(z) = \sum_q D^q(z)$ is the flavor singlet D-term.

The D-term evolves with the change of the renormalization scale according to the ERBL evolution equation [Efr80, Lep79]. Hence it is useful to decompose the D-term in a Gegenbauer series (eigenfunctions of the LO ERBL evolution equation):

$$D(z) = (1 - z^2) \left[d_1 C_1^{3/2}(z) + d_3 C_3^{3/2}(z) + d_5 C_5^{3/2}(z) + \dots \right], \quad (23)$$

$$D^g(z) = \frac{3}{4} (1 - z^2)^2 \left[d_1^G + d_3^G C_2^{5/2}(z) + d_5^G C_4^{5/2}(z) + \dots \right], \quad (24)$$

where $D^g(z)$ represents the gluon D-term. Because the D-term is a singlet quantity therefore the quark D-term $D(z)$ is mixed under evolution with the gluon D-term $D^g(z)$. Asymptotically (for a renormalization scale $\mu \rightarrow \infty$) we obtain:

$$D_{as}(z) = d \frac{N_f}{N_f + 4C_F} (1 - z^2) C_1^{3/2}(z), \quad (25)$$

$$D_{as}^g(z) = d \frac{4C_F}{N_f + 4C_F} \frac{3}{4} (1 - z^2)^2, \quad (26)$$

where $C_F = \frac{N_c^2 - 1}{2N_c}$. Furthermore, the scale independent constant d is a nonperturbative parameter characterizing the D-term at a low normalization point, $d = d_1 + d_1^G$ with d_1 from Eq. (23) and d_1^G being the first Gegenbauer coefficient of the gluon D-term (24). We see that the D-term survives in the limit $\mu \rightarrow \infty$ and therefore the complete form⁸ of the singlet quark GPDs at an asymptotically large scale μ^2 is the following:

$$\sum_q H_{\text{as}}^q(x, \xi) = \frac{N_f}{N_f + 4C_F} \left(1 - \frac{x^2}{\xi^2}\right) C_1^{3/2}\left(\frac{x}{\xi}\right) \left[\frac{5}{4\xi^2} + d\right] \theta\left(1 - \frac{x^2}{\xi^2}\right). \quad (27)$$

The asymptotic form of the corresponding gluon GPD is the following:

$$H_{\text{as}}^g(x, \xi) = \frac{4C_F}{N_f + 4C_F} \xi \left(1 - \frac{x^2}{\xi^2}\right)^2 \frac{3}{4} \left[\frac{5}{4\xi^2} + d\right] \theta\left(1 - \frac{x^2}{\xi^2}\right). \quad (28)$$

Analogously, one can obtain the asymptotic form of the singlet GPD $E(x, \xi)$:

$$\sum_q E_{\text{as}}^q(x, \xi) = -\frac{N_f}{N_f + 4C_F} d \left(1 - \frac{x^2}{\xi^2}\right) C_1^{3/2}\left(\frac{x}{\xi}\right) \theta\left(1 - \frac{x^2}{\xi^2}\right). \quad (29)$$

The asymptotic form of the corresponding gluon GPD is the following:

$$E_{\text{as}}^g(x, \xi) = -\frac{4C_F}{N_f + 4C_F} \frac{3d}{4} \xi \left(1 - \frac{x^2}{\xi^2}\right)^2 \theta\left(1 - \frac{x^2}{\xi^2}\right). \quad (30)$$

Furthermore, note that asymptotically the GPD $E(x, \xi)$ is completely determined by the D-term. Note that all expressions for the asymptotic singlet GPDs depend on the scale independent (conserved) constant d . From this point of view this constant is as fundamental as other conserved characteristics of the nucleon, such as the total momentum or total angular momentum.

Up to now we considered the polynomiality properties of the GPDs $H(x, \xi)$ and $E(x, \xi)$. For the quark helicity dependent GPDs $\tilde{H}(x, \xi)$ and $\tilde{E}(x, \xi)$ the polynomiality conditions are very similar to those for $H(x, \xi)$ and $E(x, \xi)$, see Eq. (14). The only difference is that in the case of the quark helicity dependent GPDs the highest powers of the polynomial in ξ is $N - 1$ for the singlet case and N for the nonsinglet one. This implies that the D-term is absent for the GPDs $\tilde{H}(x, \xi)$ and $\tilde{E}(x, \xi)$.

2.3 Angular momentum sum rule

The second Mellin moments of the quark helicity independent GPDs are given by the nucleon form factors of the symmetric energy momentum tensor. The quark part of the symmetric energy momentum tensor is related to the quark angular momentum operator by:

$$J_q^i = \varepsilon^{ijk} \int d^3x x^j T_q^{0k}. \quad (31)$$

⁸In the literature, to the best of our knowledge, only an incomplete form of the asymptotic singlet GPDs was presented.

This relation implies that the forward nucleon matrix element of the angular momentum operator can be related to the form factor of the symmetric energy momentum tensor. This results in the sum rule relating the second Mellin moment of the GPDs to the angular momentum carried by the quarks in the nucleon [Ji97b]:

$$\int_{-1}^1 dx \, x \, (H^q(x, \xi) + E^q(x, \xi)) = 2J^q. \quad (32)$$

In Eq. (32) J^q is the fraction of the nucleon angular momentum carried by a quark of the flavor q (i.e. the sum of spin and orbital angular momentum). The closest analogy for this sum rule is the relation between the magnetic moment of the nucleon and the electromagnetic (e.m.) form factors:

$$\mu_N = F_1^N(0) + F_2^N(0). \quad (33)$$

In this case the magnetic moment is given by the “forward” form factor $F_1^N(0)$ plus the “non-forward” form factor $F_2(0)^N$. In analogy to Eq. (31) the relation between the magnetic moment operator and the e.m. current: $\mu^i \propto \varepsilon^{ijk} \int d^3x \, x^j \, J_{\text{e.m.}}^k$ contains explicitly the coordinate operator x^j . A detailed derivation and discussion of the angular momentum sum rule (32) can be found in Refs. [Ji97b, Ji98b].

Let us discuss here the role played by the D-term in the angular momentum sum rule. Unfortunately it is very hard to find an observable in which the GPDs $H^q(x, \xi)$ and $E^q(x, \xi)$ enter as a sum. Also we should keep in mind that in a hard exclusive process, we have kinematically $\xi \neq 0$ and that the GPDs $H(x, \xi)$, $E(x, \xi)$ enter observables with different kinematical factors. Therefore, we shall discuss the angular momentum sum rule (32) separately for the functions H and E . We rewrite Ji’s sum rule (32) in the following equivalent way [Ji97a]

$$\begin{aligned} \int_{-1}^1 dx \, x \, \sum_q H^q(x, \xi) &= M_2^Q + \frac{4}{5} d_1 \xi^2, \\ \int_{-1}^1 dx \, x \, \sum_q E^q(x, \xi) &= (2J^Q - M_2^Q) - \frac{4}{5} d_1 \xi^2. \end{aligned} \quad (34)$$

Here d_1 is the first Gegenbauer coefficient in the expansion of the D-term (23), $J^Q = \sum_q J^q$ and M_2^Q is the momentum fraction carried by the quarks and antiquarks in the nucleon:

$$M_2^Q = \sum_q \int_0^1 dx \, x \, (q(x) + \bar{q}(x)). \quad (35)$$

We see that the sum rule (34) is sensitive only to the combination $2J^Q - M_2^Q$. What can we say about this combination? Asymptotically one has that $\lim_{\mu \rightarrow \infty} 2J^Q - M_2^Q = 0$ [Ji96]. At some finite scale, the value of $2J^q - M_2^q$ which one would like to extract from the data should be compared with the contribution of the D-term on the *rhs* of the sum rule (34). We shall see below that estimates in the chiral quark-soliton model for the first

Gegenbauer coefficient of the D-term give the value $d_1 \approx -4$, which leads at $\xi = 0.15$ to a value of 0.07 for the second term in Eq. (34). Therefore at accessible values of ξ the extraction of the angular momentum carried by the quarks from the observables requires (among other things) an accurate knowledge of the D-term. The size of the D-term can be determined from the observables which are sensitive to the real part of the amplitude of the corresponding process. An example of such an observable is the DVCS charge asymmetry (accessed by reversing the charge of the lepton beam), see a detailed discussion in Sec. 4.3.4.

2.4 Chiral properties of GPDs

Here we shall argue that the spontaneously broken chiral symmetry of QCD plays an important role in determining the properties of the generalized parton distributions. We shall illustrate this on examples of the D-term and the GPD $\tilde{E}(x, \xi, t)$.

2.4.1 Spontaneously broken chiral symmetry and the D-term

First we will discuss how the physics of spontaneously broken chiral symmetry plays an important role in determining the size and the sign of the D-term. In particular, this role is seen clearly in the case of the GPDs in the pion. In this case the value of the coefficient d_1 in the parametrization of the pion D-term (23) can be computed in a model independent way and it is strictly nonzero. To compute the pion D-term we use the soft-pion theorem for the singlet GPD in the pion derived in [Pol99a]. This soft-pion theorem has been derived using the fact that the pion is a (pseudo)Goldstone boson of the spontaneously broken chiral symmetry. The theorem states that the singlet GPD in the pion vanishes for $\xi = \pm 1$ and momentum transfer squared $t = 0$ (corresponding to a pion with vanishing four momentum):

$$\sum_q H_q^{(\pi)}(x, \xi = \pm 1) = 0. \quad (36)$$

Hence (see also [Pol99b]),

$$\int_{-1}^1 dx x \left(\sum_q H_q^{(\pi)}(x, \xi) \right) = (1 - \xi^2) M_2^{Q\pi}. \quad (37)$$

Evaluating Eq. (37) at $\xi = 0$, determines :

$$M_2^{Q\pi} = \int_0^1 dx x \sum_q [q^{(\pi)}(x) + \bar{q}^{(\pi)}(x)], \quad (38)$$

being the fraction of the momentum carried by the quarks and antiquarks in the pion. As the highest power in ξ in Eq. (37) (i.e. the term in ξ^2) originates solely from the D-term, one easily obtains the following expression for pion D-term :

$$D^{(\pi)}(z) = -\frac{5M_2^Q}{4} (1 - z^2) \left[C_1^{3/2}(z) + \dots \right]. \quad (39)$$

We see therefore that the first Gegenbauer coefficient of the pion D-term is *negative* and strictly nonzero. Its value is fixed by the chiral relations in terms of the momentum fraction carried by the partons in the pion.

The nucleon D-term is not fixed by general principles. However one may expect that the contribution of the pion cloud of the nucleon can be significant. Indeed in the chiral quark-soliton model, which emphasizes the role of broken chiral symmetry in the nucleon structure, the D-term is large and has the sign of the pion D-term. Quantitatively for the coefficients d_1, d_3, d_5 (see Eq. 23), the estimate which is based on the calculation of GPDs in the chiral quark soliton model [Pet98] at a low normalization point $\mu \approx 0.6$ GeV, gives [Kiv01b] (see also Sec. 3.2.1) :

$$d_1 \approx -4.0, \quad d_3 \approx -1.2, \quad d_5 \approx -0.4, \quad (40)$$

and higher moments (denoted by the ellipses in Eq. (23)) are small. Notice the negative sign of the Gegenbauer coefficients for the D-term in Eq. (40), as obtained in the chiral quark-soliton model. The coincidence of the signs in the nucleon and pion D-terms hints that the D-term in the nucleon is intimately related to the spontaneous breaking of the chiral symmetry. The chiral contributions of the long range two-pion exchange shown in Fig. 3 to the GPDs of the nucleon are sizeable giving large and negative contribution to the leading Gegenbauer coefficient of the nucleon D-term d_1 . The sign is related to the negative sign of the pion D-term which is fixed by the soft pion theorem (39).



Figure 3: Two-pion exchange graphs giving the chiral contributions to the nucleon form factors of the energy momentum tensor. The dashed lines represent the pion, and the solid lines represent the nucleon. The black blob is the operator of the energy momentum tensor.

2.4.2 Pion pole contribution to the GPD $\tilde{E}(x, \xi, t)$

The role of the spontaneously broken chiral symmetry in the structure of GPDs is seen particularly clearly in the case of the quark helicity dependent GPD $\tilde{E}(x, \xi, t)$. We remind that this GPD satisfies the sum rule of Eq. (11), in terms of the pseudoscalar nucleon nucleon form factor $h_A^q(t)$. It is well known (see e.g. Ref. [Adl68]) that due to the spontaneously broken chiral symmetry this form factor at small t is dominated by the contribution of the pion pole of the form:

$$\lim_{t \rightarrow m_\pi^2} h_A^q(t) = \frac{1}{2} \tau_{qq}^3 \frac{4g_A m_N^2}{m_\pi^2 - t}, \quad (41)$$

where $g_A \approx 1.267$ is the nucleon isovector axial charge and τ^3 is the Pauli matrix in the flavor space. The presence of the chiral singularity on the *rhs* of the sum rule (11) implies that one should also expect the presence of the chiral singularity in the GPD $\tilde{E}^q(x, \xi, t)$

at small momentum transfer squared t [Fra98a]. The form of this singularity has been specified in Refs. [Man99a, Fra99a, Pen00a] to be:

$$\lim_{t \rightarrow m_\pi^2} \tilde{E}^q(x, \xi, t) = \frac{1}{2} \tau_{qq}^3 \frac{4g_A m_N^2}{m_\pi^2 - t} \theta[\xi - |x|] \frac{1}{\xi} \Phi_\pi\left(\frac{x}{\xi}\right), \quad (42)$$

where $\Phi_\pi\left(\frac{x}{\xi}\right)$ is the pion distribution amplitude entering e.g. description of the pion e.m. form factor at large momentum transfer and the hard reaction $\gamma^* \gamma \rightarrow \pi^0$. In Ref. [Pen00a] in the framework of the chiral quark-soliton model Eq. (42) and the deviations from it have been computed. The corresponding results are discussed in Sec. 3.2.

The presence of the pion pole singularity in the GPD \tilde{E} leads, in particular, to a strong dependence of the differential cross section of, for example, hard π^+ production on the *transverse* polarization of the target [Fra99a]. The dependence of the *exclusive* cross section on the transverse polarization of the proton target has the following dominant structure⁹:

$$\sigma \propto |S_\perp| \sin \Phi \frac{\sqrt{t_{\min} - t}}{-t + m_\pi^2} \times \left[2 \left(\tilde{H}^u(\xi, \xi, t) - \tilde{H}^d(\xi, \xi, t) \right) - \left(\tilde{H}^u(-\xi, \xi, t) - \tilde{H}^d(-\xi, \xi, t) \right) \right], \quad (43)$$

where $\sin \Phi$ is the azimuthal angle between lepton plane and the plane spanned by 3-vectors of the virtual photon and produced meson. The specific t -dependence of the cross section is due to the contribution of the chiral singularity (pion pole) to the “truly non-forward” GPD \tilde{E} whose presence is dictated by the chiral dynamics of QCD.

2.5 Twist-3 GPDs

Recently the DVCS amplitude has been computed in Refs. [Ani00, Pen00b, Bel00b, Rad00, Rad01b] including the terms of the order $O(1/Q)$. The inclusion of such terms is mandatory to ensure the electromagnetic gauge invariance of the DVCS amplitude to the order $\sqrt{-t}/Q$. At the order $1/Q$ the DVCS amplitude depends on a set of new generalized parton distributions. Let us introduce generic generalized “vector” $\mathcal{F}^\mu(x, \xi)$ and “axial” $\tilde{\mathcal{F}}^\mu(x, \xi)$ distributions¹⁰:

$$\begin{aligned} \mathcal{F}^\mu(x, \xi, t) &= \frac{\bar{P}^+}{2\pi} \int_{-\infty}^{\infty} dy^- e^{ix\bar{P}^+y^-} \langle p' | \bar{\psi}(-y/2) \gamma^\mu \psi(y/2) | p \rangle \Big|_{y^+ = y_\perp = 0}, \\ \tilde{\mathcal{F}}^\mu(x, \xi, t) &= \frac{\bar{P}^+}{2\pi} \int_{-\infty}^{\infty} dy^- e^{ix\bar{P}^+y^-} \langle p' | \bar{\psi}(-y/2) \gamma^\mu \gamma_5 \psi(y/2) | p \rangle \Big|_{y^+ = y_\perp = 0}. \end{aligned} \quad (44)$$

If in the above equations the index μ is projected onto the “plus” light-cone direction (i.e. $\mu = +$) we reproduce the twist-2 GPDs, see definition (5). The case of $\mu = -$, according

⁹Detailed expressions and quantitative estimates are shown in Sec. 4.5.2

¹⁰In this section we do not specify the flavor index as all formulae here are valid for each flavor separately.

to the general twist counting rules of Ref. [Jaf91] corresponds to the twist-4 GPDs which contribute to the DVCS amplitude at the order of $O(1/Q^2)$. The twist-3 GPDs correspond to $\mu = \perp$. For a detailed discussion of the DVCS observables to the twist-3 accuracy see Sec. 4.3.3. Here we first discuss the general properties of the twist-3 GPDs and then will show that they can be related to the twist-2 GPDs in the so-called Wandzura-Wilczek approximation.

2.5.1 General properties of the twist-3 GPDs

Several properties of the twist-3 GPDs can be derived without invoking any approximation.

Forward limit: In the forward limit the “vector” GPD \mathcal{F}_μ can be parametrized as follows:

$$\lim_{\Delta \rightarrow 0} \mathcal{F}_\mu(x, \xi) = 2[q(x)\tilde{p}_\mu + m_N^2 f_4(x)n_\mu], \quad (45)$$

where $q(x)$ is the unpolarized forward quark (antiquark for $x \leq 0$) distribution of twist-2, $f_4(x)$ is the twist-4 quark distribution, see [Jaf91]. Also we introduced the light-cone vectors \tilde{p}^μ and n^μ , the former has only “plus” non-zero component $\tilde{p}^+ = \bar{P}^+$ and the latter only “minus” component $n^- = 1/\bar{P}^+$. As it could be expected, the twist-3 part of \mathcal{F}_μ disappears in the forward limit, because unpolarized parton densities of twist-3 are absent.

The forward limit for the twist-3 part of the “axial” GPD $\tilde{\mathcal{F}}_{\mu\perp}^{WW}$ is nontrivial:

$$\lim_{\Delta \rightarrow 0} \tilde{\mathcal{F}}_{\mu\perp}(x, \xi) = 2S_\mu^\perp \Delta_T q(x).$$

Here $\Delta_T q(x)$ is the transverse spin quark distribution which can be measured in DIS on a transversely polarized target.

Sum rules: Performing the integral over x of the distributions $\mathcal{F}^\mu(x, \xi)$ and $\tilde{\mathcal{F}}^\mu(x, \xi)$ given by Eq. (44) we obtain on the *rhs* the nucleon matrix elements of the local vector and axial currents. This results in the sum rules:

$$\begin{aligned} \int_{-1}^1 dx \mathcal{F}_\mu(x, \xi, t) &= \bar{N}(p') \gamma_\mu N(p) F_1(t) + \bar{N}(p') \frac{i\sigma_{\mu\nu} \Delta^\nu}{2m_N} N(p) F_2(t), \\ \int_{-1}^1 dx \tilde{\mathcal{F}}_\mu(x, \xi, t) &= \bar{N}(p') \gamma_\mu \gamma_5 N(p) g_A(t) + \frac{\Delta_\mu}{2m_N} \bar{N}(p') \gamma_5 N(p) h_A(t). \end{aligned} \quad (46)$$

These sum rules can be viewed as a generalization of the Burkhard-Cottingham sum rule for the transverse polarized distribution $\Delta_T q(x)$ [BurC70]. Indeed, in the forward limit the sum rule (46) for twist-3 GPD $\tilde{\mathcal{F}}_{\mu\perp}$ corresponds directly to the Burkhard-Cottingham sum rule

$$\int_0^1 dx \Delta_T q(x) = \int_0^1 dx \Delta q(x).$$

The second Mellin moment of GPDs $\mathcal{F}^\mu(x, \xi)$ and $\tilde{\mathcal{F}}^\mu(x, \xi)$ can be also computed in terms of moments of twist-2 GPDs without invoking any approximation [Pen00b, Kiv01c]. Indeed taking the x -moment of Eq. (44) we obtain on the *rhs* the local operator of the type

$\bar{\psi}\gamma_\mu(\gamma_5)\overleftrightarrow{\nabla}^+\psi$ which with the help of QCD equations of motion can be reduced to either the local operators of twist-2 or their total derivatives. Let us illustrate how this works on the example of the twist-3 part of the “vector” GPD $\mathcal{F}_{\mu\perp}(x, \xi)$. From the definition (44) we obtain:

$$\int_{-1}^1 dx \, x \, \mathcal{F}^{\mu\perp}(x, \xi) = \frac{i}{P^+} \langle p' | \bar{\psi}\gamma_\perp^\mu \overleftrightarrow{\nabla}^+ \psi | p \rangle. \quad (47)$$

Here ∇_α is the gauge covariant derivative in the fundamental representation. We rewrite the operator in Eq. (47) identically as:

$$\begin{aligned} \bar{\psi}\gamma_\perp^\mu \overleftrightarrow{\nabla}^+ \psi &= \frac{1}{2} \left[\bar{\psi}\gamma^\alpha \overleftrightarrow{\nabla}^\beta \psi + \bar{\psi}\gamma^\beta \overleftrightarrow{\nabla}^\alpha \psi - \frac{1}{2} g^{\alpha\beta} \bar{\psi}\gamma_\nu \overleftrightarrow{\nabla}^\nu \psi \right] \\ &+ \frac{1}{2} \left[\bar{\psi}\gamma^\alpha \overleftrightarrow{\nabla}^\beta \psi - \bar{\psi}\gamma^\beta \overleftrightarrow{\nabla}^\alpha \psi \right] \Big|_{\alpha=\mu_\perp, \beta=+}. \end{aligned} \quad (48)$$

The first bracket is the operator of the twist-2 (it is symmetric and traceless) and can be expressed in terms of the Mellin moments of the twist-2 GPDs H, E . The operator in the second bracket can be reduced to the total derivative of the axial current with the help of QCD equation of motion for a massless quark: $\overleftrightarrow{\nabla}\psi = 0$. Indeed, starting with the identities of the type $\bar{\psi}\gamma_\alpha\gamma_\beta\overleftrightarrow{\nabla}\psi = 0$ one derives the following identity:

$$\bar{\psi}(x) \left[\gamma_\alpha \overleftrightarrow{\nabla}_\beta - \gamma_\beta \overleftrightarrow{\nabla}_\alpha \right] \psi(x) = i\varepsilon_{\alpha\beta\rho\sigma} \partial^\sigma \left[\bar{\psi}(x) \gamma^\rho \gamma_5 \psi(x) \right], \quad (49)$$

which can be used to reduce the second bracket in Eq. (47) to the total derivative of the axial current. The latter is obviously the operator of twist-2.

Putting everything together we obtain the following sum rules [Pen00b, Kiv01a]:

$$\begin{aligned} \int_{-1}^1 dx \, x \, \mathcal{F}_{\mu\perp}(x, \xi, t) &= \bar{N}(p') \gamma_\mu^\perp N(p) \\ &\times \frac{1}{2} \left[\int_{-1}^1 dx \, x \{ H(x, \xi, t) + E(x, \xi, t) \} + g_A(t) \right] \\ &+ \frac{\Delta_\mu^\perp}{4m_N} \bar{N}(p') N(p) \frac{\partial}{\partial \xi} \int_{-1}^1 dx \, x \, E(x, \xi, t). \end{aligned} \quad (50)$$

We see that the GPD $\mathcal{F}_{\mu\perp}$ is sensitive to the combination

$$\int_{-1}^1 dx \, x \{ H(x, \xi, t) + E(x, \xi, t) \} + g_A(t)$$

which is related to the spin structure of the nucleon in the forward limit:

$$\lim_{\Delta \rightarrow 0} \int_{-1}^1 dx \, x \{ H^q(x, \xi, t) + E^q(x, \xi, t) \} + g_A(t) = 2J^q + \Delta q, \quad (51)$$

where J^q is for a given flavor a fraction of the total angular momentum of the nucleon carried by quarks and Δq is the corresponding fraction of the spin. To derive Eq. (51) we made use of angular momentum sum rule (32). We see that the twist-3 DVCS observables can be used to probe the spin structure of the nucleon. In principle, this part of the amplitude can be extracted from the data through the angular, spin and Q dependence of the differential cross section [Die97, Bel00a, Bel01b]. As will be discussed further in Sec. 4.3.4 and Sec. 4.3.5, this may provide us with additional possibility to probe J^q in the nucleon.

In the case of the axial transverse GPD $\tilde{\mathcal{F}}_{\mu\perp}$ we obtain in the same way the following result for the corresponding second moment:

$$\begin{aligned} \int_{-1}^1 dx \, x \, \tilde{\mathcal{F}}_{\mu\perp}(x, \xi, t) &= \bar{N}(p') \gamma_\mu^\perp \gamma_5 N(p) \frac{1}{2} \left[\int_{-1}^1 dx \, x \, \tilde{H}(x, \xi) + \xi^2 \{F_1(t) + F_2(t)\} \right] \\ &+ \text{other structures.} \end{aligned} \quad (52)$$

For simplicity we do not write all possible spinor structures which appear on the *rhs*. The sum rule (52) can be viewed as the generalization of the Efremov-Leader-Teryaev sum rule [Efr97] for the polarized structure function $\Delta_T q(x)$. The reason for such sum rules is the absence of the genuine twist-3 local gauge invariant operators of the form $\bar{\psi} G \psi$ (G is the gluon field strength) having dimension four. The third and higher Mellin moments are not generically related to the moments of twist-2 GPDs H, E and \tilde{H}, \tilde{E} , they get additional contributions from the genuine twist-3 local gauge invariant operators of the form $\bar{\psi} G \psi$. For instance the third Mellin moment of the GPDs \mathcal{F}^μ and $\tilde{\mathcal{F}}^\mu$ has the following structure:

$$\begin{aligned} \int_{-1}^1 dx \, x^2 \, \mathcal{F}^\mu(\tilde{\mathcal{F}}^\mu) &= \frac{1}{3(\bar{P}^+)^2} \langle p' | \bar{\psi} \gamma^+ (\gamma_5) g \tilde{G}^{+\mu} \psi | p \rangle \\ &+ \text{moments of } H, E, \tilde{H}, \tilde{E}. \end{aligned} \quad (53)$$

Here $\tilde{G}^{\mu\nu} = \frac{i}{2} \varepsilon^{\mu\nu\alpha\beta} G_{\alpha\beta}$ is a dual gluon field strength tensor. Generically the value of the matrix element of the genuine twist-3 $\bar{\psi} G \psi$ operator in the above equation is comparable with the size of matrix elements of twist-2 operators. The genuine twist-3 matrix element in Eq. (53) in the forward kinematics has been estimated using QCD sum rules [Bra87, Ste95], in the instanton model of the QCD vacuum [Balla98] and recently in lattice QCD [Goc01].

In the instanton model of the QCD vacuum the matrix elements of genuine twist-3 operators are parametrically (and numerically) suppressed relative to the corresponding matrix elements of twist-2 operators [Balla98, Dres00a]. This suppression is due to the small packing fraction of instantons in the QCD vacuum which is related to the ratio of the average size of the instantons to their average relative distance: $\frac{\bar{\rho}}{R} \approx \frac{1}{3}$. The dependence of the twist-3 to twist-2 parts of forward matrix elements on this small parameter was obtained in Refs. [Balla98, Dres00a] as:

$$\frac{\text{twist} - 3}{\text{twist} - 2} \sim \frac{\bar{\rho}^4}{R^4} \log \left(\frac{\bar{\rho}^2}{R^2} \right). \quad (54)$$

Several indications for the smallness of the above ratio have been provided recently by measurements of the transverse spin structure functions at SLAC [Mit99, Bos00]. We see that,

at least for the forward matrix elements, the genuine twist-3 operators can be neglected relative to the twist-2 ones. If one does so, one can express the twist-3 GPDs in terms of twist-2 ones. Such approximation is called Wandzura-Wilczek (WW) approximation [Wan77].

The twist-3 GPDs in the Wandzura-Wilczek approximation are discussed in the next section.

2.5.2 Wandzura-Wilczek approximation for the twist-3 GPDs

The aim of this section is the calculation of the matrix elements (44) in the Wandzura-Wilczek (WW) approximation. The operators entering the definition of the GPDs \mathcal{F}^μ and $\tilde{\mathcal{F}}^\mu$ of Eq. (44) can be decomposed in a gauge invariant way into two parts, one of which is fixed by the twist-2 GPDs H, E, \tilde{H} and \tilde{E} , and another – the “genuine twist-3” part – associated with operators of the type $\bar{\psi}G\psi$. The latter operators are interaction dependent and measure quark-gluon correlations in the target hadron. The WW approximation consists in the *assumption* that the nucleon matrix elements of the interaction dependent operators are small and can be neglected.

To obtain the WW relation we make use of the operator identities¹¹ derived in [Bel00b, Kiv01c, Rad00, Kiv01a, Rad01a] on the basis of technique developed in Ref. [Bal89]:

$$\begin{aligned} \bar{\psi}(x)\gamma_\mu\psi(-x) &= \frac{\mathcal{D}_\mu}{(\mathcal{D}x)}\bar{\psi}(x)\not{x}\psi(-x) \\ &+ \left[\partial_\mu - \frac{\mathcal{D}_\mu}{(x\mathcal{D})}(x\partial) \right] \frac{1}{2} \int_0^1 d\alpha \left\{ e^{\bar{\alpha}(x\mathcal{D})} + e^{-\bar{\alpha}(x\mathcal{D})} \right\} \bar{\psi}(\alpha x)\not{x}\psi(-\alpha x) \\ &+ \left[i\varepsilon_{\mu\alpha\beta\rho}x^\alpha \frac{\mathcal{D}^\beta}{(\mathcal{D}x)}\partial^\rho \right] \frac{1}{2} \int_0^1 d\alpha \left\{ e^{-\bar{\alpha}(x\mathcal{D})} - e^{\bar{\alpha}(x\mathcal{D})} \right\} \bar{\psi}(\alpha x)\not{x}\gamma_5\psi(-\alpha x) + \dots \end{aligned} \quad (55)$$

where $\bar{\alpha} = 1 - \alpha$ and ellipses stand for the contributions of either twist-3 quark gluon operators or twist-4 operators which both are neglected in the WW approximation. An analogous expression for the operator $\bar{\psi}(x)\gamma_\mu\gamma_5\psi(-x)$ can be obtained from Eq. (55) by the replacement $\not{x} \rightarrow \not{x}\gamma_5$ on *rhs* of this equation. The symbol \mathcal{D} denotes the derivative with respect to the total translation:

$$\mathcal{D}_\alpha \left\{ \bar{\psi}(tx)\Gamma[tx, -tx]\psi(-tx) \right\} \equiv \frac{\partial}{\partial y^\alpha} \left\{ \bar{\psi}(tx+y)\Gamma[tx+y, -tx+y]\psi(-tx+y) \right\} \Big|_{y \rightarrow 0}, \quad (56)$$

with a generic Dirac matrix structure Γ and $[x, y] = \text{Pexp}[ig\int_0^1 dt (x-y)_\mu A^\mu(tx + (1-t)y)]$. Note that in the matrix elements the total derivative can be easily converted into the momentum transfer:

$$\langle p' | \mathcal{D}_\mu \bar{\psi}(tx)\Gamma[tx, -tx]\psi(-tx) | p \rangle = i(p' - p)_\mu \langle p' | \bar{\psi}(tx)\Gamma[tx, -tx]\psi(-tx) | p \rangle \quad (57)$$

and therefore in the matrix elements one can associate \mathcal{D} with the momentum transfer Δ .

The identity (55) allows to express the matrix elements of the non-local “vector” and “axial” operators (*lhs* of (55)) in terms of matrix elements of symmetric operators generated by non-local operators $\bar{\psi}(x)\not{x}(\gamma_5)\psi(-x)$ standing on the *rhs* of Eq. (55). Since

¹¹Alternative derivation based on generalized rotational invariance can be found in Ref. [Ani01].

eventually (after performing differential operations on the *rhs* of Eq. (55)) the coordinate x^μ is put on the light-cone the symmetric operators on the *rhs* are reduced to the twist-2 operators and their total derivatives¹². This allows us to obtain the WW-relations for twist-3 nucleon GPDs [Bel00b, Kiv01a]:

$$\begin{aligned}\mathcal{F}_\mu^{WW}(x, \xi) &= \frac{\Delta_\mu}{2m_N\xi} \bar{N}(p') N(p) E(x, \xi) - \frac{\Delta_\mu}{2\xi} \bar{N}(p') \not{n} N(p) (H + E)(x, \xi) \\ &+ \int_{-1}^1 du G_\mu(u, \xi) W_+(x, u, \xi) + i\epsilon_{\perp\mu k} \int_{-1}^1 du \tilde{G}^k(u, \xi) W_-(x, u, \xi),\end{aligned}\quad (58)$$

$$\begin{aligned}\tilde{\mathcal{F}}_\mu^{WW}(x, \xi) &= \frac{\Delta_\mu}{2m_N\xi} \bar{N}(p') \gamma_5 N(p) \tilde{E}(x, \xi) - \frac{\Delta_\mu}{2\xi} \bar{N}(p') \not{n} \gamma_5 N(p) \tilde{H}(x, \xi) \\ &+ \int_{-1}^1 du \tilde{G}_\mu(u, \xi) W_+(x, u, \xi) + i\epsilon_{\perp\mu k} \int_{-1}^1 du G^k(u, \xi) W_-(x, u, \xi).\end{aligned}\quad (59)$$

The following notations are used :

$$\begin{aligned}G^\mu(u, \xi) &= \bar{N}(p') \gamma_\perp^\mu N(p) (H + E)(u, \xi) + \frac{\Delta_\perp^\mu}{2\xi m_N} \bar{N}(p') N(p) \left[u \frac{\partial}{\partial u} + \xi \frac{\partial}{\partial \xi} \right] E(u, \xi) \\ &- \frac{\Delta_\perp^\mu}{2\xi} \bar{N}(p') \not{n} N(p) \left[u \frac{\partial}{\partial u} + \xi \frac{\partial}{\partial \xi} \right] (H + E)(u, \xi),\end{aligned}\quad (60)$$

$$\begin{aligned}\tilde{G}^\mu(u, \xi) &= \bar{N}(p') \gamma_\perp^\mu \gamma_5 N(p) \tilde{H}(u, \xi) + \frac{\Delta_\perp^\mu}{2m_N\xi} \bar{N}(p') \gamma_5 N(p) \left[1 + u \frac{\partial}{\partial u} + \xi \frac{\partial}{\partial \xi} \right] \tilde{E}(u, \xi) \\ &- \frac{\Delta_\perp^\mu}{2\xi} \bar{N}(p') \not{n} \gamma_5 N(p) \left[u \frac{\partial}{\partial u} + \xi \frac{\partial}{\partial \xi} \right] \tilde{H}(u, \xi).\end{aligned}\quad (61)$$

The functions $W_\pm(x, u, \xi)$ can be called Wandzura-Wilczek kernels. They were introduced in Ref. [Bel00b, Kiv01a] and are defined as :

$$\begin{aligned}W_\pm(x, u, \xi) &= \frac{1}{2} \left\{ \theta(x > \xi) \frac{\theta(u > x)}{u - \xi} - \theta(x < \xi) \frac{\theta(u < x)}{u - \xi} \right\} \\ &\pm \frac{1}{2} \left\{ \theta(x > -\xi) \frac{\theta(u > x)}{u + \xi} - \theta(x < -\xi) \frac{\theta(u < x)}{u + \xi} \right\}.\end{aligned}\quad (62)$$

We also introduce the metric and totally antisymmetric tensors in the two dimensional transverse plane ($\varepsilon_{0123} = +1$) :

$$(-g^{\mu\nu})_\perp = -g^{\mu\nu} + n^\mu \tilde{p}^\nu + n^\nu \tilde{p}^\mu, \quad \epsilon_{\mu\nu}^\perp = \epsilon_{\mu\nu\alpha\beta} n^\alpha \tilde{p}^\beta. \quad (63)$$

¹²Note that in the pioneering approach of Ref. [Blu00] to the WW relations for GPDs the total derivatives were neglected. In this paper the reader can find a detailed discussion of the mathematical aspects of the twist decomposition of light-cone operators.

In Sec. 4.3.4 and Sec. 4.3.5 we shall use the WW-relations (58,59) in order to estimate the contributions of the twist-3 effects to various DVCS observables.

In the rest of this section, we discuss properties of the twist-3 GPDs peculiar for the WW approximation. Let us start with a discussion of the properties of the WW-kernels (62). We introduce the following notations for the action of the WW kernels on a function $f(u, \xi)$:

$$W_{\pm} \otimes f[x, \xi] \equiv \int_{-1}^1 du W_{\pm}(x, u, \xi) f(u, \xi), \quad (64)$$

with W_{\pm} given by Eq. (62). We shall call “WW transform” the resulting functions $W_{\pm} \otimes f[x, \xi]$ and we shall call the “WW transformation” the action of the WW kernels.

Limiting cases. We consider two limiting cases of the WW transformation: the forward limit $\xi \rightarrow 0$ and the ‘meson’ limit $\xi \rightarrow 1$. In the forward limit we easily obtain:

$$\begin{aligned} \lim_{\xi \rightarrow 0} W_+ \otimes f[x, \xi] &= \theta(x \geq 0) \int_x^1 \frac{du}{u} f(u, \xi = 0) - \theta(x \leq 0) \int_{-1}^x \frac{du}{u} f(u, \xi = 0), \\ \lim_{\xi \rightarrow 0} W_- \otimes f[x, \xi] &= 0. \end{aligned} \quad (65)$$

We can see that the action of the W_+ in the forward limit reproduces the Wandzura–Wilczek relation for the spin structure function g_T [Wan77]. The term with $\theta(x \geq 0)$ corresponds to the quark distributions and the term with $\theta(x \leq 0)$ to the antiquark distributions. The W_- kernel disappears in the forward limit, so that this kernel is a ‘genuine non-forward’ object.

In the limit $\xi \rightarrow 1$ the generalized parton distributions have properties of meson distribution amplitudes. In this limit the WW transforms have the form (we use the notation $f(u, \xi = 1) = \varphi(u)$):

$$\lim_{\xi \rightarrow 1} W_{\pm} \otimes f[x, \xi] = \frac{1}{2} \left\{ \int_{-1}^x \frac{du}{1-u} \varphi(u) \pm \int_x^1 \frac{du}{1+u} \varphi(u) \right\},$$

which corresponds to the WW relations for the meson distribution amplitudes derived in [Ball96, Ball98].

We can see that WW transforms of generalized parton distributions interpolate between WW relations for parton distributions and for the meson distribution amplitude. The general form of the WW kernels (62) also allows us to derive WW relations for distribution amplitudes of a meson of arbitrary spin.

Mellin moments: One can easily derive the Mellin moments of the WW transform. The result has the form:

$$\int_{-1}^1 dx x^N W_{\pm} \otimes f[x, \xi] = \frac{1}{N+1} \int_{-1}^1 du \left[\frac{u^{N+1} - \xi^{N+1}}{u - \xi} \pm \frac{u^{N+1} - (-\xi)^{N+1}}{u + \xi} \right] f(u, \xi). \quad (66)$$

From this simple exercise we can see an important property of the WW transformation, namely, if the function $f(u, \xi)$ satisfies the polynomiality condition, *i.e.*:

$$\int_{-1}^1 du u^N f(u, \xi) = \text{polynomial in } \xi \text{ of the order } N+1, \quad (67)$$

its WW transform also satisfies the same polynomiality condition.

Discontinuities. In Refs. [Kiv01c, Rad00, Rad01a] it was demonstrated that the twist-3 skewed parton distributions in the WW approximation exhibit discontinuities at the points $x = \pm\xi$. This feature is related to the properties of the WW kernels. Let us compute the discontinuities of a WW transform at the points $x = \pm\xi$:

$$\begin{aligned} \lim_{\delta \rightarrow 0} [W_{\pm} \otimes f[\xi + \delta, \xi] - W_{\pm} \otimes f[\xi - \delta, \xi]] &= \frac{1}{2}vp \int_{-1}^1 \frac{du}{u - \xi} f(u, \xi), \\ \lim_{\delta \rightarrow 0} [W_{\pm} \otimes f[-\xi + \delta, \xi] - W_{\pm} \otimes f[-\xi - \delta, \xi]] &= \pm \frac{1}{2}vp \int_{-1}^1 \frac{du}{u + \xi} f(u, \xi). \end{aligned} \quad (68)$$

Here vp means an integral in the sense of *valeur principale*. We see that for a very wide class of functions $f(u, \xi)$, the discontinuity of the corresponding WW transforms is nonzero. This feature of the WW transformation may lead to the violation of the factorization for the twist-3 DVCS amplitude.

Using general properties of the WW transformation (68) and Eqs. (58,59) one obtains that \mathcal{F}_{μ}^{WW} and $\tilde{\mathcal{F}}_{\mu}^{WW}$ have discontinuities at the points $x = \pm\xi$. But using a certain symmetry of the Eqs. (58) and (59), one can find that some combinations of the distributions \mathcal{F}_{μ}^{WW} and $\tilde{\mathcal{F}}_{\mu}^{WW}$ are free of discontinuities. For example, using Eq. (68) one can see that the combination:

$$\mathcal{F}_{\mu}^{WW}(x, \xi) - i\varepsilon_{\perp\mu\rho} \tilde{\mathcal{F}}_{\rho}^{WW}(x, \xi), \quad (69)$$

has no discontinuity at $x = \xi$. On the other hand, the ‘dual’ combination:

$$\mathcal{F}_{\mu}^{WW}(x, \xi) + i\varepsilon_{\perp\mu\rho} \tilde{\mathcal{F}}_{\rho}^{WW}(x, \xi), \quad (70)$$

is free of the discontinuity at $x = -\xi$. The cancellation of discontinuities in these particular combinations of the GPDs ensures the factorization of the twist-3 DVCS amplitude on the nucleon, as given in Sec. 4.3.3,

Pion pole contribution: The generalized parton distribution \tilde{E} at small t is dominated by chiral contribution of the pion pole, see Eq. (42). In the WW relation (58) the twist-2 GPD \tilde{E} enters only in the combination:

$$\left[1 + u \frac{\partial}{\partial u} + \xi \frac{\partial}{\partial \xi} \right] \tilde{E}(u, \xi). \quad (71)$$

One can easily see that the contribution of the pion pole (42) nullifies under the action of the differential operator in Eq. (71). The only place where the pion pole contribution survives is the GPD $\tilde{\mathcal{F}}_{\mu}$, see Eq. (59). In this way we obtain the following simple results for the contribution of the pion pole to the twist-3 GPDs in the WW approximation:

$$\begin{aligned} \mathcal{F}_{\mu}^{WW, \text{pion pole}}(x, \xi) &= 0, \\ \tilde{\mathcal{F}}_{\mu}^{WW, \text{pion pole}}(x, \xi) &= \frac{\Delta_{\mu}}{2m_N} \bar{N}(p') \gamma_5 N(p) \frac{4g_A^2 m_N^2}{m_{\pi}^2 - t} \frac{1}{\xi} \Phi_{\pi} \left(\frac{x}{\xi} \right) \theta(\xi - |x|). \end{aligned} \quad (72)$$

We see an interesting result that the pion pole contribution to the twist-3 GPDs is expressed in terms of twist-2 pion distributions amplitude. This observation is in nice agreement with the fact that in the WW approximation there exists no twist-3 pion distribution amplitude associated with vector- and axial-vector operators [Ball96].

D-term contribution: Now we discuss the D-term contribution to the twist-3 GPDs. If we substitute the D-term contributions (20) for the GPDs H and E into the WW relations of Eqs. (58,59) we see that the result is:

$$\begin{aligned}\mathcal{F}_\mu^{\text{WW D-term}}(x, \xi) &= -\frac{\Delta_\mu}{2\xi m_N} \bar{N}(p') N(p) D\left(\frac{x}{\xi}\right) \theta(|x| \leq \xi), \\ \tilde{\mathcal{F}}_\mu^{\text{WW D-term}}(x, \xi) &= 0.\end{aligned}\tag{73}$$

In some sense the D-term is an eigenfunction of the WW transformation.

2.6 GPDs for $N \rightarrow \Lambda, \Sigma$ transitions : SU(3) relations and beyond

The studies of hard exclusive processes with strangeness production give an access to the flavor non-diagonal generalized parton distributions [Fra99b]. These distributions correspond to the process where a quark of one flavor is taken out of the initial nucleon at the space-time point $y/2$, and then a quark with another flavor (say a strange quark) is put back exciting a hyperon at the space-time point $-y/2$. The strangeness changing distributions for $N \rightarrow Y$ transitions ($Y = \Sigma, \Lambda$) can be defined as (cf. Eq. (5)):

$$\begin{aligned}& \frac{\bar{P}^+}{2\pi} \int dy^- e^{ix\bar{P}^+ y^-} \langle p', Y | \bar{s}_\beta(-y/2) q_\alpha(y/2) | p, N \rangle \Big|_{y^+ = \bar{y}_\perp = 0} \\ &= \frac{1}{4} \left\{ (\gamma^-)_{\alpha\beta} \left[H^{N \rightarrow Y}(x, \xi, t) \bar{Y}(p') \gamma^+ N(p) \right. \right. \\ & \quad \left. \left. + E^{N \rightarrow Y}(x, \xi, t) \bar{Y}(p') i\sigma^{+\kappa} \frac{\Delta_\kappa}{2m_N} N(p) \right] \right. \\ & \quad \left. + (\gamma_5 \gamma^-)_{\alpha\beta} \left[\tilde{H}^{N \rightarrow Y}(x, \xi, t) \bar{Y}(p') \gamma^+ \gamma_5 N(p) \right. \right. \\ & \quad \left. \left. + \tilde{E}^{N \rightarrow Y}(x, \xi, t) \bar{Y}(p') \gamma_5 \frac{\Delta^+}{2m_N} N(p) \right] \right\},\end{aligned}\tag{74}$$

where $s_\beta(-y/2)$ is the field operator of a strange quark, $q(y/2)$ is the field operator of a nonstrange quark (with $q = u$ or d depending on the charge of the hyperon Y).

The flavor non-diagonal GPDs provide a new tool to study the non-perturbative structure of various nucleon-hyperon transitions. Below we shall relate strangeness changing $N \rightarrow Y$ GPDs to $N \rightarrow N$ GPDs with help of flavor $SU(3)$ relations. But before doing this let us discuss some interesting features of the $N \rightarrow Y$ GPDs which are related to the $SU(3)$ symmetry breaking effects.

Let us start with a discussion of the form factor sum rules for strangeness changing $N \rightarrow Y$ GPDs. Integrating the *lhs* of Eq. (74) over x one gets the local $\bar{s}q$ operator sandwiched between a nucleon and a hyperon state. Such matrix elements are parametrized in terms of vector and axial $N \rightarrow Y$ transition form factors entering the description of

semi-leptonic decays of hyperons (see e.g. [Gar85])¹³:

$$\begin{aligned}\langle p', Y | \bar{s} \gamma^\mu q | p, N \rangle &= \bar{Y}(p') \left[f_1^{N \rightarrow Y} \gamma^\mu + f_2^{N \rightarrow Y} \frac{i \sigma^{\mu\nu} \Delta_\nu}{2m_N} + f_3^{N \rightarrow Y} \frac{\Delta^\mu}{2m_N} \right] N(p), \\ \langle p', Y | \bar{s} \gamma^\mu \gamma_5 q | p, N \rangle &= \bar{Y}(p') \left[g_1^{N \rightarrow Y} \gamma^\mu + g_2^{N \rightarrow Y} \frac{i \sigma^{\mu\nu} \Delta_\nu}{2m_N} + g_3^{N \rightarrow Y} \frac{\Delta^\mu}{2m_N} \right] \gamma_5 N(p).\end{aligned}\quad (75)$$

We see that for the strangeness changing transitions two additional form factors $f_3^{N \rightarrow Y}(t)$ and $g_2^{N \rightarrow Y}(t)$ related to the second class currents (g_2 is also often referred to as weak electricity) appear. Both these form-factors are proportional to flavor $SU(3)$ breaking ($\sim m_s$) effects and they are absent for transitions without strangeness change.

The form factor sum rules for strangeness changing GPDs have the following form:

$$\begin{aligned}\int_{-1}^1 dx H^{N \rightarrow Y}(x, \xi, t) &= f_1^{N \rightarrow Y}(t) - \xi \frac{m_Y + m_N}{2m_N} f_3^{N \rightarrow Y}(t), \\ \int_{-1}^1 dx E^{N \rightarrow Y}(x, \xi, t) &= f_2^{N \rightarrow Y}(t) + \xi f_3^{N \rightarrow Y}(t), \\ \int_{-1}^1 dx \tilde{H}^{N \rightarrow Y}(x, \xi, t) &= g_1^{N \rightarrow Y}(t) + \frac{m_Y - m_N}{2m_N} g_2^{N \rightarrow Y}(t), \\ \int_{-1}^1 dx \tilde{E}^{N \rightarrow Y}(x, \xi, t) &= g_3^{N \rightarrow Y}(t) + \frac{1}{\xi} g_2^{N \rightarrow Y}(t).\end{aligned}\quad (76)$$

One sees that in contrast to the corresponding sum rules for the GPDs without strangeness changing (see Eqs. (8-11)) the sum rules (76) get additional contributions from the $SU(3)$ symmetry breaking form factors $f_3(t)$ and $g_2(t)$, associated with the second class currents. Note that these additional contributions also violate the symmetry of GPDs under the transformation $\xi \rightarrow -\xi$ [Man98a]. The reason is that for the derivation of this symmetry the time inversion transformation has been used. Under this transformation the initial and final baryon states are exchanged. In the case when this transition occurs between baryons belonging to the same symmetry multiplet the T -invariance gives the symmetry property under $\xi \rightarrow -\xi$. However for the case of transitions between baryons from different multiplets the T -invariance is not restrictive (it gives only the realness of the GPDs).

Studies of semileptonic hyperon decays showed (see e.g. [Gar85]) that the assumption of the $SU(3)$ flavor symmetry works very well for form factors g_1 , f_1 , and f_2 . Unfortunately the semileptonic decays of hyperons are not sensitive to f_3 , g_2 and g_3 . On general grounds we can state that the form factors f_3 and g_2 are proportional to the explicit $SU(3)$ breaking, *i.e.* they are proportional to the strange quark mass, therefore their effect can be non-negligible. For the form factor $g_3(t)$ we can apply the generalized PCAC relations to obtain the contribution of the kaon pole:

$$g_3^{N \rightarrow Y}(t) \approx \frac{2g_{KNY}f_K}{m_K^2 - t}, \quad (77)$$

¹³We change the definitions of the form factors f_2, g_2 and g_3 by a factor of two to have correspondence with the standard definition of the nucleon form factors.

where g_{KNY} are the KNY coupling constants, and $f_K \approx 159$ MeV is the kaon decay constant. Comparing the t -dependence of this equation with the one of the pion pole contribution to pseudoscalar nucleon form factor (41) we notice a big difference due to the large difference between the kaon and pion masses. This shows that $SU(3)$ symmetry breaking effects are sizeable for $g_3^{N \rightarrow Y}(t)$.

From the sum rules (76) we see that the $SU(3)$ symmetry breaking effects are suppressed for the GPDs H , E , and \tilde{H} , at least they are suppressed in the sum rules by either ξ (like for H and E) or $m_Y - m_N$ (like for \tilde{H}). On contrary, the sum rule for GPD $\tilde{E}^{N \rightarrow Y}(x, \xi, t)$ shows that the flavor symmetry breaking effects can be very strong for this GPD. Indeed the first term on the *rhs* of the sum rule is proportional to $g_3^{N \rightarrow Y}(t)$ for which one expects large symmetry breaking effects (see discussion above). Additionally the weak electricity (symmetry breaking) form factor enters the corresponding sum rule with the factor of $1/\xi$. This, in particular, implies that in the limit $\xi \rightarrow 0$ the function is divergent¹⁴, and this divergency is dominated by weak electricity. This observation opens an exciting possibility to study the weak electricity of nucleon-hyperon transitions (otherwise hardly accessible) in hard exclusive strange meson production. In this respect, the transverse spin azimuthal asymmetry in the production of kaons on the nucleon is a very promising observable as it is sensitive to the function $\tilde{E}^{N \rightarrow Y}$, see Sec. 4.5.4 and qualitative discussion below.

Given the large expected $SU(3)$ symmetry breaking effects for the GPD $\tilde{E}^{N \rightarrow Y}$ we model this function by the contribution of the kaon pole plus the weak electricity contribution:

$$\begin{aligned} \tilde{E}^{N \rightarrow Y}(x, \xi, t) &= \frac{2g_{KNY}m_N f_K}{m_K^2 - t} \theta[\xi - |x|] \frac{1}{\xi} \Phi_K\left(\frac{x}{\xi}\right) \\ &+ \frac{1}{\xi} \tilde{E}_{WE}^{N \rightarrow Y}(x, \xi, t), \end{aligned} \quad (78)$$

where $\Phi_K(z)$ is the kaon distribution amplitude and $\tilde{E}_{WE}^{N \rightarrow Y}(x, \xi, t)$ is the “weak electricity” GPD normalized to the corresponding weak electricity form factor $g_2^{N \rightarrow Y}(t)$:

$$\int_{-1}^1 dx \tilde{E}_{WE}^{N \rightarrow Y}(x, \xi, t) = g_2^{N \rightarrow Y}(t). \quad (79)$$

This GPD is proportional to explicit $SU(3)$ symmetry breaking effects ($\sim m_s$). If for the weak electricity GPD we use the following rough (asymptotic) ansatz $\tilde{E}_{WE}^{N \rightarrow Y} = 3/4(1 - x^2/\xi^2)/\xi g_2^{N \rightarrow Y}(t)$ the transverse spin asymmetry in production of the kaons has the dominant contribution (*cf.* Eq. (43)):

$$\sigma^{N \rightarrow YK} \propto |S_\perp| \sin \Phi \sqrt{t_{\min} - t} \left[\frac{g_{KNY}m_N f_K}{-t + m_K^2} + \frac{g_2^{N \rightarrow Y}(t)}{2\xi} \right] \tilde{H}^{N \rightarrow Y}(\xi, \xi, t).$$

¹⁴One can introduce an “ovecomplete” set of GPDs adding to the *rhs* of Eq. (74) one additional “weak electricity” GPD $\tilde{E}_{WE}^{N \rightarrow Y} \sigma^{+\nu} \Delta_\nu \gamma_5 / 2m_N$. In this way one avoids working with GPDs non normalizable at $\xi = 0$.

This expression illustrates that at small ξ the measurement of hard exclusive kaon production can give us (among other exciting things!) an access to the symmetry breaking weak electricity form factor $g_2^{N \rightarrow Y}(t)$. The contribution of the weak electricity is enhanced at small x_B . For example for the $\gamma^* p \rightarrow \Lambda K^+$ processes at $-t = 0.5 \text{ GeV}^2$ and $x_B \approx 0.05$ the contribution of the weak-electricity part in (80) is of the same order as the contribution of the kaon pole. We take for this estimate the value of $g_2^{p \rightarrow \Lambda}(0) \approx 0.1$ obtained in Ref. [Kim98] in the framework of the chiral quark-soliton model. This simple estimate shows that the studies of the second class currents are feasible in hard exclusive reactions with production of strangeness.

For the strangeness changing GPDs $H^{N \rightarrow Y}$, $E^{N \rightarrow Y}$ and $\tilde{H}^{N \rightarrow Y}$ we can apply the flavor $SU(3)$ relations as it seems that for these GPDs the effects of the symmetry breaking are small. The $SU(3)$ relations for these functions have the following form [Fra99a]:

$$\begin{aligned} H^{p \rightarrow \Lambda}(x, \xi, t) &= -\frac{1}{\sqrt{6}} (2H^u - H^d - H^s) , \\ H^{p \rightarrow \Sigma^0}(x, \xi, t) &= -\frac{1}{\sqrt{2}} (H^d - H^s) , \\ H^{p \rightarrow \Sigma^+}(x, \xi, t) &= -(H^d - H^s) , \end{aligned} \tag{80}$$

and similar expressions for GPDs $E^{N \rightarrow Y}$ and $\tilde{H}^{N \rightarrow Y}$. For transitions from the neutron we can analogously derive:

$$\begin{aligned} H^{n \rightarrow \Lambda}(x, \xi, t) &= -\frac{1}{\sqrt{6}} (2H^d - H^u - H^s) , \\ H^{n \rightarrow \Sigma^0}(x, \xi, t) &= -\frac{1}{\sqrt{2}} (H^u - H^s) , \\ H^{n \rightarrow \Sigma^-}(x, \xi, t) &= -(H^u - H^s) . \end{aligned} \tag{81}$$

The $SU(3)$ relations (80,81) give us a possibility to access strange quark distributions in the nucleon. Indeed, using these relations we can derive the following obvious relations [we show only the example of \tilde{H}]:

$$\begin{aligned} \lim_{\Delta \rightarrow 0} \tilde{H}^{p \rightarrow \Lambda}(x, \xi, t) &= -\frac{1}{\sqrt{6}} (2\Delta u(x) - \Delta d(x) - \Delta s(x)) , \\ \lim_{\Delta \rightarrow 0} \tilde{H}^{p \rightarrow \Sigma^0}(x, \xi, t) &= -\frac{1}{\sqrt{2}} (\Delta d(x) - \Delta s(x)) , \\ \lim_{\Delta \rightarrow 0} \tilde{H}^{p \rightarrow \Sigma^+}(x, \xi, t) &= -(\Delta d(x) - \Delta s(x)) . \end{aligned} \tag{82}$$

This illustrates that measurements of strangeness changing GPDs can give us important information about strange (anti-)quark polarized distributions.

2.7 GPDs for $N \rightarrow \Delta$ transition

In the hard exclusive processes with an excitation of the Δ one accesses the parton distributions for $N \rightarrow \Delta$ transition [Fra98a, Fra00a]. A knowledge of such distributions would

give us the detailed information about the physics of $N \rightarrow \Delta$ transition, in particular it would allow us to understand the physics of this transition at the level of partons.

The $N \rightarrow \Delta$ quark distributions can be defined through nondiagonal matrix elements of products of quark fields at light-cone separation. We give the definitions of $N \rightarrow \Delta$ generalized quark distributions for $p \rightarrow \Delta^+$ transition. The GPDs of other transitions, e.g. $p \rightarrow \Delta^{++}$, $p \rightarrow \Delta^0$, etc. can be obtained with the help of the following isospin factors:

$$[p \rightarrow \Delta^{++}] = \sqrt{\frac{3}{2}} [p \rightarrow \Delta^+], \quad [p \rightarrow \Delta^0] = \sqrt{\frac{1}{2}} [p \rightarrow \Delta^+], \quad (83)$$

and analogous relations for transitions from the neutron. Keeping in mind this simple isospin relations, we introduce for the $p \rightarrow \Delta^+$ transition the following three GPDs (cf. Eq. 5 with $y^\mu = \lambda n^\mu$):

$$\begin{aligned} \int \frac{d\lambda}{2\pi} e^{i\lambda x} \langle \Delta, p' | \bar{\psi}(-\lambda n/2) \not{n} \tau^3 \psi(\lambda n/2) | N, p \rangle = \\ \sqrt{\frac{2}{3}} \bar{\psi}^\beta(p') [H_M(x, \xi, t) \mathcal{K}_{\beta\mu}^M n^\mu + H_E(x, \xi, t) \mathcal{K}_{\beta\mu}^E n^\mu + H_C(x, \xi, t) \mathcal{K}_{\beta\mu}^C n^\mu] N(p). \end{aligned} \quad (84)$$

Here n_μ is a light-cone vector,

$$n^2 = 0, \quad n \cdot \bar{P} = 1, \quad \bar{P}^\mu = \frac{1}{2}(p + p')^\mu \quad (85)$$

Δ is the four-momentum transfer,

$$\Delta = p' - p, \quad (86)$$

$\psi^\beta(p')$ is the Δ Rarita-Schwinger spinor, $N(p)$ is the nucleon Dirac spinor. The $N \rightarrow \Delta$ quark distributions $H_{M,E,C}(x, \xi, \Delta^2)$ are regarded as functions of the variable x , the square of the four-momentum transfer, t , and its longitudinal component

$$\xi = -\frac{1}{2}(n \cdot \Delta). \quad (87)$$

The covariants $\mathcal{K}_{\beta\mu}^{M,E,C}$ are magnetic dipole, electric quadrupole and Coulomb quadrupole covariants [Jon73]:

$$\begin{aligned} \mathcal{K}_{\beta\mu}^M &= -i \frac{3(m_\Delta + m_N)}{2m_N((m_\Delta + m_N)^2 - t)} \varepsilon_{\beta\mu\lambda\sigma} \bar{P}^\lambda \Delta^\sigma, \\ \mathcal{K}_{\beta\mu}^E &= -\mathcal{K}_{\beta\mu}^M - \frac{6(m_\Delta + m_N)}{m_N Z(t)} \varepsilon_{\beta\sigma\lambda\rho} \bar{P}^\lambda \Delta^\rho \varepsilon_{\mu\kappa\delta}^{\sigma} \bar{P}^\kappa \Delta^\delta \gamma^5, \\ \mathcal{K}_{\beta\mu}^C &= -i \frac{3(m_\Delta + m_N)}{m_N Z(t)} \Delta_\beta (t \bar{P}_\mu - \Delta \cdot \bar{P} \Delta_\mu) \gamma^5, \end{aligned} \quad (88)$$

where we introduced the notation $Z(t) = [(m_\Delta + m_N)^2 - t][(m_\Delta - m_N)^2 - t]$. We choose such definition of the $N \rightarrow \Delta$ quark distributions in order to have the following sum rules:

$$\int_{-1}^1 dx H_{M,E,C}(x, \xi, t) = 2 G_{M,E,C}^*(t), \quad (89)$$

where $G_{M,E,C}^*(t)$ are the standard magnetic dipole, electric quadrupole and Coloumb quadrupole transition form factors respectively [Jon73].

Analogously to Eq. (84) we introduce the following quark helicity dependent $p \rightarrow \Delta^+$ generalized quark distributions:

$$\begin{aligned} \int \frac{d\lambda}{2\pi} e^{i\lambda x} \langle \Delta, p' | \bar{\psi}(-\lambda n/2) \not{n} \gamma^5 \tau^3 \psi(\lambda n/2) | N, p \rangle = \\ \bar{\psi}^\beta(p') \left[C_1(x, \xi, t) n_\beta + C_2(x, \xi, t) \frac{\Delta_\beta (n \cdot \Delta)}{m_N^2} + C_3(x, \xi, t) \frac{1}{m_N} \{ n_\beta \not{\Delta} - \Delta_\beta \not{n} \} \right. \\ \left. + C_4(x, \xi, t) \frac{1}{m_N^2} \{ \bar{P} \cdot \Delta n_\beta - 2 \Delta_\beta \} \right] N(p). \end{aligned} \quad (90)$$

Actually in this definition not all the functions C_i are independent, for example the function C_4 can be absorbed in a redefinition of the functions C_1 and C_2 . We choose the “overcomplete” definition (90) to have simple (ξ -independent) sum rules for the first Mellin moment of generalized distributions C_i :

$$\begin{aligned} \int_{-1}^1 dx \, C_1(x, \xi, t) &= 2 \, C_5^A(t), & \int_{-1}^1 dx \, C_2(x, \xi, t) &= 2 \, C_6^A(t), \\ \int_{-1}^1 dx \, C_3(x, \xi, t) &= 2 \, C_3^A(t), & \int_{-1}^1 dx \, C_4(x, \xi, t) &= 2 \, C_4^A(t). \end{aligned} \quad (91)$$

Here $C_i^A(t)$ are axial $N \rightarrow \Delta$ transition form factors in the notations of Adler [Adl75]:

$$\begin{aligned} \langle \Delta^+, p' | \bar{\psi}(0) \gamma_\mu \gamma_5 \psi(0) | p, p \rangle = \\ \bar{\psi}^\beta(p') \left[C_5^A(t) g_{\mu\beta} + C_6(t) \frac{\Delta_\beta \Delta_\mu}{m_N^2} + C_3^A(t) \frac{1}{m_N} \{ g_{\beta\mu} \not{\Delta} - \Delta_\beta \gamma_\mu \} \right. \\ \left. + C_4^A(t) \frac{2}{m_N^2} \{ \bar{P} \cdot \Delta g_{\beta\mu} - \bar{P}_\mu \Delta_\beta \} \right] N(p). \end{aligned} \quad (92)$$

In Sec. 3 we shall derive large N_c relations between the $N \rightarrow \Delta$ generalized quark distributions and the usual $N \rightarrow N$ ones.

For the $N \rightarrow \Delta$ GPDs one can repeat almost word for word the discussion of such issues as polynomiality, pion pole contribution, etc. However in applications for hard exclusive processes with excitation of Δ (see Sec. 4.4 and Sec. 4.5.4) we shall use only the large N_c relations derived in Sec. 3.1.1. Therefore here we restrict ourselves to discussion of these relations. They have the following form:

$$\begin{aligned} H_M(x, \xi, t) &= \frac{2}{\sqrt{3}} [E^u(x, \xi, t) - E^d(x, \xi, t)], \\ C_1(x, \xi, t) &= \sqrt{3} [\tilde{H}^u(x, \xi, t) - \tilde{H}^d(x, \xi, t)], \\ C_2(x, \xi, t) &= \frac{\sqrt{3}}{4} [\tilde{E}^u(x, \xi, t) - \tilde{E}^d(x, \xi, t)]. \end{aligned} \quad (93)$$

All other $N \rightarrow \Delta$ GPDs are zero at leading order of $1/N_c$ expansion. Let us also note that if we take the first moment of the Eqs. (93) and take into account the sum rules for $N \rightarrow N$ GPDs (8-11) we reproduce the well known result of soliton models for the $N \rightarrow \Delta$ transition form factors. Integrating H_M , given by the large N_c relation of Eq. 93, over x at $t = 0$ gives the relation between magnetic moments:

$$\mu_{N\Delta} = \frac{1}{\sqrt{2}}(\mu_p - \mu_n) , \quad (94)$$

which is satisfied rather well by the experimental data on magnetic moments. As we discussed in Sec. 2.4.2, the GPD \tilde{E} contains a contribution of the pion pole. From the large N_c relation for C_2 in Eq. (93) we conclude that the $N \rightarrow \Delta$ GPD $C_2(x, \xi, t)$ also contain the pion pole contribution of the form:

$$\lim_{t \rightarrow m_\pi^2} C_2(x, \xi, t) = \sqrt{3} \frac{g_A m_N^2}{m_\pi^2 - t} \theta[\xi - |x|] \frac{1}{\xi} \Phi_\pi\left(\frac{x}{\xi}\right) . \quad (95)$$

The $N \rightarrow \Delta$ distribution $H_M(x, \xi, t)$ in the large N_c limit contains information about the isovector part of the angular momentum of the nucleon carried by the quarks – $J^u - J^d$. Indeed with help of angular momentum sum rule (34) we easily obtain

$$\lim_{t \rightarrow 0, N_c \rightarrow \infty} \int_{-1}^1 dx \, x \, H_M(x, \xi, t) = \frac{2}{\sqrt{3}} [2(J^u - J^d) - M_2^u + M_2^d] , \quad (96)$$

where, as usually:

$$M_2^q = \int_0^1 dx \, x \, [q(x) + \bar{q}(x)] .$$

Note that the contribution of the D-term does not appear in the $N \rightarrow \Delta$ transition, because the D-term is a flavor singlet quantity.

Obviously one can easily introduce GPDs for other $N \rightarrow N^*$ (N^* is a nucleon resonance) transitions which enter description of hard exclusive processes with excitation of baryonic resonances. Such kind of reactions can be viewed as a new tool for the study of baryon spectroscopy (spectroscopy by light-cone operators).

2.8 Further generalizations: GPDs for $N \rightarrow \pi N$ transitions

The transitions of the nucleon to a πN system with low invariant mass can also be studied by light-cone probes encoded in the $N \rightarrow \pi N$ GPDs¹⁵ which can be introduced as follows (we only show the parametrization of the “vector” bilocal quark operator):

$$\begin{aligned} & \frac{\bar{P}^+}{2\pi} \int dy^- e^{ix\bar{P}^+ y^-} \langle \pi(k) N(p') | \bar{\psi}(-y/2) \gamma^+ \psi(y/2) | N(p) \rangle \Big|_{y^+ = \bar{y}_\perp = 0} \\ &= \frac{1}{f_\pi} \left[H_1^{\pi N}(x, \xi, t, \alpha, t_\pi, m_{\pi N}) \bar{N}(p') \gamma^+ \gamma_5 N(p) \right] \end{aligned}$$

¹⁵Previously $N \rightarrow \pi N$ GPDs were briefly discussed in Ref. [Pol98]

$$\begin{aligned}
& + H_2^{\pi N}(x, \xi, t, \alpha, t_\pi, m_{\pi N}) \bar{N}(p') \frac{i\sigma^{+\nu} k_\nu}{2m_N} \gamma_5 N(p) \\
& + H_3^{\pi N}(x, \xi, t, \alpha, t_\pi, m_{\pi N}) \bar{N}(p') \frac{\not{k}}{2m_N} \gamma_5 N(p) \\
& + H_4^{\pi N}(x, \xi, t, \alpha, t_\pi, m_{\pi N}) \bar{N}(p') \gamma_5 N(p) \Big].
\end{aligned} \tag{97}$$

Here $f_\pi \approx 92.4$ MeV is the pion decay constant and we introduced the following kinematical variables:

$$\bar{P} \equiv \frac{p + p' + k}{2}, \tag{98}$$

and the momentum transfer

$$\Delta \equiv p' + k - p. \tag{99}$$

n is a light-cone vector, i.e. $n^2 = 0$, which is normalized such that $n \cdot \bar{P} = 1$. The $N \rightarrow \pi N$ GPDs $H_i^{\pi N}$ are the functions of the invariants on which the matrix elements depend. These are the skewedness:

$$\xi \equiv -\frac{n \cdot \Delta}{2}, \tag{100}$$

the square of the momentum transfer $t = \Delta^2$, the square of the nucleon momentum difference $t_\pi = (p' - p)^2$, the invariant mass of the final πN system $m_{\pi N}$ and the light-cone fraction α , which characterizes the longitudinal fraction of the final pion:

$$\alpha \equiv \frac{n \cdot k}{1 - \xi}. \tag{101}$$

These GPDs can be used to describe the hard “semi-exclusive” processes of the type:

$$\gamma^* + N \rightarrow \gamma + (\pi N), \quad \gamma^* + N \rightarrow M + (\pi N), \tag{102}$$

in which the target nucleon dissociates into a low mass πN system. The description of such reactions is important because in the high energy experiments the resolution in the missing mass of the recoil baryonic system can be rather low. In such cases the data for e.g. $\gamma^* N \rightarrow \gamma N$ always include the $\gamma^* N \rightarrow \gamma(\pi N)$ ‘contamination’ due to a soft pion.

Another motivation for studies of $N \rightarrow \pi N$ GPDs is that in the threshold region, where $m_{\pi N} \rightarrow m_\pi + m_N$, $\alpha \rightarrow m_\pi / (m_\pi + m_N)$, etc, the πN GPDs can be expressed in terms of nucleon and pion GPDs [Mos01, Str01]. Additionally one can develop the systematic chiral perturbation theory for the $N \rightarrow \pi N$ GPDs. Indeed the first Mellin moment of the $N \rightarrow \pi N$ GPDs (97) corresponds to the amplitude of the pion electroproduction off the nucleon. Near the threshold this process has been described by chiral perturbation theory, for the review see [Ber94]. The second Mellin moment of the $N \rightarrow \pi N$ GPDs corresponds to pion production by the operator of the energy momentum tensor, this can be rephrased as the pion production by a graviton. This simple example shows that the studies of the hard reactions of the type (102) open a new, large field for applications of chiral perturbation theory. Measurements of these GPDs would give a new sensitive tool for studies of chiral symmetry breaking mechanism in QCD.

The $N \rightarrow \pi N$ GPDs in the resonance region, i.e. for $m_{\pi N} \approx m_R$, give us a new tool for studying of the resonance spectroscopy, i.e. the spectroscopy with light-cone probes.

3 GPDs IN THE LARGE N_c LIMIT

The large N_c limit in QCD [tHo74, Wit79] proved to be an useful tool to analyze the properties of mesons and baryons. The idea is that our world with the number of colors $N_c = 3$ is not qualitatively different from an imaginary world with large number of colors. For the comprehensive review of applications of the large N_c expansion in hadronic physics see Ref. [Mano98]. In this section we study the GPDs of the nucleon in the large N_c limit, first discussing general properties of the GPDs in this limit and then presenting calculations of the GPDs in the specific dynamical realization of the low-energy large N_c QCD – chiral quark-soliton model.

3.1 Generalized parton distributions at large N_c : general properties

In order to consider the generalized parton distributions in the large N_c limit we start from the quark correlator $\langle B_2 | \psi(x_2) \bar{\psi}(x_1) | B_1 \rangle$. The Hartree picture of the large N_c nucleon described in [Wit79] leads to the following form of this correlation function [Pob00]:

$$\begin{aligned} \langle B_1, \mathbf{p}_1 | \bar{\psi}_{s_1 f_1}(x_1^0, \mathbf{x}_1) \psi_{s_2 f_2}(x_2^0, \mathbf{x}_2) | B_2, \mathbf{p}_2 \rangle &= 2m_B N_c \int d^3 \mathbf{X} e^{i(\mathbf{p}_2 - \mathbf{p}_1) \cdot \mathbf{X}} \\ &\times \int dR \phi_{B_1}^*(R) \phi_{B_2}(R) \left[R_{f_2 f'_2} F_{s_2 f'_2, s_1 f'_1} \left(x_1^0 - x_2^0, \mathbf{x}_1 - \mathbf{X}, \mathbf{x}_2 - \mathbf{X} \right) (R^{-1})_{f'_1 f_1} \right]. \end{aligned} \quad (103)$$

Here $F_{s_2 f'_2, s_1 f'_1}(x_1^0 - x_2^0, \mathbf{x}_1, \mathbf{x}_2)$ is the correlation function $\langle \psi(x_2) \bar{\psi}(x_1) \rangle$ corresponding to the static solution of the Hartree equation, s_i are Dirac spinor indices and f_i are $SU(2)$ isospin indices. The $x^0 - y^0$ time dependence expresses the fact that we deal with a static solution. The solution $F_{s_2 f'_2, s_1 f'_1}(x_2^0 - x_1^0, \mathbf{x}_2, \mathbf{x}_1)$ also violates the $SU(2)$ flavor and the 3-space translation invariance. Therefore in Eq. (103) we used plane waves $e^{i\mathbf{p} \cdot \mathbf{X}}$ and the $SU(2)$ rotator wave functions $\phi_B(R)$ expressed in terms of Wigner finite rotation functions [Adk83]:

$$\phi_{S_3 T_3}^{S=T}(R) = \sqrt{2S+1} (-1)^{T+T_3} D_{-T_3, S_3}^{S=T}(R), \quad (104)$$

in order to construct baryon states with given spin, isospin and momentum. The expression in the square brackets in Eq. (103) (where one puts $(x - y)^2 = 0$) can be called a parton distribution of a soliton.

Since the exact form of the effective Hartree hamiltonian corresponding to the large N_c limit generically is not known we do not know the function $F_{s_2 f'_2, s_1 f'_1}(x_2^0 - x_1^0, \mathbf{x}_2, \mathbf{x}_1)$ either¹⁶. However, following [Wit79] we assume that this solution has the spin-flavor symmetry:

$$S_{s_2 s'_2}(R) R_{f_2 f'_2} F_{s'_2 f'_2, s'_1 f'_1} \left(x^0 - y^0, O_{space}(R) \mathbf{x}, O_{space}(R) \mathbf{y} \right) (R^{-1})_{f'_1 f_1} S_{s'_1 s_1}(R^{-1}) \quad (105)$$

$$= F_{s_2 f_2, s_1 f_1}(x^0 - y^0, \mathbf{x}, \mathbf{y}) \quad (106)$$

Here we use the notation $S_{s_2 s'_2}(R)$ for spin rotations and $O_{space}(R)$ for space rotations, which are parametrized by a $SU(2)$ matrix R .

¹⁶In the next section we shall use the chiral quark-soliton model to compute this function

Using the expression (103), one can obtain any quark parton distribution function in the large N_c limit. Using the spin-flavor symmetry (106) of the soliton distribution (the expression in square brackets of Eq. (103)) we can write explicitly the dependence on the orientation angles R of particular $\bar{\psi}\psi$ operators entering the definition of GPDs, see Eq. (5). In the leading order of $1/N_c$ we have:

$$\begin{aligned} & \frac{1}{2\pi} \int dy^- e^{ix\bar{P}^+ y^-} \langle \text{sol } P' | \bar{\psi}_{f'}(-y/2) \gamma^+ \psi_f(y/2) | \text{sol } P \rangle \Big|_{y^+=y_\perp=0} \\ &= H_0(x, \xi, t) \delta_{ff'} - i \frac{H_1(x, \xi, t)}{m_N} \frac{1}{2} \text{Tr}(R^\dagger M^{(ff')} R \tau_j) \cdot \varepsilon_{3jk} \Delta_k, \end{aligned} \quad (107)$$

where R is $SU(2)$ matrix which defines the orientation of the soliton in the spin-flavor space, $M^{(ff')}$ is the matrix, of which all elements are zero except the element in row f and column f' which is unity. Furthermore in Eq. 107, $H_{0,1}(x, \xi, t)$ are the universal GPDs of the soliton. Analogously we can write for the quark helicity dependent GPDs of the soliton:

$$\begin{aligned} & \frac{1}{2\pi} \int dy^- e^{ix\bar{P}^+ y^-} \langle \text{sol } P' | \bar{\psi}_{f'}(-y/2) \gamma^+ \gamma_5 \psi_f(y/2) | \text{sol } P \rangle \Big|_{y^+=y_\perp=0} \\ &= \left[\tilde{H}_0(x, \xi, t) \delta^{i3} - \tilde{E}_1(x, \xi, t) \frac{\Delta^3 \Delta^i}{m_N^2} \right] \frac{1}{2} \text{Tr}(R^\dagger M^{(ff')} R \tau_i). \end{aligned} \quad (108)$$

Now to get the GPDs for a baryon with particular quantum numbers (or for transition GPDs) we have to sandwich equations (107,108) between rotational states (104) of the soliton which corresponds to baryons from the octet and/or decuplet, i.e.

$$\langle S' = T', S'_3, T'_3 | \dots | S = T, S_3, T_3 \rangle = \int dR \phi_{S'_3 T'_3}^{* S' = T'}(R) \dots \phi_{S_3 T_3}^{S = T}(R). \quad (109)$$

We note here that in the derivation of Eqs. (107,108) we used that in the large N_c limit the baryon masses rise linearly with N_c , with mass splitting $m_\Delta - m_N \sim 1/N_c$. Therefore in the first approximation we can neglect nucleon- Δ mass difference and consider them as nonrelativistic particles if $-t \ll m_N^2$. It is useful to work in the Breit frame, where:

$$\begin{aligned} \vec{p}' &= -\vec{p} = \vec{\Delta}/2 \sim N_c^0, \\ \bar{P}^\mu &= \frac{1}{2}(P'^0 + P^0, 0, 0, 0) \approx (m_N, 0, 0, 0) \sim (N_c, 0, 0, 0), \end{aligned} \quad (110)$$

we introduce a light-like vector n which is normalized by $n \cdot \bar{P} = 1$. In the large N_c limit, we can choose it in the form

$$n^\mu = \frac{1}{m_N}(1, 0, 0, -1) \sim \frac{1}{N_c}(1, 0, 0, -1), \quad (111)$$

which leads to

$$t \sim N_c^0 \quad \text{and} \quad \xi = -\frac{1}{2}(n \cdot \Delta) \approx \frac{\Delta^3}{2m_N} \sim 1/N_c. \quad (112)$$

These relations fix the large N_c counting rules for baryon masses and kinematical variables in the problem.

Let us first apply the expressions for GPDs of the soliton (107,108) to the case of $N \rightarrow N$ GPDs. The projection of the *rhs* of Eqs. (107,108) onto particular nucleon states can be done with help of the standard integral:

$$\int dR \phi_{S'_3 T'_3}^{* S'=T'}(R) \phi_{S_3 T_3}^{S=T}(R) \frac{1}{2} \text{Tr} (R^\dagger \tau^a R \tau^b) = \frac{\sqrt{2S+1}}{\sqrt{2S'+1}} C_{T-T_3;1a}^{T'-T'_3} C_{SS_3;1b}^{S'S'_3}, \quad (113)$$

where $C_{j_1 m_2; j_2 m_2}^{jm}$ is the Clebsch-Gordan coefficient. Performing the projection we observe that in the leading order of the $1/N_c$ expansion only the following flavor combinations of nucleon GPDs are nonzero:

$$H^u(x, \xi, t) + H^d(x, \xi, t), \quad \tilde{H}^u(x, \xi, t) - \tilde{H}^d(x, \xi, t), \quad (114)$$

and

$$E^u(x, \xi, t) - E^d(x, \xi, t), \quad \tilde{E}^u(x, \xi, t) - \tilde{E}^d(x, \xi, t). \quad (115)$$

Complementary combinations are zero in the leading order of the $1/N_c$ expansion. Further, taking into account the N_c counting rules for kinematical variables and for the nucleon form factors (see e.g. Ref. [Das95, Mano98]) we obtain the following counting rules for the nucleon GPDs:

$$\left. \begin{aligned} H^u(x, \xi, t) + H^d(x, \xi, t) \\ \tilde{H}^u(x, \xi, t) - \tilde{H}^d(x, \xi, t) \end{aligned} \right\} \sim N_c^2 f(N_c x, N_c \xi, t),$$

$$\left. \begin{aligned} H^u(x, \xi, t) - H^d(x, \xi, t) \\ \tilde{H}^u(x, \xi, t) + \tilde{H}^d(x, \xi, t) \end{aligned} \right\} \sim N_c f(N_c x, N_c \xi, t), \quad (116)$$

and

$$\begin{aligned} E^u(x, \xi, t) - E^d(x, \xi, t) &\sim N_c^3 f(N_c x, N_c \xi, t), \\ \tilde{E}^u(x, \xi, t) - \tilde{E}^d(x, \xi, t) &\sim N_c^4 f(N_c x, N_c \xi, t), \\ E^u(x, \xi, t) + E^d(x, \xi, t) &\sim N_c^2 f(N_c x, N_c \xi, t), \\ \tilde{E}^u(x, \xi, t) + \tilde{E}^d(x, \xi, t) &\sim N_c^3 f(N_c x, N_c \xi, t). \end{aligned} \quad (117)$$

In the above equations $f(x_1, x_2, t)$ is a generic function stable in the large N_c limit. Also note that for the “truly non-forward” functions E, \tilde{E} the overall powers of N_c are higher than for the GPDs H, \tilde{H} because of the kinematical factor $1/m_N \sim 1/N_c$ and $\xi/m_N \sim 1/N_c^2$ in the definition of the GPDs E and \tilde{E} respectively (see Eq. (5)).

Taking the forward limit $\xi \rightarrow 0, t \rightarrow 0$ of the large- N_c counting rules (116) we reproduce the corresponding counting rules for polarized and unpolarized nucleon parton distributions derived in Refs. [Dia96, Dia97].

Let us analyse the large N_c behaviour of particular contributions to GPDs. We start with the D-term contribution, see Sec. 2.2. The large- N_c counting for the D-term can be extracted from either (116) or from (117), because the D-term contributes to both functions H and E in the same way (up to the sign). For the isosinglet component of the D-term we obtain:

$$D^u(z) + D^d(z) \sim N_c^2 f(z). \quad (118)$$

When we turn to the isovector D-term we see that the counting rules for $H^u - H^d$ and $E^u - E^d$ are different the latter being the dominant one in the large N_c limit. It implies that for the counting of the large N_c behaviour of the isovector D-term $D^u(z) - D^d(z)$ one has to use Eq. (116). One obtains:

$$D^u(z) - D^d(z) \sim N_c f(z). \quad (119)$$

Comparing Eqs. (118) and (119), one sees that the isovector D-term is suppressed relative to the isoscalar one in the large N_c limit.

Next let us check that the pion pole contribution of Eq. (42) to $\tilde{E}^u - \tilde{E}^d$ corresponds to the general counting rule (117). Indeed, taking into account that $g_A \sim N_c$ and $m_N \sim N_c$ we easily reproduce (117) from Eq. (42).

In section 3.2 we shall discuss the results obtained in the chiral quark-soliton model for the “large” GPDs (114,115). Before doing this we derive the large N_c relations between $N \rightarrow N$ and $N \rightarrow \Delta$ GPDs introduced in Sec. 2.7.

3.1.1 GPDs for octet to decuplet transition in the large N_c limit

In order to derive the large N_c relations between the $N \rightarrow \Delta$ GPDs and usual ones we shall use the fact that in the large N_c limit the nucleon and Δ states are simply different rotational excitations of the same classical object – soliton [Fra98a].

To obtain the relations we sandwich Eqs. (107,108) between rotational states of the soliton which corresponds to baryons from octet and decuplet. Doing this we obtain the expressions for $N \rightarrow N$ and $N \rightarrow \Delta$ GPDs in terms of the universal functions $H_{0,1}$ and $\tilde{H}_{0,1}$, *i.e.* the GPDs of the soliton introduced by Eqs. (107,108). Since both $N \rightarrow N$ and $N \rightarrow \Delta$ GPDs are expressed in terms of the *same* GPDs of a soliton $H_{0,1}$ and $\tilde{H}_{0,1}$ we obtain the following relations [The $N \rightarrow \Delta$ GPDs are defined by Eqs. (84,90)]:

$$\begin{aligned} H_M(x, \xi, t) &= \frac{2}{\sqrt{3}} [E^u(x, \xi, t) - E^d(x, \xi, t)] , \\ C_1(x, \xi, t) &= \sqrt{3} [\tilde{H}^u(x, \xi, t) - \tilde{H}^d(x, \xi, t)] , \\ C_2(x, \xi, t) &= \frac{\sqrt{3}}{4} [\tilde{E}^u(x, \xi, t) - \tilde{E}^d(x, \xi, t)] . \end{aligned} \quad (120)$$

All other $N \rightarrow \Delta$ GPDs are zero at leading order of $1/N_c$ expansion. The properties of these relations were discussed in Sec. 2.7.

3.2 GPDs in the chiral-quark soliton model

Model calculations of the nucleon GPDs are important firstly to understand how non-perturbative mechanisms generate various structures in GPDs. In this respect the chiral models should be very useful because as we saw in Sec. 2.4 the spontaneously broken chiral symmetry plays a prominent role in the physics of GPDs. Secondly, model calculations allow us to develop an intuition about the structure of the GPDs which is important for the construction of phenomenological parameterizations for GPDs.

Model calculations of nucleon GPDs were first performed in Ref. [Ji97a] where GPDs were computed in the MIT bag model. Unfortunately in the bag model the chiral symmetry is not respected and also the non field theoretic nature of this model leads to problems with positivity of antiquark distributions. Calculations of the nucleon GPDs in the chiral quark-soliton model [Dia88] do not show these deficiencies and have been performed in Refs. [Pet98, Pen00a]. The chiral quark-soliton model is field theoretic model of the nucleon which stresses the dominant role of spontaneous chiral symmetry breaking in the dynamics of the nucleon bound state. The review of foundations of this model and its applications to calculations of the parton distributions can be found in [Dia98, Dia00]. The review of applications to calculations of nucleon form factors and many static observables can be found in Refs. [Chr96, Alk96]. We refer the reader to above reviews for details. Here we remind only some basics of this model.

The chiral quark-soliton model is essentially based on the $1/N_c$ expansion. Although in reality the number of colors $N_c = 3$, the academic limit of large N_c is known to be a useful guideline. At large N_c the nucleon is heavy and can be viewed as a classical soliton of the pion field [Wit79, Adk83]. In the previous section we derived from this large- N_c semiclassical picture of the nucleon general large N_c counting rules for various nucleon GPDs (see Eqs. (116,117)) and relations between $N \rightarrow N$ and $N \rightarrow \Delta$ GPDs (see Eq. (120)). In order to compute the nucleon GPDs we have to specify the dynamics of the low energy QCD. Here we work with the effective chiral action given by the functional integral over quarks in the background pion field [Dia83, Dia86]:

$$\exp(iS_{\text{eff}}[\pi(x)]) = \int D\psi D\bar{\psi} \exp\left(i \int d^4x \bar{\psi}(i\not{\partial} - MU^{\gamma_5})\psi\right),$$

$$U = \exp[i\pi^a(x)\tau^a], \quad U^{\gamma_5} = \exp[i\pi^a(x)\tau^a\gamma_5] = \frac{1+\gamma_5}{2}U + \frac{1-\gamma_5}{2}U^\dagger. \quad (121)$$

Here ψ is the quark field, M the effective quark mass, which is due to the spontaneous breakdown of chiral symmetry (generally speaking, it is momentum dependent), and U is the $SU(2)$ chiral pion field. The effective chiral action given by Eq. (121) is known to contain automatically the Wess–Zumino term and the four-derivative Gasser–Leutwyler terms, with correct coefficients. Equation (121) has been derived from the instanton model of the QCD vacuum [Dia86], which provides a natural mechanism of chiral symmetry breaking and enables one to express the dynamical mass M and the ultraviolet cutoff intrinsic in (121) through the Λ_{QCD} parameter. The ultraviolet regularization of the effective theory is provided by the specific momentum dependence of the mass, $M(p^2)$, which drops to zero for momenta of order of the inverse instanton size in the instanton vacuum, $1/\rho \sim 600$ MeV. We also note the the inverse instanton size sets the renormalization scale for computed parton distributions at $\mu = 0.6$ GeV.

An immediate application of the effective chiral theory (121) is the chiral quark-soliton model of baryons of Ref. [Dia88]. According to this model nucleons can be viewed as N_c “valence” quarks bound by a self-consistent pion field (the “soliton”) whose energy coincides with the aggregate energy of the quarks of the negative-energy Dirac continuum. Similarly to the Skyrme model the large N_c limit is needed as a parameter to justify the use of the mean-field approximation; however, the $1/N_c$ -corrections can be — and, in some cases, have been — computed [Chr96].

Let us remind the reader how the nucleon is described in the effective low-energy theory Eq. (121). Integrating out the quarks in (121) one finds the effective chiral action,

$$S_{\text{eff}}[\pi^a(x)] = -N_c \text{Sp} \log D(U), \quad D(U) = i\partial_0 - H(U), \quad (122)$$

where $H(U)$ is the one-particle Dirac hamiltonian,

$$H(U) = -i\gamma^0 \gamma^k \partial_k + M\gamma^0 U^{\gamma_5}, \quad (123)$$

and $\text{Sp} \dots$ denotes the functional trace. For a given time-independent pion field $U = \exp(i\pi^a(\mathbf{x})\tau^a)$ one can determine the spectrum of the Dirac hamiltonian,

$$H\Phi_n = E_n\Phi_n. \quad (124)$$

It contains the upper and lower Dirac continua (distorted by the presence of the external pion field), and, in principle, also discrete bound-state level(s), if the pion field is strong enough. If the pion field has unity winding number, there is exactly one bound-state level which travels all the way from the upper to the lower Dirac continuum as one increases the spatial size of the pion field from zero to infinity [Dia88]. We denote the energy of the discrete level as E_{lev} , $-M \leq E_{\text{lev}} \leq M$. One has to occupy this level to get a non-zero baryon number state. Since the pion field is color blind, one can put N_c quarks on that level in the antisymmetric state in color.

The limit of large N_c allows us to use the mean-field approximation to find the nucleon mass. To get the nucleon mass one has to add $N_c E_{\text{lev}}$ and the energy of the pion field. Since the effective chiral lagrangian is given by the determinant (122) the energy of the pion field coincides exactly with the aggregate energy of the lower Dirac continuum, the free continuum subtracted. The self-consistent pion field is thus found from the minimization of the functional [Dia88]

$$m_N = \min_U N_c \left\{ E_{\text{lev}}[U] + \sum_{E_n < 0} (E_n[U] - E_n^{(0)}) \right\}. \quad (125)$$

From symmetry considerations one looks for the minimum in a hedgehog ansatz:

$$U_c(\mathbf{x}) = \exp[i\pi^a(\mathbf{x})\tau^a] = \exp[in^a \tau^a P(r)], \quad r = |\mathbf{x}|, \quad \mathbf{n} = \frac{\mathbf{x}}{r}, \quad (126)$$

where $P(r)$ is called the profile of the soliton.

The minimum of the energy (125) is degenerate with respect to translations of the soliton in space and to rotations of the soliton field in ordinary and isospin space. For the hedgehog field (126) the two rotations are equivalent. The projection on a nucleon state with given spin (S_3) and isospin (T_3) components is obtained by integrating over all spin-isospin rotations, R , see Eq. (109). Analogously, the projection on a nucleon state with given momentum \mathbf{P} is obtained by integrating over all shifts, \mathbf{X} , of the soliton,

$$\langle \mathbf{P}' | \dots | \mathbf{P} \rangle = \int d^3\mathbf{X} e^{i(\mathbf{P}' - \mathbf{P}) \cdot \mathbf{X}} \dots \quad (127)$$

Recently it was shown that the chiral quark-soliton model of the nucleon provides a framework for a successful calculation not only of nucleon form factors [Chr96] but also

of the nucleon parton distributions, both unpolarized and polarized, at a low normalization point [Dia96, Dia97, Pob96, Wei97, Gam98, Wak98, Wak99, Pob99]. Because both cases are limiting cases of the GPDs, the chiral quark-soliton model is a promising tool to calculate them. Since the chiral quark-soliton model is a quantum field-theoretical description of the nucleon, with explicit quark degrees of freedom, it allows an unambiguous identification of the quark as well as antiquark distributions in the nucleon. We were able to demonstrate that all general properties of the quark and antiquark distributions (positivity, sum rules, Soffer inequalities [Pob96, Pob00], *etc.*).

All GPDs can be expressed in terms of a matrix element of a non-local quark bilinear operator in the nucleon states with definite 4-momenta P, P' and spin and isospin components, see general large N_c expression Eq. (103). Since in the chiral quark-soliton model the dynamics of the mean-field is specified, one can write the explicit expression for correlator of the type of Eq. (103). [We write explicitly all the flavor ($f, g = 1, 2$) and the Dirac ($i, j = 1, \dots, 4$) indices for clarity]:

$$\begin{aligned} & \langle \mathbf{P}', S'_3, T'_3 | \bar{\psi}_{fi}(x^0, \mathbf{x}) \psi^{gj}(y^0, \mathbf{y}) | \mathbf{P}, S_3, T_3 \rangle = \\ & 2m_N N_c \int d^3 \mathbf{X} e^{i(\mathbf{P}' - \mathbf{P}) \cdot \mathbf{X}} \int dR \phi_{S'_3 T'_3}^\dagger(R) \phi_{S_3 T_3}(R) \\ & \times \left[R_{g'}^g \sum_{\text{occup.}} \exp[iE_n(x^0 - y^0)] \Phi_{n, f'i}^\dagger(\mathbf{x} - \mathbf{X}) \Phi_n^{g'j}(\mathbf{y} - \mathbf{X}) (R^\dagger)_f^{f'} \right]. \end{aligned} \quad (128)$$

The functions Φ_n are eigenstates of energy E_n of the Dirac hamiltonian (123) in the external (self-consistent) pion field U_c , they can be found numerically by diagonalization of the hamiltonian. In this way we compute the function F in general large- N_c Eq. (103).

3.2.1 Results for H and E

Having the expression (128) for nucleon matrix elements of quark bilocal operators in the chiral quark-soliton model we can now express various nucleon GPDs as the sum over occupied quark orbitals in the external pion field U_c . We start with GPDs H and E . One immediately observes that, in accordance with general large- N_c counting rules (116–117), in the leading N_c order only the flavor singlet part of $H(x, \xi, t)$ and the flavor-nonsinglet part of $E(x, \xi, t)$ are non-zero. They are given, respectively, by

$$\begin{aligned} \sum_q H^q(x, \xi, \Delta^2) &= \frac{N_c m_N}{2\pi} \int dz^0 \int d^3 \mathbf{X} \exp[i\Delta \cdot \mathbf{X}] \\ &\times \sum_{\text{occup.}} \exp\{iz^0[(x + \xi)m_N - E_n]\} \Phi_n^\dagger(\mathbf{X}) (1 + \gamma^0 \gamma^3) \Phi_n(\mathbf{X} - z^0 \mathbf{e}_3), \end{aligned} \quad (129)$$

$$\begin{aligned} E^u(x, \xi, t) - E^d(x, \xi, t) &= -\frac{iN_c m_N^2}{3\pi} \int dz^0 \int d^3 \mathbf{X} \exp[i\Delta \cdot \mathbf{X}] \frac{\epsilon^{3jk} \Delta^j}{\Delta^2} \\ &\times \sum_{\text{occup.}} \exp\{iz^0[(x + \xi)m_N - E_n]\} \Phi_n^\dagger(\mathbf{X}) \tau^k (1 + \gamma^0 \gamma^3) \Phi_n(\mathbf{X} - z^0 \mathbf{e}_3). \end{aligned} \quad (130)$$

The isovector part of $H(x, \xi, \Delta^2)$ and the isosinglet part of $E(x, \xi, \Delta^2)$ appear only in the next-to-leading order of the $1/N_c$ -expansion, *i.e.*, after taking into account the finite angular velocity of the soliton rotation.

First we would like to demonstrate that the two limiting cases of the GPDs — usual parton distributions and elastic form factors — are correctly reproduced within the chiral quark-soliton model. Taking in Eq.(129) the forward limit, $\Delta \rightarrow 0$, one recovers the formula for the usual singlet (anti-) quark distributions in the chiral quark-soliton model which was obtained in Ref. [Dia96]. Thus the forward limit, Eq. (6), is reproduced. On the other hand, integrating Eqs. (129,130) over $-1 \leq x \leq 1$ one obtains (up to corrections parametrically small in $1/N_c$) the expressions for the electromagnetic formfactors of the nucleon derived in Ref. [Dia88]:

$$\int_{-1}^1 dx \sum_q H^q(x, \xi, t) = N_c \int d^3\mathbf{X} \exp[i\mathbf{\Delta} \cdot \mathbf{X}] \sum_{\text{occup.}} \Phi_n^\dagger(\mathbf{X}) \Phi_n(\mathbf{X}) = F_1^{(T=0)}(t), \quad (131)$$

$$\begin{aligned} \int_{-1}^1 dx [E^u(x, \xi, t) - E^d(x, \xi, t)] &= \frac{iN_cm_N}{\Delta^2} \varepsilon_{3ki} \Delta^i \int d^3\mathbf{X} \exp[i\mathbf{\Delta} \cdot \mathbf{X}] \\ &\times \sum_{\text{occup.}} \Phi_n^\dagger(\mathbf{X}) \gamma^0 \gamma^3 \tau^k \Phi_n(\mathbf{X}) = F_2^{(T=1)}(t). \end{aligned} \quad (132)$$

The electromagnetic formfactors computed in the chiral quark soliton model on the basis of these formulae compare rather well with the experimentally measured ones up to momenta of order $-t \sim 1 \text{ GeV}^2$ [Chr96]. One can also check that [Pet98, Pen00a] the GPDs given by Eqs.(129,130) satisfy the polynomiality condition (14).

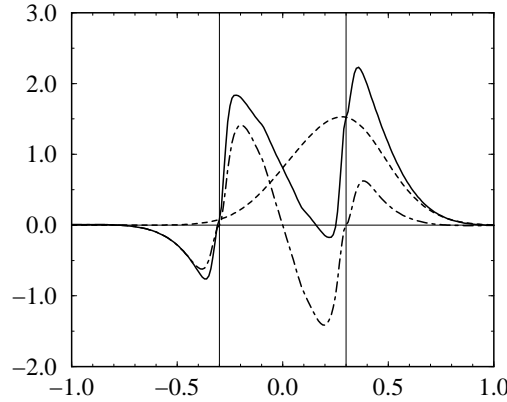


Figure 4: The GPD $H^u(x, \xi, t) + H^d(x, \xi, t)$ as a function of x at $\xi = 0.3$ and $t = t_{\min} = -0.35 \text{ GeV}^2$. Dashed curve: contribution from valence level. Dashed-dotted curve: contribution of the Dirac continuum. Solid curve: the total distribution (sum of the dashed and dashed-dotted curves). The vertical lines mark the crossover points $x = \pm\xi$.

Eqs. (129,130) express the GPDs as a sum over quark single-particle levels in the soliton field. This sum runs over *all* occupied levels, including both the discrete bound-state level and the negative polarized Dirac continuum. We remind the reader that in the case of usual parton distributions it was demonstrated that in order to ensure the positivity of the

antiquark distributions it is essential to take into account the contributions of *all* occupied levels of the Dirac Hamiltonian [Dia96]. The so-called “valence level approximation” advocated in Refs. [Wei97, Gam98] for structure functions in the chiral quark-soliton model leads to unacceptable *negative* antiquark distributions. We shall see below that also in the off-forward case the contribution of the Dirac continuum drastically changes the shape of the distribution function, leading to characteristic crossovers of $H(x, \xi, \Delta)$ at $|x| = \xi$, in addition this contribution generates the large and negative D-term.

Now we present results for calculations of the contributions of the discrete bound-state level and the negative Dirac continuum to Eqs. (129,130). Technical details and methods of calculations can be found in Refs. [Pet98, Pen00a].

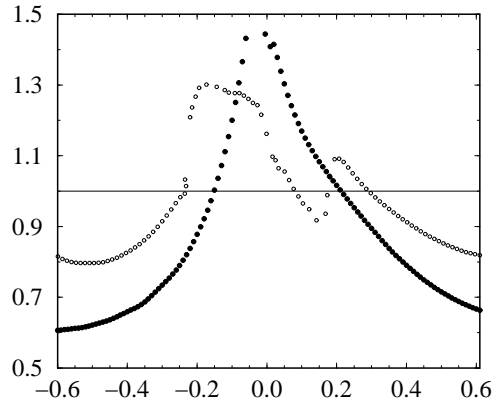


Figure 5: Ratio Eq. (134) as a function of x showing the deviation from the factorization ansatz for the t -dependence of the GPD H for the values of $\xi = 0$ (filled circles) and $\xi = 0.2$ (open circles) with $t_0 = -4m_N^2\xi^2/(1 - \xi^2)$ and $t_1 = t_0 - 0.5 \text{ GeV}^2$.

In Fig. 4 a typical shape of the GPD $H^u(x, \xi, t) + H^d(x, \xi, t)$ as a function of the variable x is shown at $\xi = 0.3$ and $t = t_{\min}$, with

$$t_{\min} = -4m_N^2\xi^2/(1 - \xi^2).$$

For $\xi = 0.3$ one has $t_{\min} = -0.35 \text{ GeV}^2$. On this figure we show separately the contributions of the valence level and of the Dirac continuum as well as their sum. We see that the Dirac continuum contribution is essential especially in the region $-\xi \leq x \leq \xi$, also in the region $x \leq -\xi$, corresponding to minus antiquark distributions, the Dirac continuum contribution ensures the positivity of antiquarks. We also computed several Mellin moments at various values of ξ and t (in the model calculations the values of ξ is limited by $\xi^2 \leq -t/(4m_N^2 - t)$) and with the help of Eq. (21) we determined the value of the first few coefficients in a Gegenbauer expansion of the D-term (23). The result extrapolated to the value of $t = 0$ is:

$$\sum_{q=u,d,s,\dots} D^q(z) = (1 - z^2) \left[-4.0 C_1^{3/2}(z) - 1.2 C_3^{3/2}(z) - 0.4 C_5^{3/2}(z) + \dots \right]. \quad (133)$$

We shall use this result for the D-term in Sec. 4 for estimates of various observables.

Calculations of GPDs in the chiral quark-soliton model give a possibility to study their t -dependence. In modeling the t -dependence of GPDs usually the factorization ansatz: $H(x, \xi, t) = H(x, \xi)F_1(t)$ is adopted. In order to illustrate numerically the non-

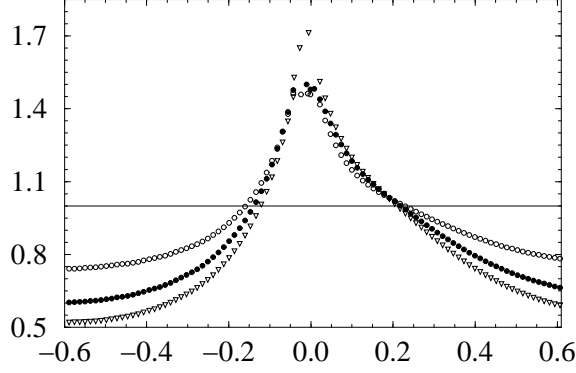


Figure 6: Ratio Eq. (134) as a function of x for a fixed value of $\xi = 0$ and for $t_0 = 0$ and for $t_1 = -0.25$ (open circles), -0.5 (filled circles), -0.75 (triangles) GeV^2 .

factorability of the t -dependence of $H(x, \xi, t)$ we show in Fig. 5 the following ratio :

$$R = \frac{H(x, \xi, t_0)}{H(x, \xi, t_1)} \frac{\int_{-1}^1 dx H(x, \xi, t_1)}{\int_{-1}^1 dx H(x, \xi, t_0)}, \quad (134)$$

$[H = H^u + H^d]$ as a function of x taking $t_0 = t_{\min}$ and $t_1 = t_{\min} - 0.5 \text{ GeV}^2$, and $\xi = 0$ (filled circles), $\xi = 0.2$ (open circles). If the t -dependence of the GPDs factors out then $R = 1$ independently of t_0, t_1 and x, ξ . From Fig. 5 we see that the ratio (134) can deviate considerably from unity and it depends in a non-trivial way on both variables x and ξ .

To illustrate the dependence of the ratio (134) on the value of t_1 we plot in Fig 6 this ratio as the function of x with $\xi = 0$ and $t_0 = 0$ for several values of $t_1 = -0.25, 0.5, 0.75 \text{ GeV}^2$. The results of the chiral quark-soliton model on the t -dependence of GPDs shown in Fig. 5 and Fig. 6 illustrate that the assumption of factorization of the t -dependence for GPDs should be taken with caution and that more work on t -dependence of phenomenological parametrizations of GPDs should be done.

It is interesting to note that the features of the t -dependence of GPDs shown on Fig. 6 can be qualitatively reproduced by the following ansatz for $H^q(x, \xi = 0, t)$:

$$H^q(x, \xi = 0, t) = \frac{1}{x^{\alpha' t}} q(x), \quad (135)$$

where α' can be interpreted as the slope of a Regge trajectory. This Regge theory motivated ansatz reproduces all qualitative feature of Fig. 6 obtained in the chiral quark-soliton model. As a curiosity we note that a rough fit of the curves on Fig. 6 by the ansatz (135) gives $\alpha' \approx 0.8 \text{ GeV}^{-2}$, amazingly close to the slopes of meson Regge trajectories.

Let us now discuss results for the GPD $E^u - E^d$. In Fig. 7 we plot the GPD $E^u(x, \xi, t) - E^d(x, \xi, t)$ at $\xi = 0.3$ and $t = t_{\min}$. We see that in this case the Dirac continuum contribution is also essential and it generates a symmetric sea contribution to the GPD $E^u - E^d$. Computing several Mellin moments of the function $E^u(x, \xi, t) - E^d(x, \xi, t)$ we are able to extract the value of the isovector D-term $D^u(z) - D^d(z)$. The leading- N_c result for this flavor combination is zero, i.e.

$$D^u(z) - D^d(z) = 0.$$

This is in accordance with general large N_c counting rules for the D-term (119). Therefore we conclude that the D-term is independent of quark flavor.

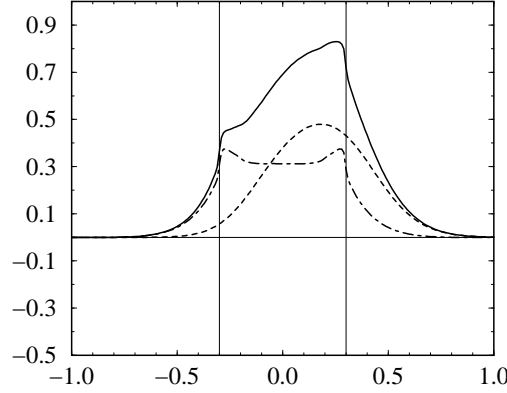


Figure 7: The GPD $E^u(x, \xi, t) - E^d(x, \xi, t)$ as a function of x at $\xi = 0.3$ and $t = t_{\min} = 0.35 \text{ GeV}^2$. Dashed curve: contribution from valence level. Dashed-dotted curve: contribution of the Dirac continuum. Solid curve: the total distribution (sum of the dashed and dashed-dotted curves). The vertical lines mark the crossover points $x = \pm\xi$.

For the construction of the phenomenological model for the GPD E^q we shall need the forward limit of this functions which we denote as $e^q(x)$:

$$e^q(x) = \lim_{\Delta \rightarrow 0} E^q(x, \xi, t). \quad (136)$$

In Fig. 8 we present the result of the model calculation of $e^u(x) - e^d(x)$. We see that it consists of the valence contribution and of the sea part peaked around $x = 0$. With help of sum rules for the function $e^u(x) - e^d(x)$:

$$\begin{aligned} \int_{-1}^1 dx [e^u(x) - e^d(x)] &= \kappa^p - \kappa^n, \\ \int_{-1}^1 dx x [e^u(x) - e^d(x)] &= 2[J^u - J^d] - M_2^u + M_2^d \end{aligned} \quad (137)$$

where κ^N is an anomalous magnetic moment of a nucleon $N = p, n$ and J^q and M_2^q are the parts of angular and of total momentum carried by a quark, we obtain in the model:

$$\kappa^p - \kappa^n = 1.0_{val} + 2.22_{sea} = 3.22 \text{ vs. } 3.7 \text{ (exp.)},$$

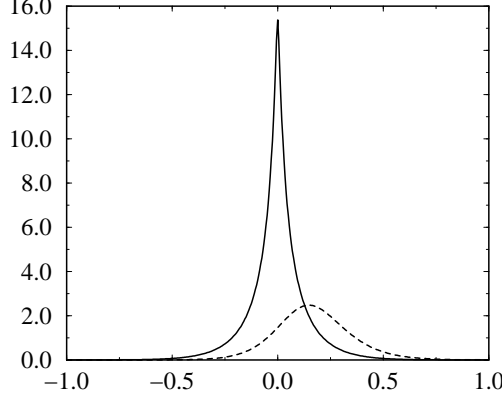


Figure 8: The GPD $E^u(x, \xi = 0, t = 0) - E^d(x, \xi = 0, t = 0) = e^u(x) - e^d(x)$ as a function of x . Dashed curve: contribution from valence level. Solid curve: contribution of the Dirac continuum.

$$2[J^u - J^d] - M_2^u + M_2^d = 0.18_{val} + 0_{sea} = 0.18. \quad (138)$$

Here we show also the individual contributions from the valence and sea parts. We see that the value of the anomalous magnetic moment is dominated by the sea contribution and its value is close to the experimental number. The model prediction for $2J^{u-d} - 2M_2^{u-d}$ is dominated by the valence contribution.

Since the combination $J^u - J^d$ of angular momenta is dominated by the valence part of the function $e^u(x) - e^d(x)$ ¹⁷ it is instructive to compare the shapes of the valence contributions to $e^q(x)$ and to $q(x)$ with each other. The corresponding comparison is shown in Fig. 9 where we plot

$$\frac{e_{val}^u(x) - e_{val}^d(x)}{\int_{-1}^1 dx (e_{val}^u(x) - e_{val}^d(x))} \quad \text{versus} \quad \frac{q_{val}^u(x) + q_{val}^d(x)}{\int_{-1}^1 dx (q_{val}^u(x) + q_{val}^d(x))},$$

computed in the chiral quark-soliton model. We see that the shapes of both these valence distributions in the model are very close. This observation will motivate us in Sec. 4.2.3 for the ansatz:

$$e_{val}^q(x) = A^q q_{val}(x), \quad (139)$$

where A^q is a x -independent constant.

The qualitative features of the GPDs H and E obtained in the chiral quark-soliton model will be used in Sec. 4.2 for the construction of phenomenological parametrization of these distributions.

3.2.2 Results for \tilde{H} and \tilde{E}

Now we turn to the results for the quark helicity dependent GPDs \tilde{H} and \tilde{E} . Expressions for these distributions in terms of a summation over occupied quark orbitals in the external pion mean field can be found in Ref. [Pen00a]. Here we discuss only the main results.

¹⁷As shown in Ref. [Pob99] the $M_2^u - M_2^d$ is also dominated by valence level contributions.

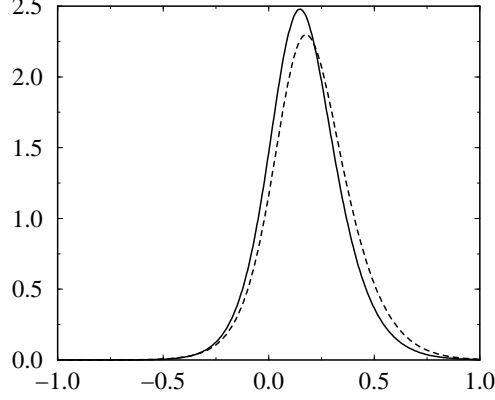


Figure 9: Comparison of shapes of the valence level contributions to $u(x) + d(x)$ (solid curve) and to $e^u(x) - e^d(x)$ (dashed curve). Both contributions are normalized to unity.

According to the general large N_c counting rules derived in Sec. 3.1 at the leading order only isovector combinations of GPDs $\tilde{H}^u - \tilde{H}^d$ and $\tilde{E}^u - \tilde{E}^d$ are non-zero. This general counting is fulfilled in the chiral quark-soliton model.

Before presenting the numerical results for the GPDs \tilde{H} and \tilde{E} let us discuss specific contribution to these GPDs originating from the long range pion tail of the pion mean-field. The behaviour of the mean pion field at large distances is governed by linearized equations of motion and PCAC:

$$\lim_{|\vec{x}| \rightarrow \infty} U(x) = 1 + \frac{3g_A}{8\pi f_\pi^2 |\vec{x}|^2} \left(1 + m_\pi |\vec{x}|\right) \frac{ix^a \tau^a}{|\vec{x}|} \exp(-m_\pi |\vec{x}|), \quad (140)$$

where $g_A \approx 1.267$ is the axial charge of the nucleon, $f_\pi \approx 92.4$ MeV is the pion decay constant. Contribution of this long-range tail to \tilde{E} can be computed analytically (see details in Ref. [Pen00a]) with the result:

$$\begin{aligned} \tilde{E}_\pi^{u-d}(x, \xi, t) &= \frac{m_N F(t)}{f_\pi^2} \int \frac{d^4 p}{(2\pi)^4} \delta \left[(x - \xi) m_N - p^0 + p^3 \right] \\ &\times \frac{M^{1/2} [(p + \Delta)^2]}{[(p + \Delta)^2 - M^2 + i0]} \frac{M^{3/2} [(p - \Delta)^2]}{[(p - \Delta)^2 - M^2 + i0]} + \left(\xi \rightarrow -\xi, \quad \Delta \rightarrow -\Delta \right). \end{aligned} \quad (141)$$

Here $M[p^2]$ is the momentum dependent constituent quark mass as obtained in the theory of the instanton vacuum [Dia86]. It provides the UV regularization of the effective theory (121). In the Eq. (141) we introduced the following form factor:

$$F(-\vec{k}^2) = \frac{4m_N^2 f_\pi^2}{3k^3} \int d^3 x \exp(i\vec{k} \cdot \vec{x}) \text{Tr} \left[(U(\vec{x}) - 1) \tau^3 \right]. \quad (142)$$

The small momentum asymptotic of this form factor can be obtained by substituting into Eq. (142) the long-range asymptotic of the mean-field (140). The result is:

$$\lim_{t \rightarrow m_\pi^2} F(t) = \frac{4g_A m_N^2}{m_\pi^2 - t}. \quad (143)$$

Now the crucial observation [Pen00a] is that the integral over p in Eq. (141) coincides *exactly* (up to trivial renaming of variable) with the expression for the light-cone pion distribution amplitude in the instanton model of the QCD vacuum [Pet99]. Therefore the expression (141) for the \tilde{E}_π at $t \rightarrow m_\pi^2$ can be written in the compact form:

$$\tilde{E}^{u-d}(x, \xi, t) = \frac{4g_A m_N^2}{m_\pi^2 - t} \theta[\xi - |x|] \frac{1}{\xi} \Phi_\pi\left(\frac{x}{\xi}\right). \quad (144)$$

This is exactly the general result obtained in Sec. 2.4.2, see Eq. (42).

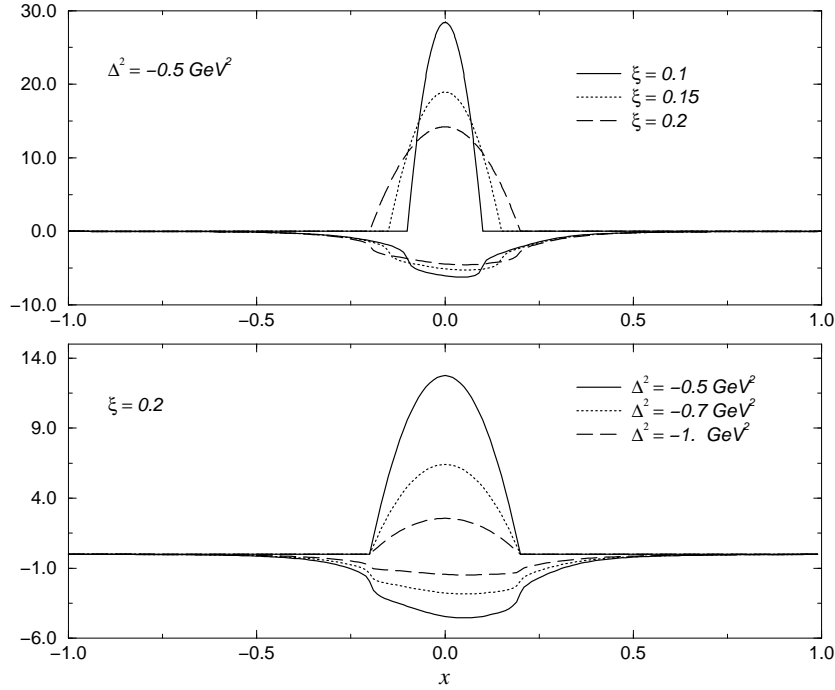


Figure 10: Comparison of pion pole contribution and non-pole part of the isovector GPD \tilde{E} at various values of t and ξ . The positive curves correspond to pion pole contributions.

In Ref. [Pen00a] the non-pole contributions to $\tilde{E}^u - \tilde{E}^d$ have been computed in the chiral quark-soliton model. The corresponding results are presented in Fig. 10. We see that for wide range of t and ξ the pion pole contribution dominates, the non-pole part being negative. The result of the chiral quark-soliton model for $\tilde{H}^u(x, \xi, t) - \tilde{H}^d(x, \xi, t)$ at $\xi = 0.3$ and $t = t_{\min}$ is presented in Fig. 11. We observe the sizeable contribution of the Dirac continuum.

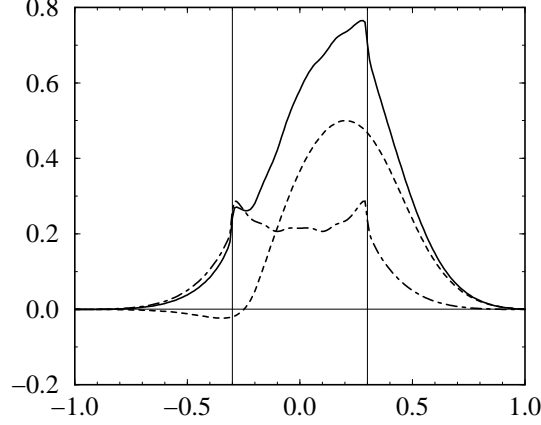


Figure 11: The GPD $\tilde{H}^u(x, \xi, t) - \tilde{H}^d(x, \xi, t)$ as a function of x at $\xi = 0.3$ and $t = t_{\min} = -0.35 \text{ GeV}^2$. Dashed curve: contribution from valence level. Dashed-dotted curve: contribution of the Dirac continuum. Solid curve: the total distribution (sum of the dashed and dashed-dotted curves). The vertical lines mark the crossover points $x = \pm \xi$.

To illustrate the non-factorizability of the t -dependence also for the GPD \tilde{H} we plot in Fig. 12 the ratio analogous to Eq. (134) with the same values of all parameters

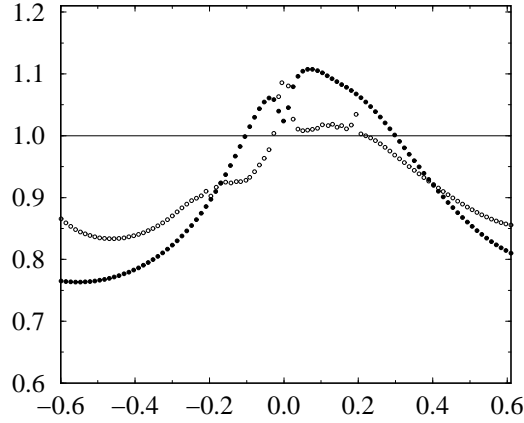


Figure 12: The same as Fig. 5 but for the GPD $\tilde{H}^u(x, \xi, t) - \tilde{H}^d(x, \xi, t)$.

replacing GPD $H^u(x, \xi, t) + H^d(x, \xi, t)$ by $\tilde{H}^u(x, \xi, t) - \tilde{H}^d(x, \xi, t)$. We observe again a noticeable deviation from the factorization ansatz for the t -dependence, though in this case the deviation is smaller.

With these lessons from chiral quark-soliton model calculations we next turn to a discussion of the phenomenological applications of the GPDs to various hard exclusive reactions.

4 GPDs FROM HARD ELECTROPRODUCTION REACTIONS

4.1 Introduction

In this section, we show how one can access the GPDs through the measurement of hard exclusive reactions. As discussed in Sec. 2.1, in leading twist there are four GPDs for the nucleon, i.e. H , E , \tilde{H} and \tilde{E} , which are defined for each quark flavor (u , d , s). These GPDs depend upon the different longitudinal momentum fractions $x + \xi$ ($x - \xi$) of the initial (final) quark and upon the overall momentum transfer t to the nucleon. Therefore, these functions contain a wealth of new nucleon structure information.

In the following, it will be shown how the different GPDs enter in the observables for different hard exclusive processes. We will discuss in detail the deeply virtual Compton scattering (DVCS) process on the nucleon and hard electroproduction of vector and pseudoscalar mesons (HMP) on the nucleon. Besides the hard processes involving nucleon GPDs, it will also be discussed how the $N \rightarrow \Delta$ DVCS process and the hard electroproduction of $\pi\Delta$ final states depend upon GPDs for the $N \rightarrow \Delta$ transition, providing new information on the quark structure of the Δ resonance. Furthermore, it will be discussed how the electroproduction of kaon-hyperon (KY) final states contains GPDs for the $N \rightarrow Y$ transitions, yielding information on the quark structure of hyperons.

It is clear that to extract all those different GPDs from hard electroproduction reactions and to map out their dependencies on the three variables (x, ξ, t) is a quite challenging program. As a first step towards this goal, one strategy is to use phenomenological parametrizations for the GPDs which include all general constraints and which are flexible enough to allow for a fit to different hard electroproduction observables. The aim of this section is to present such phenomenological and physically motivated parametrizations of the GPDs and to test then their sensitivity on observables.

4.2 Phenomenological parametrization of GPDs

In the following, we discuss successively the parametrizations for the GPDs H^q , E^q , \tilde{H}^q and \tilde{E}^q for each quark flavor q ($= u, d, s$). As we address here mainly hard exclusive reactions in the valence region at relatively small values of $-t$ ($< 1 \text{ GeV}^2$), we start by parametrizing the GPDs at $t = 0$ and discuss firstly their x and ξ dependencies. For each GPD, we then come back to their t -dependence.

4.2.1 Parametrization of the GPD H^q

For the function H^q (for each flavor q), the t -independent part $H^q(x, \xi) \equiv H^q(x, \xi, t = 0)$ is parametrized by a two-component form :

$$H^q(x, \xi) = H_{DD}^q(x, \xi) + \theta(\xi - |x|) \frac{1}{N_f} D\left(\frac{x}{\xi}\right), \quad (145)$$

where H_{DD}^q is the part of the GPD which is obtained as a one-dimensional section of a two-variable double distribution (DD) F^q [Rad99], imposing a particular dependence on

the skewedness ξ , as given by Eq. (17)

$$H_{DD}^q(x, \xi) = \int_{-1}^1 d\beta \int_{-1+|\beta|}^{1-|\beta|} d\alpha \delta(x - \beta - \alpha\xi) F^q(\beta, \alpha) . \quad (146)$$

The D-term contribution D in Eq. (145) completes the parametrization of GPDs, restoring the correct polynomiality properties of GPDs [Ji98b, Pol99b] as discussed in Sec. 2.2. It has a support only for $|x| \leq |\xi|$, so that it is ‘invisible’ in the forward limit. Because the D-term is an isoscalar contribution, it adds the same function for each flavor. In Eq. (145), $N_f = 3$ is the number of active flavors (u, d, s).

For the double distributions, entering Eq. (146), we follow Radyushkin’s suggestion [Rad99] to use the following model

$$F^q(\beta, \alpha) = h(\beta, \alpha) q(\beta), \quad (147)$$

where $q(\beta)$ is the forward quark distribution (for the flavor q) and where $h(\beta, \alpha)$ denotes a profile function. In the following estimates, we parametrize the profile function through a one-parameter ansatz, following Refs. [Rad99, Rad01b] :

$$h(\beta, \alpha) = \frac{\Gamma(2b+2)}{2^{2b+1}\Gamma^2(b+1)} \frac{[(1-|\beta|)^2 - \alpha^2]^b}{(1-|\beta|)^{2b+1}} . \quad (148)$$

In Eq. (148), the parameter b characterizes the strength of the ξ dependence of the GPD $H(x, \xi)$. The limiting case $b \rightarrow \infty$ corresponds to the ξ independent ansatz for the GPD, i.e. $H(x, \xi) = q(x)$, as used in Refs. [Gui98, Vdh98]. The power b in Eq. (148) is a free parameter for the valence contribution (b_{val}) and for the sea/antiquark contribution (b_{sea}) to the GPD, which can be used in such an approach as fit parameters in the extraction of GPDs from hard electroproduction observables. As an example, the twist-2 DVCS predictions of Ref. [Vdh99] and the twist-3 DVCS predictions of Ref. [Kiv01b] correspond to the choice $b_{val} = b_{sea} = 1.0$. In the following, we discuss the dependence of DVCS observables on the shape of the profile function, i.e. on the choice of the parameters b_{val} and b_{sea} .

In Eq. (147), we use the phenomenological forward quark distributions $q(\beta)$ as measured from DIS as input, ensuring the correct forward limit for the GPDs, i.e. $H^u(x, 0) = u(x)$, $H^d(x, 0) = d(x)$, $H^s(x, 0) = s(x)$. Specifically, the calculations shown in the following were performed using the NLO quark distributions of [Mar98a] (more precisely, their so-called “central gluon parametrization”). We checked explicitly however that the results in the valence region practically do not change when using another current parametrization for the NLO quark distributions, as those parametrizations are very close to each other in the valence region which we consider here. As an illustration, we show in Figs. 13, 14 the parametrization of Eqs. (145-148) for the double distribution part to the u -quark GPD $H^u(x, \xi)$ and d -quark GPD $H^d(x, \xi)$ respectively, for the parameter value $b_{val} = b_{sea} = 1$. One sees how the GPDs approach the forward u - and d -quark distributions as $\xi \rightarrow 0$. Note that the negative x -range at $\xi = 0$ corresponds to the anti-quark distribution, i.e. $q(-x) = -\bar{q}(x)$.

Fig. 15 shows, at a fixed value of $\xi = 0.3$, the dependence of the DD part to the GPD H^u on the parameters b_{val}, b_{sea} . In the limit $b_{val} = b_{sea} = \infty$, one finds back the forward u -quark distribution.

We next discuss the parametrization of the t -dependence of the double distribution

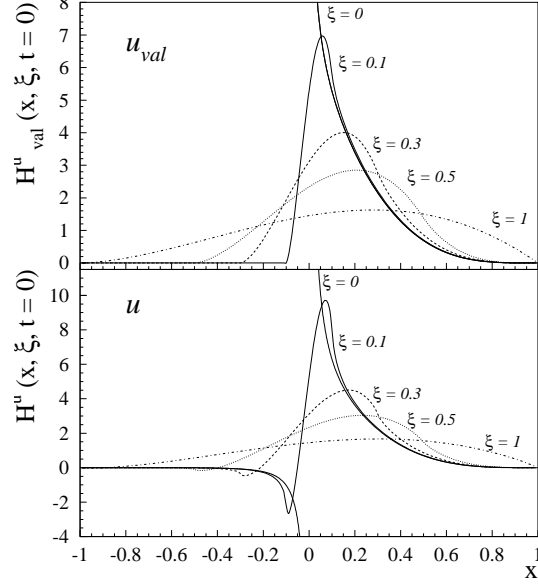


Figure 13: Double distribution part to the u -quark GPD H^u at $t = 0$ for different ξ , using the ansatz (146) as described in the text for $b_{val} = b_{sea} = 1$. Upper panel : valence u -quark GPD, lower panel : total (valence and sea) u -quark GPD. The thin lines ($\xi = 0$) show the ordinary forward u -quark distributions (MRST98 parametrization at $\mu^2 = 2 \text{ GeV}^2$).

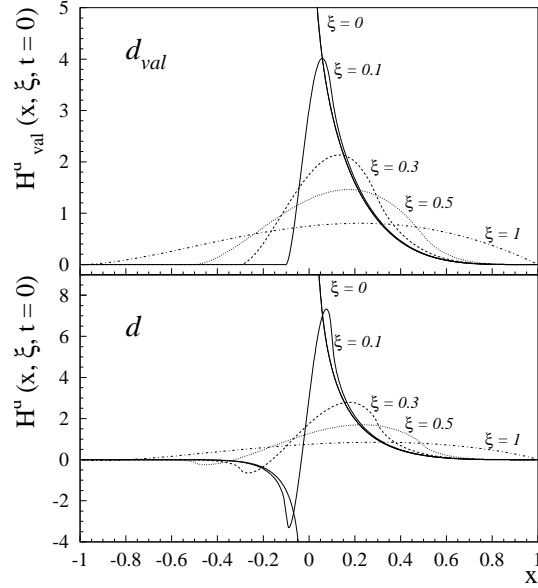


Figure 14: The same as Fig. 13 but for the double distribution part to the d -quark GPD H^d at $t = 0$.

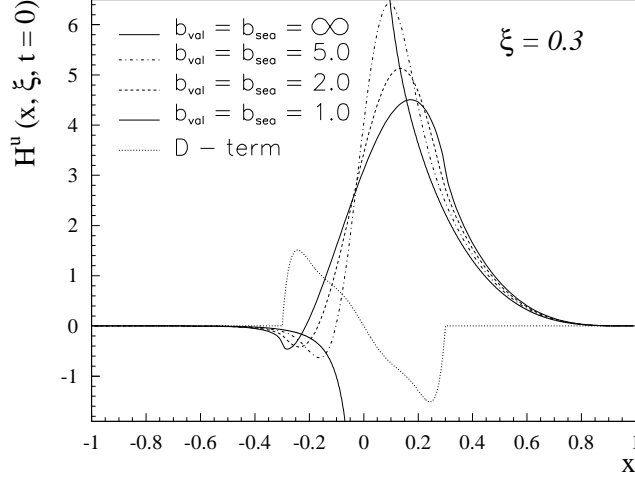


Figure 15: Double distribution part to the GPD $H^u(x, \xi, t = 0)$ at $\xi = 0.3$ for different values of the parameters b_{val} , b_{sea} . The limit $b_{val} = b_{sea} = \infty$ corresponds to the forward u -quark distribution. The D-term contribution to H^u , as it comes out from the chiral quark soliton model (see Eq. (133)) is shown by the dotted curve, and should be added to the double distribution part to obtain the total GPD H^u .

part to the GPD $H^q(x, \xi, t)$. As for the hard exclusive reactions which we discuss t should be a small scale compared to the hard scale Q^2 of the reaction, we will only be concerned here with the small $-t < 1 \text{ GeV}^2$ region. The main constraint which one has on the t -dependence of the GPDs comes through the sum rules of Eqs. (8-10), through which the first moment of the GPDs is given by the elastic nucleon form factors. For the GPD H^q and for a quark of flavor q , the first moment is determined through Eq.(8). in terms of the elastic Dirac form factors $F_1^q(t)$ for a quark of flavor q in the nucleon. In Eq. (12), the strange form factor F_1^s , which is not so well known and expected to be small, is set equal to zero in the following numerical evaluations.

The simplest parametrization of the t dependence of the GPD H^q in the small $-t$ region which fulfills the sum rule of Eq. (8), consists of the factorized ansatz for the t -dependence :

$$\begin{aligned} H^u(x, \xi, t) &= H^u(x, \xi) F_1^u(t) / 2 , \\ H^d(x, \xi, t) &= H^d(x, \xi) F_1^d(t) , \\ H^s(x, \xi, t) &= 0 , \end{aligned} \tag{149}$$

where $F_1^u(t)$ and $F_1^d(t)$ are determined through Eq. (12) using the empirical parametrizations for the proton and neutron Dirac form factors. Besides satisfying the sum rule constraint, the ansatz of Eq. (149) also yields the correct forward limit for u - and d -quark distributions, i.e. $H^u(x, \xi = 0, t = 0) = H^u(x, \xi = 0) = u(x)$ and $H^d(x, \xi = 0, t = 0) = H^d(x, \xi = 0) = d(x)$.

Note that the sum rule of Eq. (8) only gives a constraint for the valence quark part to

the GPD, as the sea-quark contribution drops out of this sum rule. Indeed at $\xi = 0$, where the GPDs reduce to the forward quark distributions, one sees from $q(x) = q_{val}(x) + \bar{q}(x)$ and $q(-x) = -\bar{q}(x)$ that the sea-quark and the anti-quark contributions cancel each other in the sum rule of Eq. (8). One could therefore use a different t -dependence for the sea-quark part to the GPD H^q . However, in lack of more information, we adopt here the same t -dependence for both valence and sea-quark parts.

Such factorized forms for the t -dependence as in Eq. (149) have been used in practically all theoretical estimates for hard exclusive reactions at small $-t$ up to now. It remains to be investigated how realistic such parametrizations are if one goes away from the $t = 0$ region. In particular, the t -dependence of the differential cross section for ρ^0 electroproduction on the proton, in which the GPDs H^u and H^d enter (see further), has been measured at HERMES at values of x_B around 0.1 - 0.15 [Tyt01]. These cross sections clearly display an exponential fall-off with $-t$ in the range $t_{min} < -t < 0.4 \text{ GeV}^2$. A form factor type ansatz as in Eq. (149), even if it gives the correct normalization at t_{min} , deviates over this t range already noticeably from an exponential fall-off.

We also saw in Sec. 3.2.1 that the calculations of GPDs in the chiral quark-soliton model indicate a deviation from the factorization ansatz (149) for the t -dependence of GPDs, as seen from Figs. 5,6. The chiral quark-soliton model results for the t -dependence of GPDs in the small $-t$ region and at a low normalization point can be described by a simple Regge theory motivated ansatz (135). If one uses such a simple ansatz for $H^q(x, \xi = 0, t)$ then the nucleon form factors follow from the sum rule Eq. (8):

$$F_1^q(t) = \int_0^1 dx \frac{1}{x^{\alpha't}} q_{val}(x). \quad (150)$$

Here $q_{val}(x)$ is the valence quark distribution at a low normalization point. The ansatz of Eq. (150) is only valid for the small $-t$ region, because at larger values of $-t$ the integral in Eq. (150) is dominated by the large x region, for which a Regge ansatz does not hold. Furthermore, note that the model of Eq. (150) for the nucleon Dirac form factor as well as the ansatz of Eq. (135) is valid only at a low normalization point. Strictly speaking the form of the ansatz of Eq. (135) should be changed when one goes to a higher normalization point. In particular, when increasing the normalization point, the slope α' should decrease [Bro94, Fra96]. This should lead for instance to the disappearance of the shrinkage of the diffractive cone in hard exclusive processes when increasing Q^2 [Fra96].

In Fig. 16 we show the ratio of the proton Dirac form factor $F_1^p(t)$ obtained from Eq. (150), using the MRST98 parametrization for the valence quark distributions at the scale $\mu^2 = 1.4 \text{ GeV}^2$ (which will be relevant in the discussion of observables further on) to the dipole form of this form factor, given by:

$$F_1^{\text{dipole}}(t) = \frac{1 - (1 + \kappa^p) t/4m_N^2}{1 - t/4m_N^2} \frac{1}{(1 - t/0.71)^2}. \quad (151)$$

The result is shown for several values of the slope $\alpha' = 0.75, 0.8$ and 0.85 GeV^{-2} , which are close to the phenomenological slope of Regge trajectories. It is seen from Fig. 16 that the simple model of Eq. (150) with e.g. $\alpha' = 0.8 \text{ GeV}^{-2}$ gives a rather satisfactory description of the proton Dirac form factor over the range $0 < -t < 1 \text{ GeV}^2$. This finding therefore suggests that the Regge theory motivated ansatz of Eq. (135) can be used as a guide for

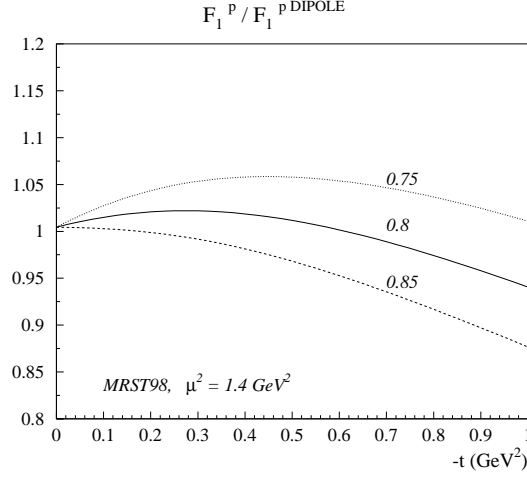


Figure 16: The ratio of the proton Dirac form factor obtained from Eq. (150) to the dipole form of the Dirac form factor (151) for different values of the slope α' (in GeV^{-2}) as indicated in the figure.

a more realistic parametrizations of the t -dependence of the GPDs. From the theoretical point of view it can give a clue for understanding the interplay between the Regge and partonic pictures of hard processes.

The ξ -dependence of the Regge type ansatz of Eq. (135) for $H(x, \xi = 0, t)$ can be restored from Eq. (17) by using the following model for the double distribution :

$$F^q(\beta, \alpha, t) = h(\beta, \alpha) q(\beta) \frac{1}{|\beta|^{\alpha' t}}. \quad (152)$$

where $h(\beta, \alpha)$ is a profile function as in Eq. (148).

In Fig. 17, we compare the factorized model of Eq. (149) for the ‘envelope’ function $H(\xi, \xi, t)$ (i.e. along the line $x = \xi$) with the unfactorized model of Eq. (152). One sees that the unfactorized model leads to an increasingly larger reduction when going to smaller ξ (typical for a Regge type ansatz) and to an enhancement at the larger ξ .

Since the theoretical status of the ansätze of the type (135,152) still remains to be clarified, we restrict ourselves in the discussion of most observables, to the simple factorization ansatz (149) unless explicitly indicated. In some observables (like spin asymmetries for hard meson production) the t -dependence of the GPDs tends to cancel in the ratio of cross sections and therefore these observables are not very sensitive to the explicit form for the t -dependence of the GPDs. However, for absolute cross sections and also for the DVCS single spin asymmetry, the ansatz for the t -dependence of the GPDs can influence the prediction, as will be shown in Sec. 4.3.5.

4.2.2 Parametrization of the D-term

To complete the parametrization of the GPD H , we next specify the D-term part in Eq. (145). The D-term contributes only to the singlet GPDs $H(x, \xi)$, i.e. yields the same

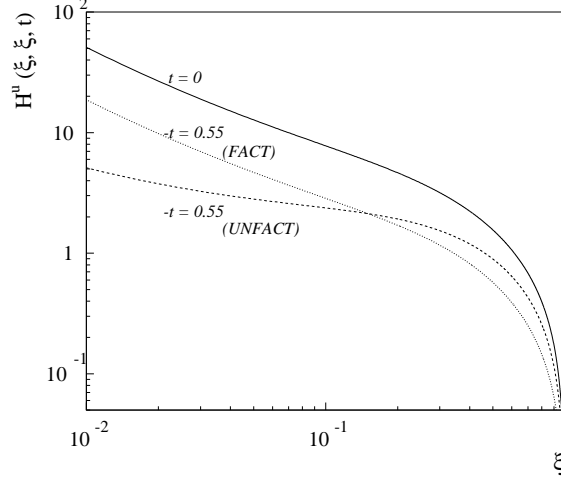


Figure 17: Comparison of the ξ -dependence of the ‘envelope’ function $H^u(\xi, \xi, t)$ at two values of $-t$ (in GeV^2). The function $H^u(\xi, \xi, 0)$ (full curve) is calculated according to the double distribution ansatz of Eq. (146) with $b_{val} = b_{sea} = 1$, using the MRST98 parametrization at a scale $\mu^2 = 1.4 \text{ GeV}^2$ for the forward u -quark distribution as input. For the function $H^u(\xi, \xi, t)$ at $-t = 0.55 \text{ GeV}^2$, the factorized model of Eq. (149) (dotted curve), is compared with the unfactorized parametrization of Eq. (152) (dashed curve).

contribution for each quark flavor.

As discussed in Sec. 2.2, the function $D(z) \equiv D(z, t = 0)$ in Eq. (145) is an odd function of its argument, i.e. $D(-z) = -D(z)$, and can be expanded in odd Gegenbauer polynomials as given by Eq. (23). The moments d_1, d_3, d_5 in such an expansion have been estimated in Eq. (133) using the calculation of GPDs in the chiral quark soliton model [Pet98] at a low normalization point $\mu \approx 0.6 \text{ GeV}$. In principle, the D-term also has a scale dependence but it will be neglected as for the moment the uncertainties in the modeling of the D-term are larger than the logarithmic scale dependence, for the scales relevant for present and planned experiments.

The general expansion of the D-term in Eq. (23) can be used in phenomenological fits to data, and the moments d_1, d_3, d_5, \dots can be used as fit parameters to be extracted from hard electroproduction observables which are sensitive to the D-term. For the following estimates, we will use the values of Eq. (133) obtained from the chiral quark soliton model calculation. The resulting D-term is represented in Fig. (15) for one quark flavor (i.e. by dividing Eq. (133) by $N_f = 3$). Note the negative sign of the Gegenbauer coefficients for the D-term in Eq. (133), as obtained in the chiral quark-soliton model, which fixes the sign of the D-term relative to the double distribution part to the GPD H^q .

In Fig. 18, we display the full x and ξ dependence of the parametrization of Eq. (145) for the GPD $H^u(x, \xi, t = 0)$, i.e. including both the DD part and the D-term. By moving along lines of constant ξ , one nicely sees how the sensitivity of the GPDs to the D-term part increases relative to the double distribution part when increasing the skewedness parameter ξ . In the end, at $\xi = 1$, the D-term contribution dominates the GPD H .

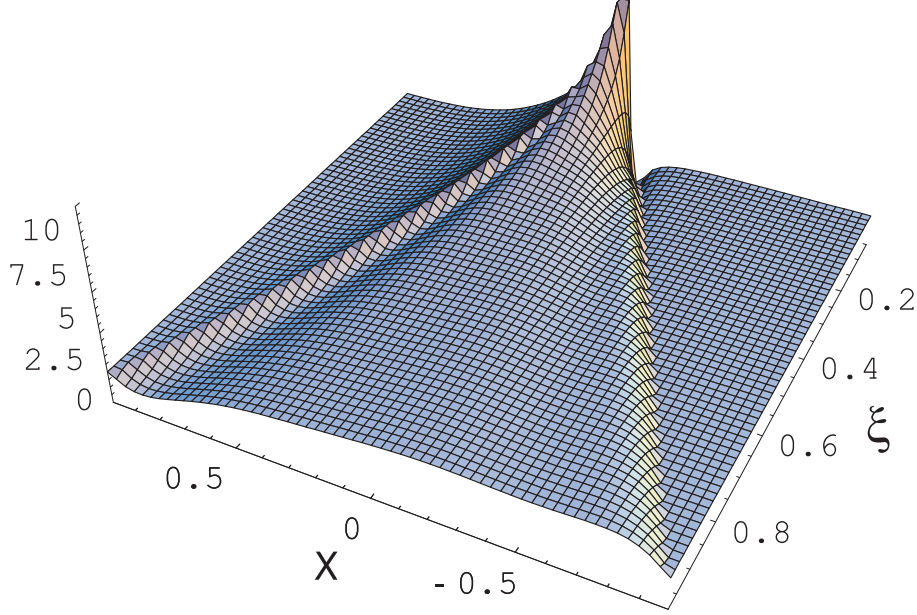


Figure 18: The x and ξ dependence of the GPD $H^u(x, \xi, t = 0)$ for the u -quark distribution, including the double distribution part (for the value $b_{val} = b_{sea} = 1$) and the D-term.

The t -dependence of the D-term is again not constrained through the sum rule of Eq. (8), because the D-term drops out of this sum rule. In absence of more information, we will assume the same t -dependence for the D-term as for the DD contribution to H^q . The study of the t -dependence of the D -term is a subject for future work.

4.2.3 Parametrization of the GPD E^q and quark contribution to the proton spin

The parametrization of E^q , which corresponds to a nucleon helicity flip amplitude, is more difficult as we don't have the DIS constraint for the x -dependence in the forward limit. In the amplitudes for hard electroproduction processes at small $-t$, E^q is multiplied by a momentum transfer and therefore its contribution is suppressed at small t in the observables.

One contribution to the GPD E^q is however determined through the polynomiality condition as explained in Sec. 2.2, which requires that the D-term contributes with opposite sign to H and E . This leads to the D-term contribution for E^q :

$$E_{\text{D-term}}^q(x, \xi, t) = -\theta(\xi - |x|) \frac{1}{N_f} D\left(\frac{x}{\xi}, t\right), \quad (153)$$

which guarantees that the D-term contribution is cancelled in the combination $H + E$. Therefore, the D-term part does not enter in the angular momentum sum rule of Eq. (32).

Similarly to Eq. (145) for H^q , one can parametrize E^q by adding a double distribution

part to the D-term of Eq. (153). This leads to the parametrization :

$$E^q(x, \xi, t) = E_{DD}^q(x, \xi, t) - \theta(\xi - |x|) \frac{1}{N_f} D\left(\frac{x}{\xi}, t\right), \quad (154)$$

where E_{DD}^q is the double distribution part.

In the forward limit, the DD part reduces to the function $e^q(x) \equiv E_{DD}^q(x, \xi = 0, t = 0)$ which is a priori unknown. However one constraint exists on the normalization of E_{DD}^q due to the form factor sum rule Eq. (9) in terms of the Pauli form factor $F_2^q(t)$ for the quark of flavor q in the proton. The quark form factors F_2^u and F_2^d are normalized at $t = 0$ through the anomalous magnetic moments of proton and neutron, i.e. $F_2^p(0) = \kappa^p = 1.793$ and $F_2^n(0) = \kappa^n = -1.913$. Defining $\kappa^u \equiv F_2^u(0)$ and $\kappa^d \equiv F_2^d(0)$, one finds :

$$\begin{aligned} \kappa^u &= 2\kappa^p + \kappa^n = 1.673, \\ \kappa^d &= \kappa^p + 2\kappa^n = -2.033. \end{aligned} \quad (155)$$

Taking Eq. (9) in the forward limit ($\xi = 0, t = 0$) leads to the normalization condition

$$\int_{-1}^{+1} dx e^q(x) = \kappa^q. \quad (156)$$

As a first guess for the function $e^q(x)$, which is consistent with this normalization condition, one can assume that it has the same x dependence as a valence quark distribution, i.e.

$$\begin{aligned} e^u(x) &= \frac{1}{2} u_{val}(x) \kappa^u, \\ e^d(x) &= d_{val}(x) \kappa^d, \\ e^s(x) &= 0. \end{aligned} \quad (157)$$

Indeed, it is seen from Fig. 9 that the chiral quark-soliton model calculation for the isovector function $e^u(x) - e^d(x)$ (which is leading in the large N_c limit) contains such a valence quark component.

Using the ansatz of Eq. (157), one obtains a prediction for the total angular momentum of the quarks in the nucleon, evaluating Ji's sum rule at $\xi = 0$:

$$J^q = \frac{1}{2} \int_{-1}^1 dx x [q(x) + e^q(x)]. \quad (158)$$

By defining the total fraction of the proton momentum carried by the quarks and antiquarks of flavor q as

$$M_2^q = \int_0^1 dx x [q(x) + \bar{q}(x)] = \int_0^1 dx x [q_{val}(x) + 2\bar{q}(x)], \quad (159)$$

and the momentum fraction carried by the valence quarks as

$$M_2^{q_{val}} = \int_0^1 dx x q_{val}(x), \quad (160)$$

the ansatz of Eq. (157) for $e^q(x)$ leads to an estimate for the total angular momentum carried by the u , d and s -quarks in the proton, J^u , J^d , and J^s respectively, as :

$$J^u = \frac{1}{2} \left(M_2^u + \frac{1}{2} \kappa^u M_2^{u_{val}} \right), \quad (161)$$

$$J^d = \frac{1}{2} \left(M_2^d + \kappa^d M_2^{d_{val}} \right), \quad (162)$$

$$J^s = \frac{1}{2} M_2^s. \quad (163)$$

	$M_2^{q_{val}} (\mu^2 = 1 \text{ GeV}^2)$	$M_2^q (\mu^2 = 1 \text{ GeV}^2)$	$2 J^q (\mu^2 = 1 \text{ GeV}^2)$
u	0.34	0.40	0.69
d	0.14	0.22	-0.07
s	0	0.03	0.03
$u + d + s$	0.49	0.65	0.65

Table 4: Estimate of $2 J^q$ at the scale $\mu^2 = 1 \text{ GeV}^2$ according to Eqs. (161-163) using the valence model of Eq. (157). For the forward parton distributions, the MRST98 parametrization (so-called ‘central gluon parametrization’ of Ref. [Mar98a]) has been used.

In Table 4, we show the values of the momentum fractions $M_2^{q_{val}}$ and M_2^q at the scale $\mu^2 = 1 \text{ GeV}^2$, using the MRST98 parametrization [Mar98a] for the forward parton distributions. We also show the estimate for J^u , J^d , and J^s of Eqs. (161-163) at the same scale. These estimates lead to a large fraction (69 %) of the total angular momentum of the proton carried by the u -quarks and a relatively small contribution carried by the d and s -quarks. Using this estimate, the sum of u , d , and s -quark contributions is around 65 % at this low scale. This estimate is in good agreement with the recent lattice QCD estimate of Ref. [Mat00] for J^q , which found the total value $2 J^q = 0.60 \pm 0.14$ at a comparable low scale, and the QCD sum rule estimate of Ref. [Bal97].

One furthermore sees from Table 4 that $2J^u + 2J^d \approx M_2^u + M_2^d$ to a rather high accuracy. For the separate u and d contributions however, one sees from Table 4 that in the ansatz of Eq. (157), $2J^u$ is quite different from M_2^u , and similarly $2J^d$ is quite different from M_2^d . This leads us to the observation that the following remarkable relation between nucleon anomalous magnetic moments and valence quark distributions in the proton seems to hold in general ¹⁸ :

$$\kappa^u \int_0^1 dx x [u(x) - \bar{u}(x)] \approx -2 \kappa^d \int_0^1 dx x [d(x) - \bar{d}(x)]. \quad (164)$$

Such a relation allows us to express the ratio of anomalous magnetic moments of proton and neutron in terms of the proton momentum fractions $M_2^{q_{val}}$ carried by the valence quarks (see definition of Eq. (160)) as follows:

$$\frac{\kappa^p}{\kappa^n} = -\frac{1}{2} \frac{4 M_2^{d_{val}} + M_2^{u_{val}}}{M_2^{d_{val}} + M_2^{u_{val}}}. \quad (165)$$

¹⁸ At this point one could say: “.....cuius rei demonstrationem mirabilem sane detexi. Hanc marginis exiguitas non caperet”

To check the validity of the above relation, we show in Fig. 19 the scale dependence of

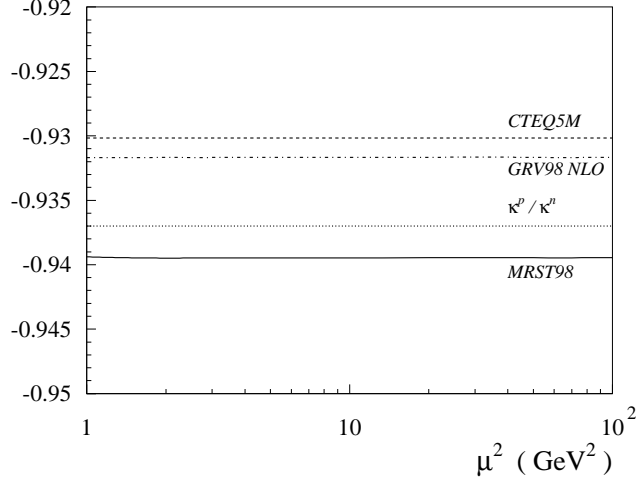


Figure 19: Scale dependence of the *rhs* of Eq. (165) for three different NLO forward parton distributions : MRST98 [Mar98a] (full curve), CTEQ5M [Lai00] (dashed curve), and GRV98 NLO($\overline{\text{MS}}$) [Glu98] (dashed-dotted curve). Also shown is the *lhs* of Eq. (165), i.e. the value κ^p/κ^n (dotted curve).

the *rhs* of Eq. (165) for three current parametrizations of the NLO parton distributions. Fig. 19 shows that the scale dependence drops out of the *rhs* of Eq. (165), although the numerator and denominator separately clearly have a scale dependence. In addition, it is seen from Fig. 19, for the three parametrizations of the NLO parton distributions, that the relation of Eq. (165) is numerically verified to an accuracy at the one percent level! Both of these observations suggest that Eq. (165) holds and that the unpolarized valence u and d -quark forward distributions contain a non-trivial information about the anomalous magnetic moments of the proton and neutron. The relation of Eq. (164) can for example be checked in a theory with weak coupling as well as in chiral perturbation theory. Note that in a simple quark model with $M_2^{uval} = 2 M_2^{dval}$, one recovers from Eq. (165) the result from $SU(6)$ symmetry, i.e. $\kappa^p = -\kappa^n$. In quark model language, the relation of Eq. (165) implies that the breaking of the $SU(6)$ symmetry follows some rule which is encoded in the valence quark distributions.

Because Eq. (164) holds to such good accuracy, when applying it to the estimates given in Eqs. (161,162), it leads to the result that $2J^u + 2J^d \approx M_2^u + M_2^d$. For the separate u and d contributions however, it was already noted from Table 4 that in the ansatz of Eq. (157), $2J^u$ is quite different from M_2^u , and similarly $2J^d$ is quite different from M_2^d . One therefore concludes that the valence ansatz of Eq. (157) for $e^q(x)$ leads to the result that the *sum* over all quarks yields the same contribution to the proton spin as to the proton momentum, at a scale as low as $\mu^2 \sim 1 \text{ GeV}^2$.

In Table 5, we show the estimate of Eqs. (161-163) for $2J^u + 2J^d + 2J^s$ at different scales, using the three different NLO forward parton distributions discussed in Fig. 19. One

firstly sees that the three estimates are very close. One furthermore sees that $J^u + J^d + J^s$ decreases (very slowly) with increasing scale. The scale dependence of the total quark (J^q) and gluon (J^g) contributions to the nucleon spin has been calculated in Ref. [Ji96]. In particular, it has been shown that as $\mu \rightarrow \infty$, there exists a fixed point solution :

$$J^q(\infty) = \frac{1}{2} \frac{3 N_f}{16 + 3 N_f}, \quad (166)$$

and J^g follows from $J^q + J^g = 1/2$. Applying Eq. (166) for $N_f = 3$, one obtains that the total quark contribution to the nucleon spin in the limit $\mu \rightarrow \infty$ amounts to 36 %.

	$2 J^q$ ($\mu^2 = 2.5 \text{ GeV}^2$)	$2 J^q$ ($\mu^2 = 10 \text{ GeV}^2$)	$2 J^q$ ($\mu^2 = 100 \text{ GeV}^2$)
$u + d + s$ (MRST98)	0.60	0.55	0.51
$u + d + s$ (CTEQ5M)	0.59	0.55	0.52
$u + d + s$ (GRV98 NLO)	0.59	0.55	0.51

Table 5: Dependence of the estimate for $2J^u + 2J^d + 2J^s$ on the scale μ^2 , using the MRST98 [Mar98a], CTEQ5M [Lai00], and GRV98 NLO($\overline{\text{MS}}$) [Glu98] forward parton distributions.

One can further interpret the spin structure of the proton by decomposing the quark contribution to the proton spin in an intrinsic part (Δq) and an orbital part (L^q) [Ji98b], for each quark flavor, as :

$$J^q(\mu) = \frac{1}{2} \Delta q(\mu) + L^q(\mu). \quad (167)$$

The flavor decomposed polarized quark contributions Δu , Δd and $\Delta \bar{q}$ to the proton spin have been determined by SMC [Ade98] at a scale $\mu^2 = 10 \text{ GeV}^2$, and by HERMES [Ack99] at a scale $\mu^2 = 2.5 \text{ GeV}^2$ from the measurement of semi-inclusive spin asymmetries. Both experiments are in good agreement when extrapolated to the same scale $\mu^2 = 2.5 \text{ GeV}^2$, as has been done in Ref. [Ack99]. The sum of the quark intrinsic spin contributions to the proton spin yields about 30 % at this scale. By using our estimate for J^q , and the measured values Δq for the different quark flavors, one can extract from Eq. (167) the corresponding orbital angular momentum contributions L^q for the u , d , and s -quarks to the proton spin, as is shown in Table 6. One sees from Table 6 that at the scale $\mu^2 = 2.5 \text{ GeV}^2$, our estimate for the total quark contribution to the proton spin yields about 60%, which is nearly entirely due to the u -quarks. The measured intrinsic spin contributions show that both Δu and Δd are large, and have opposite sign. Our estimate leads then to the picture where the quark orbital angular momenta contribute about 30 % to the proton spin, of comparable size as the intrinsic spin contribution. For the separate flavors, Table 6 shows that for the u -quarks, the dominant contribution to the proton spin comes from the intrinsic contribution Δu , with only a small amount due to orbital angular momentum.

	$2 J^q (\mu^2 = 2.5 \text{ GeV}^2)$	$\Delta q (\mu^2 = 2.5 \text{ GeV}^2)$ (HERMES)	$2 L^q (\mu^2 = 2.5 \text{ GeV}^2)$
u	0.61	0.57 ± 0.04	0.04 ∓ 0.04
d	-0.05	-0.25 ± 0.08	0.20 ∓ 0.08
s	0.04	-0.01 ± 0.05	0.05 ∓ 0.05
$u + d + s$	0.60	0.30 ± 0.10	0.30 ∓ 0.10

Table 6: Estimate of $2 L^q$ at the scale $\mu^2 = 2.5 \text{ GeV}^2$ from Eq. (167). The value of $2 J^q$ is obtained according to the model estimate of Eqs. (161-163) using the MRST98 [Mar98a] parton distributions at the same scale. The values for Δq (including both quark and anti-quark contributions) are taken from the HERMES experiment [Ack99] at this same scale. We added the errors from Ref. [Ack99] in quadrature.

For the d -quarks however, the intrinsic contribution Δd is nearly entirely cancelled by a large orbital contribution, yielding a small net value for J^d .

Having discussed a valence parametrization for the function $e^q(x)$ up to now, we next investigate a possible sea quark contribution to $e^q(x)$. It is seen from Fig. 8 that the chiral quark soliton model calculation for the leading (at large N_c) isovector GPD $E^u - E^d$ contains such a sea quark component, implying that the valence model of Eq. (157) for $e^q(x)$ is incomplete. This sea quark component to $e^q(x)$ is symmetric in x , in contrast to the sea quark contribution to $q(x)$, which is antisymmetric in x . As the chiral quark soliton model calculation indicates that this sea quark component of $e(x)$ is a very narrowly peaked function around $x = 0$, we propose to parametrize it by a δ function in x . Adding this piece to the valence parametrization of Eqs. (157) for u and d -quark flavors, leads to the following parametrization for $e^q(x)$:

$$\begin{aligned}
e^u(x) &= A^u u_{val}(x) + B^u \delta(x), \\
e^d(x) &= A^d d_{val}(x) + B^d \delta(x), \\
e^s(x) &= 0,
\end{aligned} \tag{168}$$

where the parameters A^u, A^d are related to J^u, J^d through the total angular momentum sum rule Eq. (158) as :

$$A^q = \frac{2 J^q - M_2^q}{M_2^{q_{val}}}, \tag{169}$$

and where the parameters B^u, B^d follow from the first sum rule Eq. (156) as :

$$B^u = 2 \left[\frac{1}{2} \kappa^u - \frac{2 J^u - M_2^u}{M_2^{u_{val}}} \right], \tag{170}$$

$$B^d = \kappa^d - \frac{2 J^d - M_2^d}{M_2^{d_{val}}}. \tag{171}$$

One sees that the total angular momenta carried by u - and d -quarks, J^u and J^d , enter now directly as fit parameters in the parametrization of Eq. (168), in contrast to the valence

model for $e^q(x)$ of Eq. (157), where the values J^u and J^d are fixed as in Eqs. (161,162). Therefore, such a parametrization as in Eq. (168) can be used to see the sensitivity of hard electroproduction observables on J^u and J^d , as will be shown further on.

The physical interpretation of the sea quark part of $e^q(x)$ in Eqs. (168) can be understood as being due to “vector meson exchange” because $e^q(x)$ is normalized to κ^q . In a vector meson dominance picture, the isovector (isoscalar) anomalous magnetic moments can be mainly understood as due to exchange of a ρ (ω) meson, through its tensor coupling to the nucleon.

Having specified the model for the forward distribution $e^q(x)$, i.e. Eq. (168), we now turn to the ξ -dependence of the GPD $E_{DD}^q(x, \xi) \equiv E_{DD}^q(x, \xi, t = 0)$ in Eq. (154). We generate the ξ -dependence of $E_{DD}^q(x, \xi)$ through a double distribution $K^q(\beta, \alpha)$ as given by Eq. (18) similar as in Eq. (146) :

$$E_{DD}^q(x, \xi) = \int_{-1}^1 d\beta \int_{-1+|\beta|}^{1-|\beta|} d\alpha \delta(x - \beta - \alpha\xi) K^q(\beta, \alpha) . \quad (172)$$

The double distribution $K^q(\beta, \alpha)$ is then obtained, in an analogous way as in Eq. (147), by multiplying the forward distribution $e^q(\beta)$ with a profile function as :

$$K^q(\beta, \alpha) = h(\beta, \alpha) e^q(\beta) , \quad (173)$$

and where the profile function $h(\beta, \alpha)$ is taken as in Eq. (148). Using the parametrization of Eq. (168), one obtains then for the GPD $E_{DD}^q(x, \xi)$ the expression :

$$E_{DD}^q(x, \xi) = E_{DD}^{qval}(x, \xi) + B^q \frac{\Gamma(2b+2)}{2^{2b+1}\Gamma^2(b+1)} \frac{1}{\xi} \theta(\xi - |x|) \left(1 - \frac{x^2}{\xi^2}\right)^b , \quad (174)$$

where the first (second) term in Eq. (174) is the DD part originating from the valence (sea) contribution to e^q respectively in Eq. (168). In the following, we take the power b in Eq. (174), which enters in the profile function in Eq. (173), equal to the value $b = 1$. This is motivated because this corresponds to “vector meson exchanges” with an asymptotic distribution amplitude.

In Figs. 20,21, we show the parametrization of Eq. (174) for E_{DD}^u and E_{DD}^d respectively at a fixed value $\xi = 0.3$. The two components in Eq. (174) are displayed for different values of J^u (J^d), which are the free parameters in E_{DD}^u (E_{DD}^d) respectively. The valence contribution is calculated using the forward MRST98 valence quark distributions at a scale $\mu^2 = 2 \text{ GeV}^2$. It is seen that the sea contribution due to “vector meson exchange” displays the profile of an asymptotic distribution amplitude. One also sees from Figs. 20,21, that the two components are correlated as the integral of their sum is fixed to κ^q . In particular, for the value $J^u \approx 0.32$, the sea contribution to E^u vanishes and the ansatz of Eq. (168) reduces to the valence ansatz of Eq. (157). Similarly, for the value $J^d \approx -0.03$, the sea contribution to E^d vanishes. For other values of J^u (J^d) however, the relative contribution of both components changes. As both components have a different shape in x , one gets a sensitivity on J^u and J^d in observables where the GPDs E^u and E^d enter, as will be shown further on.

In Fig. 22, we show the ξ dependence of the three contributions of the model for E^u . Besides the valence and sea contributions in the double distribution part of Eq. (172) which are shown at a fixed value of $J^u = 0.25$, the third contribution originates from the

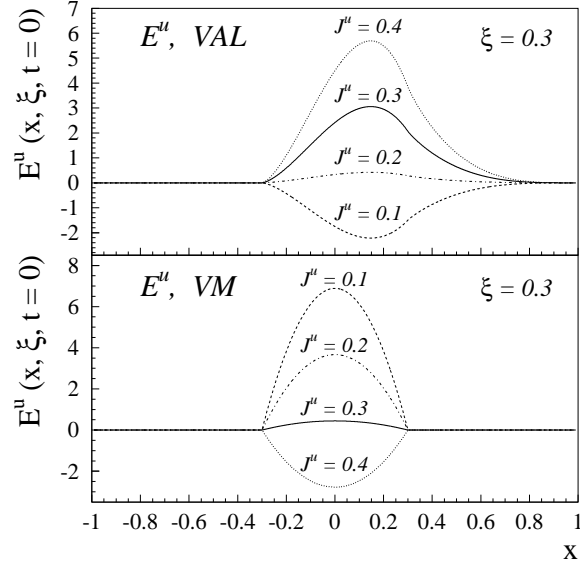


Figure 20: Double distribution part to the u -quark GPD E^u at $t = 0$ using the ansatz of Eq. (168), for different values of J^u as indicated on the curves. Upper panel : valence part (VAL), lower panel : sea contribution due to vector meson exchange (VM).

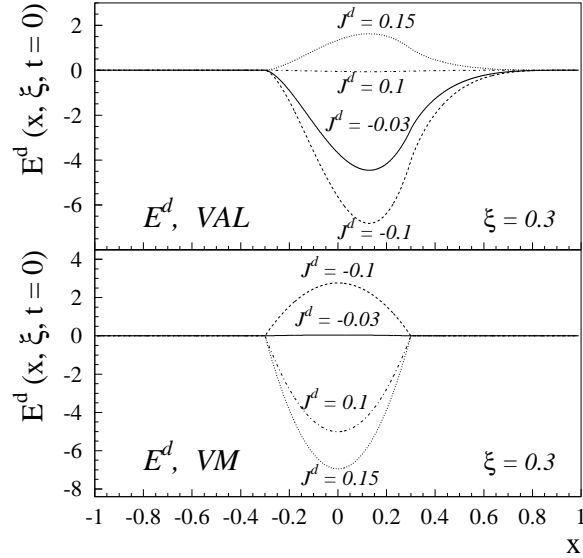


Figure 21: The same as Fig. 20 but for the double distribution part to the d -quark GPD E^d at $t = 0$, for different values of J^d .

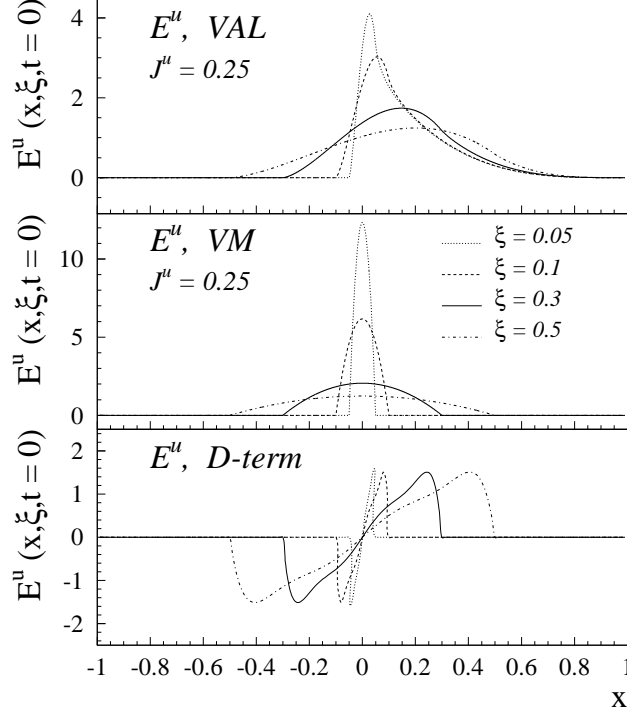


Figure 22: The three contributions of the model for the u -quark GPD E^u at $t = 0$, for different values of ξ as indicated on the figure. Upper panel : valence part (VAL) in the ansatz of Eq. (168) for $J^u = 0.25$; middle panel : sea contribution (second term in Eq. (168)) due to vector meson exchange (VM) for $J^u = 0.25$; lower panel : D-term contribution of Eq. (153) to E^u .

D-term of Eq. (153), which contributes with opposite sign to E^u as compared to H^u , and therefore drops out of the spin sum rule. Notice also from Fig. 22 that for small ξ , the sea contribution approaches a δ -function in our parametrization.

Having specified the parametrization of $E^q(x, \xi, t = 0)$, we next discuss the t -dependence of the GPD $E^q(x, \xi, t)$. This t -dependence of E^q is constrained through the first sum rule of Eq. (9), which is given by the Pauli form factor $F_2(t)$. As stated before, we are only concerned here with hard exclusive reactions in the small $-t$ region, with $-t$ small compared to the hard scale Q^2 . In this small $-t$ region, the simplest parametrization which is consistent with this sum rule constraint consists of a factorized ansatz

$$E^q(x, \xi, t) = E^q(x, \xi) \frac{1}{(1 - t/0.71)^2}, \quad (175)$$

where the t -dependence has been expressed through a dipole form factor, which is known to be a good parametrization for the t -dependence of the nucleon magnetic form factors. In all estimates at small $-t$ which contain E^q , the factorized form (in t) of Eq. (175) is used. As discussed for the GPD H^q , a more realistic estimate of the t -dependence of the

GPD E^q might also be given by a Regge ansatz analogous to Eqs. (135,152), which is postponed to a future work.

To summarize this section, we constructed a three component model for the GPDs E^q as illustrated in Fig. 22. The valence component was fixed in terms of valence forward quark distributions. This assumption is supported by the calculation in the chiral quark-soliton model (see Sec. 3.2). For the sea part, we included the two physically important contributions due to the D-term and the component associated with the “vector meson exchange”. The D-term contribution is required by the polynomiality condition (see Sec. 2.2), whereas the “vector meson exchange” component is motivated by the vector meson dominance model for the nucleon anomalous magnetic moments.

4.2.4 Parametrization of the GPD \tilde{H}^q

To model the GPD \tilde{H}^q , we need the corresponding polarized quark distributions. For this we follow the work of Ref. [Lea98], where a next to leading order QCD analysis of inclusive polarized deep-inelastic lepton-nucleon scattering was performed and which yields an excellent fit of the data. In this analysis, the input polarized densities (at a scale $\mu^2 = 1 \text{ GeV}^2$) are given by :

$$\begin{aligned}\Delta u_V(x, \mu^2) &= \eta_u A_u x^{0.250} u_V(x, \mu^2) , \\ \Delta d_V(x, \mu^2) &= \eta_d A_d x^{0.231} d_V(x, \mu^2) , \\ \Delta \bar{q}(x, \mu^2) &= \eta_{\bar{q}} A_S x^{0.576} S(x, \mu^2) ,\end{aligned}\tag{176}$$

where a $SU(3)$ symmetric sea has been assumed, i.e. $\Delta \bar{q} \equiv \Delta \bar{u} = \Delta \bar{d} = \Delta \bar{s}$ and S represents the total sea. On the *rhs* of Eqs. (176), the normalization factors A_u, A_d, A_S are determined so that the first moments of the polarized densities are given by $\eta_u, \eta_d, \eta_{\bar{q}}$ respectively. For the valence quark densities, η_u and η_d were fixed in Ref. [Lea98] by the octet hyperon β decay constants which yield :

$$\eta_u = \int_0^1 dx \Delta u_V(x) \approx 0.918 , \quad \eta_d = \int_0^1 dx \Delta d_V(x) \approx -0.339 .\tag{177}$$

The first moment of the polarized sea quark density was determined by the fit of Ref. [Lea98] which gives $\eta_{\bar{q}} \approx -0.054$.

Our ansatz for \tilde{H}^q is to generate it from a double distribution $\tilde{F}^q(\beta, \alpha, t)$, analogous to Eq. (17), for which we take

$$\begin{aligned}\tilde{F}^u(\beta, \alpha, t) &= h(\beta, \alpha) \Delta u_V(\beta) g_A^u(t)/g_A^u(0) , \\ \tilde{F}^d(\beta, \alpha, t) &= h(\beta, \alpha) \Delta d_V(\beta) g_A^d(t)/g_A^d(0) ,\end{aligned}\tag{178}$$

where $h(\beta, \alpha)$ is the profile function of Eq. (148). The parameter b in Eq. (148) can again be chosen as a free parameter in such a parametrization, but we will show all estimates with the value $b = 1$ for the GPD \tilde{H} .

One can check that Eq. (7) is verified by construction and that, using Eq. (13) to evaluate the axial form factors g_A^u and g_A^d , the sum rule of Eq. (10) is satisfied within 10 %.

The parametrization of the antiquark contribution to \tilde{H}^q remains to be investigated in future work. This might be interesting to study since a remarkable prediction of the chiral quark soliton model, noted first in Ref. [Dia96, Dia97], is the strong flavour asymmetry

of polarized antiquarks. Such a feature is missing in other models like, for instance, pion cloud models, see discussion in Ref. [Dres00b].

We stress that the factorization of the t -dependence of GPDs is not expected to hold when increasing the value of $-t$. For example, the calculations of the GPD H in the chiral quark soliton model [Pen00a] also show a deviations from the factorization ansatz for the t -dependence of GPDs as is shown in Fig. 12. In the calculations presented here, we limit ourselves to relatively small values of $-t$ and assume the factorization ansatz.

4.2.5 Parametrization of the GPD \tilde{E}^q

As for the GPD E^q , the GPD \tilde{E}^q , corresponding with the induced pseudoscalar transition at the nucleon side in the matrix element of Eq. (5), also vanishes in the forward direction and does not contribute to DIS. However, it was shown in Ref. [Man99b, Fra99a, Pen00a] that the pion exchange, which contributes to the region $-\xi \leq x \leq \xi$ of \tilde{E} , may be non negligible at small t due to the proximity of the pion pole at $t = m_\pi^2$. As discussed in Sec. 3.2.2, it was found [Pen00a] in the chiral quark-soliton model calculation that in the limit $t \rightarrow m_\pi^2$ the function \tilde{E} exactly reduces to this pion pole contribution. Furthermore it is seen from Fig. 10, that in the model calculation for \tilde{E} the pion pole part to \tilde{E} dominates over a wide range of t and ξ values.

According to these findings, the main contribution to \tilde{E} is obtained by evaluating \tilde{E} assuming it is entirely due to the pion pole. According to this hypothesis, since the pion exchange is isovector, one has

$$\tilde{E}^u = -\tilde{E}^d = \frac{1}{2} \tilde{E}_{\pi-pole} . \quad (179)$$

The t -dependence of $\tilde{E}_{\pi-pole}(x, \xi, t)$ is fixed by the sum rule of Eq. (10) in terms of the pseudoscalar form factor $h_A(t)$.

In the region $-\xi \leq x \leq \xi$, the quark and antiquark couple to the pion field of the nucleon. Therefore, this coupling should be proportional to the pion distribution amplitude. For the latter we adopt the asymptotic form. Expressing the quark's longitudinal momentum fraction z in the pion in the symmetric range $-1 \leq z \leq 1$, the asymptotic distribution amplitude Φ_{as} is given by $\Phi_{as}(z) = 3/4 (1 - z^2)$, and is normalized as $\int_{-1}^{+1} dz \Phi_{as}(z) = 1$. The light-cone momentum fractions of the quark and antiquark in the pion are respectively given by $(1 + x/\xi)/2$ and $(1 - x/\xi)/2$. Therefore, $\tilde{E}_{\pi-pole}$ is finally modelled in the estimates as :

$$\tilde{E}_{\pi-pole} = \theta(-\xi \leq x \leq \xi) h_A(t) \frac{1}{\xi} \Phi_{as}\left(\frac{x}{\xi}\right) , \quad (180)$$

which satisfies the sum rule of Eq. (11).

4.3 Deeply virtual Compton scattering (DVCS)

In order to access the GPDs experimentally, the deeply virtual Compton scattering (DVCS) process

$$\gamma^*(q) + N(p) \rightarrow \gamma(q') + N(p'), \quad (181)$$

was proposed as a practical tool in Ref. [Ji97b]. In the Bjorken regime, where the photon virtuality Q^2 is large, with $x_B \equiv Q^2/2(p \cdot q)$ fixed, the leading order DVCS amplitude in the forward direction is given by the handbag diagrams of Fig. 1 [Mul94, Rad96a, Ji97b]. These handbag diagrams express the factorization of the DVCS amplitude in a hard scattering part (which is exactly calculable in PQCD) and a soft, non-perturbative nucleon structure part, represented by the lower blobs in Fig. 1. This soft, non-perturbative object is parametrized in terms of the GPDs as given by Eq. (5). The factorization of the DVCS amplitude in a hard and soft part has been proven in Ref. [Ji98a, Rad98, Col99] for the leading power in Q and all logarithms.

To calculate the DVCS amplitude, one starts from its definition as a nucleon matrix element of the T -product of two electromagnetic currents :

$$H^{\mu\nu} = -i \int d^4x e^{-i(q \cdot x)} \langle p' | T [J_{\text{e.m.}}^\mu(x) J_{\text{e.m.}}^\nu(0)] | p \rangle, \quad (182)$$

where the four-vector index μ (ν) refers to the virtual (real) photon. The DVCS amplitude is obtained from the DVCS tensor of Eq. (182) by contracting with the photon polarization vectors as :

$$T = \varepsilon_\mu(q) \varepsilon_\nu^*(q') H^{\mu\nu}, \quad (183)$$

where $\varepsilon_\mu(q)$ ($\varepsilon_\nu^*(q')$) are the polarization vectors of the virtual (real) photons respectively.

In the following, we firstly introduce the kinematical variables entering the DVCS process. We then discuss the DVCS amplitude of Eq. (182) in the leading power in Q (twist-2 accuracy), and show its dependence upon the GPDs. In order to be able to extract the twist-2 GPDs from DVCS observables at accessible values of the hard scale Q , it is necessary to have an estimate of the effect of power suppressed (higher twist) contributions to those observables. The first power correction to the DVCS amplitude is of order $O(1/Q)$, hence it is called twist-3. We therefore discuss subsequently, the twist-3 corrections to the DVCS amplitude, which have been derived and calculated recently by several groups [Ani00, Pen00b, Bel00b, Rad00, Kiv01a, Kiv01b, Kiv01c, Rad01a, Bel00c, Bel01b] using different approaches. We then explore the experimental opportunities and discuss the different DVCS observables.

4.3.1 Kinematical variables of the DVCS process

As explained in Sec. 2.1, the calculation of the DVCS amplitude in the Bjorken regime and the parametrization of the non-perturbative matrix elements, representing the lower blobs in the handbag diagrams, is performed in a frame where the virtual photon momentum q^μ and the average nucleon momentum \bar{P}^μ are collinear along the z -axis and in opposite direction. To calculate the DVCS amplitude, it is therefore convenient to introduce lightlike vectors along the positive and negative z -directions as $\hat{p}^\mu = \bar{P}^+/\sqrt{2}(1, 0, 0, 1)$ and $n^\mu = 1/\bar{P}^+ \cdot 1/\sqrt{2}(1, 0, 0, -1)$ respectively, satisfying $\hat{p} \cdot n = 1$.

In this frame, the physical momenta entering the DVCS process (181), where $p(p')$ are the momenta of the initial (final) nucleon and $q(q')$ are the momenta of the initial (final) photon respectively, have the following decomposition [Gui98] :

$$\bar{P}^\mu = \frac{1}{2} (p^\mu + p'^\mu) = \tilde{p}^\mu + \frac{\bar{m}^2}{2} n^\mu, \quad (184)$$

$$q^\mu = - \left(2\xi' \right) \tilde{p}^\mu + \left(\frac{Q^2}{4\xi'} \right) n^\mu, \quad (185)$$

$$\Delta^\mu \equiv p'^\mu - p^\mu = - (2\xi) \tilde{p}^\mu + (\xi \bar{m}^2) n^\mu + \Delta_\perp^\mu, \quad (186)$$

$$q'^\mu \equiv q^\mu - \Delta^\mu = -2 \left(\xi' - \xi \right) \tilde{p}^\mu + \left(\frac{Q^2}{4\xi'} - \xi \bar{m}^2 \right) n^\mu - \Delta_\perp^\mu, \quad (187)$$

where Δ_\perp is the perpendicular component of the momentum transfer Δ (i.e. $\tilde{p} \cdot \Delta_\perp = n \cdot \Delta_\perp = 0$), and where the variables \bar{m}^2 , ξ' and ξ are given by

$$\bar{m}^2 = m_N^2 - \frac{\Delta^2}{4}, \quad (188)$$

$$2\xi' = \frac{\bar{P} \cdot q}{\bar{m}^2} \left[-1 + \sqrt{1 + \frac{Q^2 \bar{m}^2}{(\bar{P} \cdot q)^2}} \right] \xrightarrow{Bj} \frac{x_B}{1 - \frac{x_B}{2}}, \quad (189)$$

$$2\xi = 2\xi' \frac{Q^2 - \Delta^2}{Q^2 + \bar{m}^2 (2\xi')^2} \xrightarrow{Bj} \frac{x_B}{1 - \frac{x_B}{2}}. \quad (190)$$

To twist-3 accuracy, Eqs. (184-187) reduce to

$$\begin{aligned} \bar{P} &= \tilde{p}, & \Delta &= -2\xi \bar{P} + \Delta_\perp, \\ q &= -2\xi \bar{P} + \frac{Q^2}{4\xi} n, & q' &= \frac{Q^2}{4\xi} n - \Delta_\perp. \end{aligned} \quad (191)$$

4.3.2 Twist-2 DVCS tensor

Using the parametrization of Eq. (5) for the bilocal quark operator, the DVCS tensor in leading order in Q , $H_{\text{DVCS-LO}}^{\mu\nu}$, follows from the handbag diagrams of Fig. 1 as [Mul94, Ji97b, Rad96a] :

$$\begin{aligned} H_{\text{DVCS-LO}}^{\mu\nu} &= \frac{1}{2} (-g^{\mu\nu})_\perp \int_{-1}^{+1} dx C^+(x, \xi) \left[H_{\text{DVCS}}^p(x, \xi, t) \bar{N}(p') \not{n} N(p) \right. \\ &\quad \left. + E_{\text{DVCS}}^p(x, \xi, t) \bar{N}(p') i\sigma^{\kappa\lambda} \frac{n_\kappa \Delta_\lambda}{2m_N} N(p) \right] \\ &+ \frac{i}{2} (\epsilon^{\nu\mu})_\perp \int_{-1}^{+1} dx C^-(x, \xi) \left[\tilde{H}_{\text{DVCS}}^p(x, \xi, t) \bar{N}(p') \not{n} \gamma_5 N(p) \right. \\ &\quad \left. + \tilde{E}_{\text{DVCS}}^p(x, \xi, t) \bar{N}(p') \gamma_5 \frac{\Delta \cdot n}{2m_N} N(p) \right], \quad (192) \end{aligned}$$

where the symmetrical and antisymmetrical twist-2 tensors were introduced in Eq. (63) as :

$$(-g^{\mu\nu})_\perp = -g^{\mu\nu} + n^\mu \tilde{p}^\nu + n^\nu \tilde{p}^\mu, \quad (\epsilon_{\mu\nu})_\perp = \epsilon_{\mu\nu\alpha\beta} n^\alpha \tilde{p}^\beta. \quad (193)$$

In Eq. (192), we also introduced the coefficient functions $C^\pm(x, \xi)$, which are defined as :

$$C^\pm(x, \xi) = \frac{1}{x - \xi + i\varepsilon} \pm \frac{1}{x + \xi - i\varepsilon}. \quad (194)$$

In the DVCS process on the proton, the GPDs for each quark flavor enter in the combination

$$H_{DVCS}^p = \frac{4}{9}H^u + \frac{1}{9}H^d + \frac{1}{9}H^s, \quad (195)$$

and similarly for \tilde{H} , E and \tilde{E} . The tensor for the DVCS process on the neutron is given by Eq. (192) by replacing H_{DVCS}^p by

$$H_{DVCS}^n = \frac{1}{9}H^u + \frac{4}{9}H^d + \frac{1}{9}H^s, \quad (196)$$

and similarly for \tilde{H} , E and \tilde{E} . Note that in Eqs. (195,196) the flavor dependent GPDs H^u , H^d and H^s in our notation always refer to the corresponding quark flavor in the proton, e.g. $H^u \equiv H^{u/p}$ as explained in Sec. 4.2.

One sees from the *rhs* of the DVCS amplitude of Eq. (192) that the GPDs $H, \tilde{H}, E, \tilde{E}$ enter in a convolution integral over the quark momentum fraction x . This is a qualitative difference compared to the case of DIS, where one is only sensitive (through the optical theorem) to the imaginary part of the forward double virtual Compton amplitude. In the case of DIS, the convolution integral collapses and the quark momentum fraction x is fixed to the kinematical quantity x_B . In contrast, the non-forward DVCS amplitude of Eq. (192) displays a richer structure and has both real and imaginary parts. For the imaginary part, the convolution integral again collapses, and the value x is fixed to the kinematically determined skewedness variable ξ . Therefore, the imaginary part of the DVCS amplitudes is directly proportional to the GPDs evaluated along the line $x = \xi$ (e.g. in Fig. 18), and measures in this way the ‘envelope functions’ $H(\xi, \xi, t)$, $E(\xi, \xi, t)$, $\tilde{H}(\xi, \xi, t)$, and $\tilde{E}(\xi, \xi, t)$.

The x -dependence of the GPDs away from the line $x = \xi$ is contained in the principal value integral of the real part of the DVCS amplitude Eq. (192). As the variable x is not a kinematically accessible quantity, the extraction of GPDs away from the line $x = \xi$ is a non-trivial task. The strategy which we propose here is to start from physically motivated parametrizations for those GPDs as outlined in Sec. 4.2. One can then extract the parameters entering those parametrizations from different observables, which have a different sensitivity to the real and imaginary part of the hard electroproduction amplitudes, as shown further on.

4.3.3 Twist-3 DVCS tensor

The DVCS amplitude of Eq. (192) displays a scaling behavior as it is independent of Q . One easily sees however that this amplitude is not complete when going beyond the leading order in Q . Although the twist-2 DVCS amplitude of Eq. (192), is exactly gauge invariant with respect to the virtual photon, i.e. $q_\mu H_{DVCS-LO}^{\mu\nu} = 0$, electromagnetic gauge invariance is violated however by the real photon except in the forward direction. This violation of gauge invariance is a higher twist effect compared to the leading order term $H_{DVCS-LO}^{\mu\nu}$. Since $q'_\nu H_{DVCS-LO}^{\mu\nu} = -(\Delta_\perp)_\nu H_{DVCS-LO}^{\mu\nu}$, an improved DVCS amplitude

linear in Δ_\perp has been proposed in Refs. [Gui98, Vdh99] to restore gauge invariance (in the nonforward direction) in a heuristic way :

$$H_{\text{DVCS}}^{\mu\nu} = H_{\text{DVCS-LO}}^{\mu\nu} + \frac{\bar{P}^\nu}{(\bar{P} \cdot q')} (\Delta_\perp)_\lambda H_{\text{DVCS-LO}}^{\mu\lambda}, \quad (197)$$

leading to a correction term of higher order in Q to the twist-2 DVCS amplitude, because $(\bar{P} \cdot q') = O(Q^2)$.

Recently, the DVCS amplitude on the nucleon ¹⁹ to the order $O(1/Q)$ has been derived explicitly in a parton model approach [Pen00b] and in a light-cone expansion framework [Bel00b], yielding the result :

$$\begin{aligned} H^{\mu\nu} = & \frac{1}{2} \int_{-1}^1 dx \left\{ \left[(-g^{\mu\nu})_\perp - \frac{\bar{P}^\nu \Delta_\perp^\mu}{(\bar{P} \cdot q')} \right] n_\beta \mathcal{F}_\beta(x, \xi) C^+(x, \xi) \right. \\ & - \left[(-g^{\nu k})_\perp - \frac{\bar{P}^\nu \Delta_\perp^k}{(\bar{P} \cdot q')} \right] i(\epsilon_k^\mu)_\perp n_\beta \tilde{\mathcal{F}}_\beta(x, \xi) C^-(x, \xi) \\ & \left. - \frac{(q + 4\xi \bar{P})^\mu}{(\bar{P} \cdot q)} \left[(-g^{\nu k})_\perp - \frac{\bar{P}^\nu \Delta_\perp^k}{(\bar{P} \cdot q')} \right] \left\{ \mathcal{F}_k(x, \xi) C^+(x, \xi) - i(\epsilon_{k\rho})_\perp \tilde{\mathcal{F}}^\rho(x, \xi) C^-(x, \xi) \right\} \right\}, \end{aligned} \quad (198)$$

where the functions \mathcal{F}_μ and $\tilde{\mathcal{F}}_\mu$ are given by Eqs. (58,59).

In the expression Eq. (198) for the DVCS amplitude to the twist-3 accuracy, the first two terms correspond to the scattering of transversely polarized virtual photons. This part of the amplitude, containing $n_\beta \mathcal{F}^\beta$ and $n_\beta \tilde{\mathcal{F}}^\beta$, depends only on the twist-2 GPDs H, E and \tilde{H}, \tilde{E} and was anticipated in Refs. [Gui98, Vdh99]. The third term in Eq. (198) corresponds to the contribution of the longitudinal polarization of the virtual photon. Defining the polarization vector of the virtual photon as

$$\varepsilon_L^\mu(q) = \frac{1}{Q} \left(2\xi \bar{P}^\mu + \frac{Q^2}{4\xi} n^\mu \right), \quad (199)$$

we can easily calculate the DVCS amplitude for longitudinal polarization of the virtual photon ($L \rightarrow T$ transition), which is purely of twist-3 :

$$(\varepsilon_L)_\mu H^{\mu\nu} = \frac{2\xi}{Q} \int_{-1}^1 dx \left(\mathcal{F}_\perp^\nu C^+(x, \xi) - i\varepsilon_\perp^{\nu k} \tilde{\mathcal{F}}_{\perp k} C^-(x, \xi) \right). \quad (200)$$

It is therefore seen that this term depends only on new ‘transverse’ GPDs \mathcal{F}_\perp^μ and $\tilde{\mathcal{F}}_\perp^\mu$, which can be related to the twist-2 GPDs H, E, \tilde{H} and \tilde{E} with help of Wandzura-Wilczek relations as discussed in Sec. 2.5, and which are given by Eqs. (58-61).

The DVCS amplitude of Eq. (198) is electromagnetically gauge invariant, i.e.

$$q_\mu H^{\mu\nu} = (q - \Delta)_\nu H^{\mu\nu} = 0. \quad (201)$$

formally to the accuracy $1/Q^2$. In order to have ‘absolute’ transversality of the amplitude (i.e. such that Eq. (201) is satisfied exactly) we keep in the expression (198) terms of the

¹⁹The DVCS amplitude to twist-3 accuracy has also been derived for the analogous case of a pion target in Refs. [Ani00, Rad00, Rad01a].

order Δ^2/Q^2 , by applying the prescription of Eq. (197), i.e.

$$-g_{\perp}^{\mu\nu} \rightarrow -g_{\perp}^{\mu\nu} - \frac{\bar{P}^{\nu} \Delta_{\perp}^{\mu}}{(P \cdot q')}, \quad (202)$$

for the twist-3 terms in the amplitude. Formally such terms are beyond the twist-3 accuracy and they do not form a complete set of $1/Q^2$ contributions, but we prefer to work with the DVCS amplitude, satisfying Eq. (201) exactly.

A more systematic treatment of corrections of the order t/Q^2 for DVCS still remains to be done. Recently, the target mass corrections, which induce correction terms in powers of M^2/Q^2 , have been addressed in Ref. [Bel01b].

To calculate the twist-3 DVCS amplitude, the convolution of the leading order Wilson coefficients (194) with the WW kernels in Eq. (198) can be performed analytically, as shown in Refs. [Kiv01b, Bel00c]. In particular, it has been shown that the strongest (integrable) singularity of the resulting integrand is logarithmic only (see [Kiv01b] for technical details).

Finally, let us note that in Eq. (198), the quark flavor dependence in the GPDs \mathcal{F}_{μ} ($\tilde{\mathcal{F}}_{\mu}$) is implicitly understood, i.e.

$$\mathcal{F}_{\mu}(\tilde{\mathcal{F}}_{\mu}) \rightarrow \sum_{q=u,d,s} e_q^2 \mathcal{F}_{\mu}^q(\tilde{\mathcal{F}}_{\mu}^q). \quad (203)$$

4.3.4 DVCS cross section and charge asymmetry

In this section, we present results for the DVCS cross sections. We give all results for the invariant cross section of the $ep \rightarrow ep\gamma$ reaction, which is differential with respect to Q^2 , x_B , t , and out-of-plane angle Φ ($\Phi = 0^\circ$ corresponds to the situation where the real photon is emitted in the same half plane as the leptons). The invariant $ep \rightarrow ep\gamma$ cross section is given by :

$$\frac{d\sigma}{dQ^2 dx_B dt d\Phi} = \frac{1}{(2\pi)^4 32} \cdot \frac{x_B y^2}{Q^4} \cdot \left(1 + \frac{4m_N^2 x_B^2}{Q^2}\right)^{-1/2} \cdot \left|T_{BH} + T_{FVCS}\right|^2, \quad (204)$$

where m_N is the nucleon mass, $y \equiv (p \cdot q)/(p \cdot k)$, and k is the initial lepton four-momentum. In the $ep \rightarrow ep\gamma$ reaction, the final photon can be emitted either by the proton or by the lepton. The former process is referred to as the fully VCS process (amplitude T_{FVCS} in Eq. (204)), which includes the leptonic current. The process where the photon is emitted from the initial or final lepton is referred to as the Bethe-Heitler (BH) process (amplitude T_{BH} in Eq. (204)), and can be calculated exactly. For further technical details of the $ep \rightarrow ep\gamma$ reaction and observables, we refer to Refs. [Gui98, Bel01a, Vdh00b]²⁰.

When calculating DVCS observables, we show all results with the exact expression for the BH amplitude, i.e. we do *not* expand the BH amplitude in powers $1/Q$. Also in the actual calculations, we use the exact kinematics for the four-momenta of the participating particles as given by Eqs. (184-187). In this way we take (partially) kinematical higher twists into account. Furthermore, when referring to the twist-2 DVCS results, we include those higher twist effects which restore exact transversality of the amplitude as expressed through Eq. (202). Similarly, when referring to the twist-3 DVCS results (provided by a longitudinally polarized virtual photon), we include the gauge restoring higher twist terms.

²⁰see Ref. [Vdh00a] for a calculation of the QED radiative corrections to the VCS process.

Because the BH amplitude contains two lepton electromagnetic couplings in contrast to the FVCS process, the interference between BH and FVCS process changes sign when comparing the $e^+p \rightarrow e^+p\gamma$ and $e^-p \rightarrow e^-p\gamma$ processes. Therefore, in the difference of cross sections $\sigma_{e^+} - \sigma_{e^-}$, the BH (whose amplitude is purely real) drops out. This difference measures the real part of the BH-FVCS interference [Bro72]

$$\sigma_{e^+} - \sigma_{e^-} \sim \text{Re} \left[T^{BH} T^{FVCS*} \right], \quad (205)$$

and therefore is proportional to the *real* (principle value integral) part of the DVCS amplitude. In this way, the difference $\sigma_{e^+} - \sigma_{e^-}$ is sensitive to the GPDs away from the line $x = \xi$ (as e.g. in Fig. 18).

In the following, we firstly show results for DVCS cross sections and DVCS charge asymmetries $(\sigma_{e^+} - \sigma_{e^-})/(\sigma_{e^+} + \sigma_{e^-})$.

In Fig. 23, the Φ -dependence of the $ep \rightarrow ep\gamma$ cross section is shown for a lepton (either electron or positron) of $E_e = 27$ GeV (accessible at HERMES). The kinematics corresponds to the valence region ($x_B = 0.3$) and to a ratio $-t/Q^2 = 0.1$ (Remark that increasing the ratio $-t/Q^2$, increases the higher twist effects).

It is firstly seen from Fig. 23, that in these kinematics, the pure twist-2 DVCS process without D-term contribution (dashed curves) dominates the $ep \rightarrow ep\gamma$ cross section compared to the BH process (which is sizeable only around $\Phi = 0^\circ$, where it reaches its maximal value). In absence of the BH, the twist-2 DVCS cross section would give a Φ -independent cross section which practically saturates the $ep \rightarrow ep\gamma$ cross section at $\Phi = 180^\circ$, where the BH is vanishingly small. The Φ -dependence of the dashed curve in Fig. 23 can be understood as the sum of this constant twist-2 DVCS cross section, the cross section for the BH process, and the interference of the BH with the relatively small real part of the DVCS amplitude (in the valence kinematics, $x_B \simeq 0.3$, shown in Fig. 23, the ratio of real to imaginary part of the DVCS amplitude without D-term, is around 15 %).

When adding to the twist-2 DVCS amplitude the purely real D-term contribution, the resulting cross section for the full twist-2 DVCS process (dashed-dotted curves in Fig. 23) shows a noticeable sensitivity to the D-term. At $\Phi = 180^\circ$ (where the BH ‘contamination’ is very small), the predominantly imaginary DVCS amplitude (in absence of the D-term contribution), and the purely real D-term amplitude have only a small interference. In this region, the DVCS cross section is enhanced by about 10 %, when using the chiral quark soliton model estimate of Eq. (40) for the D-term Eq. (23). However, around $\Phi = 0^\circ$, the purely real D-term amplitude interferes maximally with the BH. This interference is destructive for the electron reaction and constructive for the positron reaction. Therefore, the effect of the D-term can be very clearly seen in the Φ -dependence of the charge asymmetry as shown on the lower panel of Fig. 23. Including the D-term contribution, the full twist-2 DVCS charge asymmetry changes sign and obtains a rather large value (≈ 0.15) at $\Phi = 0^\circ$. On the other hand, at $\Phi = 180^\circ$, where the interference with the BH (and hence the difference between e^- and e^+) is small, the charge asymmetry is correspondingly small. The pronounced Φ -dependence of the charge asymmetry and its value at $\Phi = 0^\circ$, provides therefore a useful observable to study the D-term contribution to the GPDs, and to check the chiral quark soliton model estimate of Eqs. (133).

We next study the twist-3 effects on the DVCS cross section in the WW approximation. It is seen from Fig. 23 (full curves) that they induce an additional (approximate) $\cos \Phi$ structure in the cross section. The twist-3 effects would induce an exact $\cos \Phi$ structure only when the BH amplitude is approximated by its leading term in an expansion in

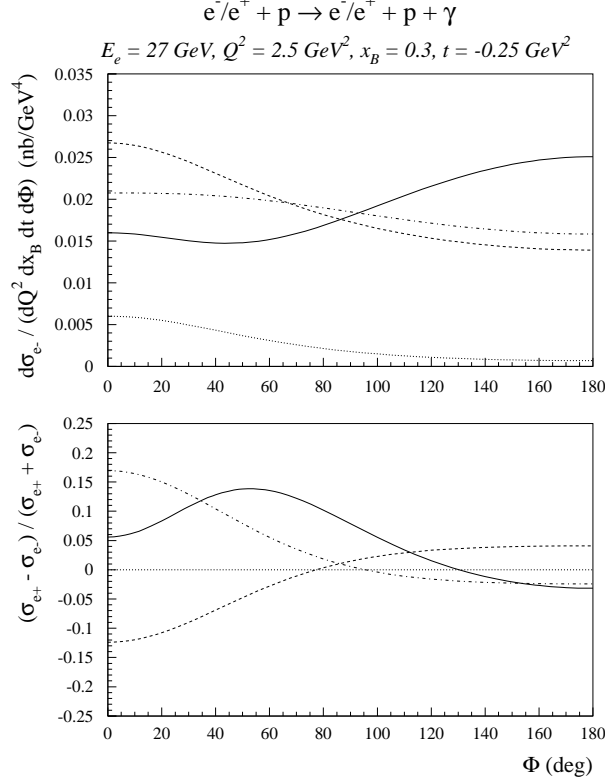


Figure 23: Invariant cross section for the $e^-p \rightarrow e^-p\gamma$ reaction (upper panel) and DVCS charge asymmetry (lower panel) at $E_e = 27 \text{ GeV}$, for the DVCS kinematics as indicated in the figure. Dotted curves : BH contribution; dashed curves : BH + twist-2 DVCS (without D-term); dashed-dotted curves : BH + twist-2 DVCS (with D-term); full curves : BH + twist-2 + twist-3 DVCS (with D-term). The calculations are performed using the values $b_{val} = b_{sea} = 1$.

$1/Q$, neglecting its additional Φ -dependence. In all calculations, we keep however the full Φ -dependence of the BH, due to the lepton propagators, which complicates the interference at the lower Q . One sees from Fig. 23 that the interference of the twist-3 amplitude with the BH + twist-2 DVCS amplitude is destructive for $\Phi \lesssim 90^\circ$, and constructive for $\Phi \gtrsim 90^\circ$. Around $\Phi = 0^\circ$, the twist-3 effects reduce the full twist-2 DVCS cross section (including the D-term) by about 25 %, whereas around $\Phi = 180^\circ$, they largely enhance the twist-2 DVCS cross section (by about 55 %).

To see how the size of the twist-3 effects on the $ep \rightarrow ep\gamma$ cross section decreases when increasing the value of Q^2 at fixed x_B and t , the cross section and charge asymmetry are shown in Fig. 24 at the same E_e , x_B , and t , as in Fig. 23, but at a value $Q^2 = 5 \text{ GeV}^2$. One firstly sees that going to higher Q^2 , at the same E_e , x_B , and t , enhances the relative contribution of the BH process compared to the DVCS process. Consequently, the cross section follows much more the Φ -behavior of the BH process. For the twist-2 cross section, one sees again clearly the effect of the D-term which leads, through its interference with

the BH amplitude, to a charge asymmetry of opposite sign as compared to the one for the twist-2 DVCS process without D-term.

The twist-3 effects in the kinematics of Fig. 24, where the ratio t/Q^2 is only half the value of Fig. 23, are correspondingly smaller. It is furthermore seen that the twist-3 effects induce an (approximate) structure $\sim A \cos(2\Phi)$ in the charge asymmetry ($A \approx -0.08$ in the kinematics of Fig. 24). Only for out-of-plane angles $\Phi \gtrsim 130^\circ$ one sees a deviation from this simple structure induced by the twist-3 amplitude, due to the more complicated Φ -dependence when calculating the BH amplitude exactly.

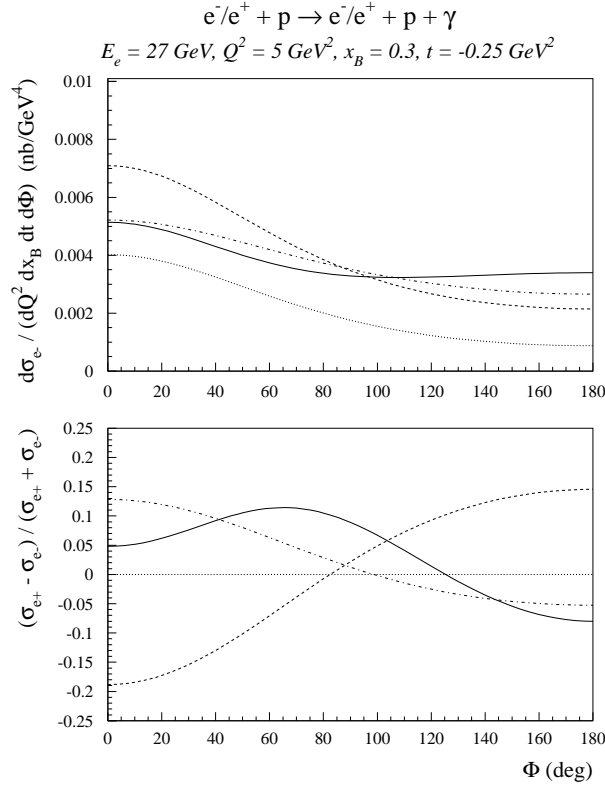


Figure 24: Same as Fig. 23, but for $Q^2 = 5 \text{ GeV}^2$.

Besides exploiting the interference between the DVCS and BH contributions to the $ep \rightarrow ep\gamma$ reaction, as e.g. through the charge asymmetry, one can also study the DVCS amplitude directly in a kinematical regime where it dominates over the BH amplitude. Indeed, it was found in Refs. [Gui98, Vdh98] that at some fixed Q^2 , x_B and t , one favors the DVCS contribution over the BH by going to higher beam energy. In particular, at intermediate values of $x_B \sim 0.15 - 0.3$, one is in such a regime at 200 GeV beam energy at COMPASS, where a DVCS experiment has been proposed [d’Ho99].

4.3.5 Electron single spin asymmetry (SSA)

At intermediate lepton beam energies, one can also extract the imaginary part of the interference between the FVCS and BH amplitudes through the $\vec{e}p \rightarrow ep\gamma$ reaction with a polarized lepton beam, by measuring the out-of-plane angular dependence of the produced photon [Kro96]. It was found in Refs. [Gui98, Vdh98] that the resulting electron single spin asymmetry (SSA)

$$\mathcal{A}^{\text{SSA}} = \frac{\sigma_{e,h=+1/2} - \sigma_{e,h=-1/2}}{\sigma_{e,h=+1/2} + \sigma_{e,h=-1/2}}, \quad (206)$$

with $\sigma_{e,h}$ the cross section for an electron of helicity h , can be sizeable for HERMES ($E_e = 27$ GeV) and JLab ($E_e = 4 - 11$ GeV) beam energies. The helicity difference ($\sigma_{e,h=+1/2} - \sigma_{e,h=-1/2}$) vanishes for the BH process and depends linearly on the imaginary part of the DVCS amplitude. This helicity difference is therefore directly proportional to the GPDs along the line $x = \xi$, and maps out the 'envelope' function $H(\xi, \xi, t)$, and analogously for E , \tilde{H} and \tilde{E} .

In the following, we discuss the SSA to twist-3 accuracy and show the sensitivity of the SSA to different parametrizations of the GPDs in kinematics at HERMES ($E_e = 27$ GeV) and JLab ($E_e = 4.23$ GeV), where this SSA has been measured recently.

In Fig. 25, we show the Φ -dependence of the DVCS cross section and of the single spin asymmetry (SSA) for the same values of Q^2 and t as in Figs. 23 and 24, and for a value of $x_B = 0.15$, accessible at HERMES. Note that, due to parity invariance, the SSA is odd in Φ . We therefore display only half of the Φ range, i.e. Φ between 0° and 180° .

When comparing Figs. 23, 24 with Fig. 25, it is firstly seen that the cross sections for the $ep \rightarrow ep\gamma$ process increases strongly when decreasing x_B at fixed Q^2 and fixed t , mainly due to the growth of the BH amplitude. Due to this large BH amplitude, the relative twist-3 effect on the cross section in Fig. 25 is smaller than the ones in Figs. 23, 24. However, the large BH amplitude leads to a large value for the SSA through its interference with the DVCS process. At (pure) twist-2 level, the SSA originates from the interference of the imaginary part of the DVCS amplitude and the (real) BH amplitude. In case the BH is approximated by its leading term in an expansion in $1/Q$, the twist-2 SSA displays a pure $\sin \Phi$ structure. Due to the more complicated Φ -dependence of the BH at the lower values of Q^2 , this form gets distorted and its maximum displaced. Note that, for practical considerations, our "twist-2" DVCS calculations include kinematical higher twist terms as well as the gauge restoring terms according to Eq. (202). Their effect can be seen in the slight change in the SSA (of the percent level), due to the DVCS process by itself (i.e. when increasing the real part of the DVCS amplitude by adding the D-term contribution, the curves for the SSAs are slightly displaced).

We next discuss the twist-3 effects, calculated in WW approximation, on the SSA for the DVCS process. One sees from Fig. 25 that the twist-3 corrections induce an (approximate) $\sin(2\Phi)$ structure in the SSA. The amplitude of the $\sin(2\Phi)$ term is however rather small and the twist-3 effects change the SSA by less than 5 % in the kinematics corresponding to $t/Q^2 = 0.1$. It was checked that at $x_B = 0.3$ and for a value $t/Q^2 = 0.1$, the twist-3 effects on the SSA are of similar size. One therefore observes that although the twist-3 effects in WW approximation can provide a sizeable contribution to the real part of the amplitude (see Fig. 23), they modify the imaginary part, and hence the SSA, to a much lesser extent.

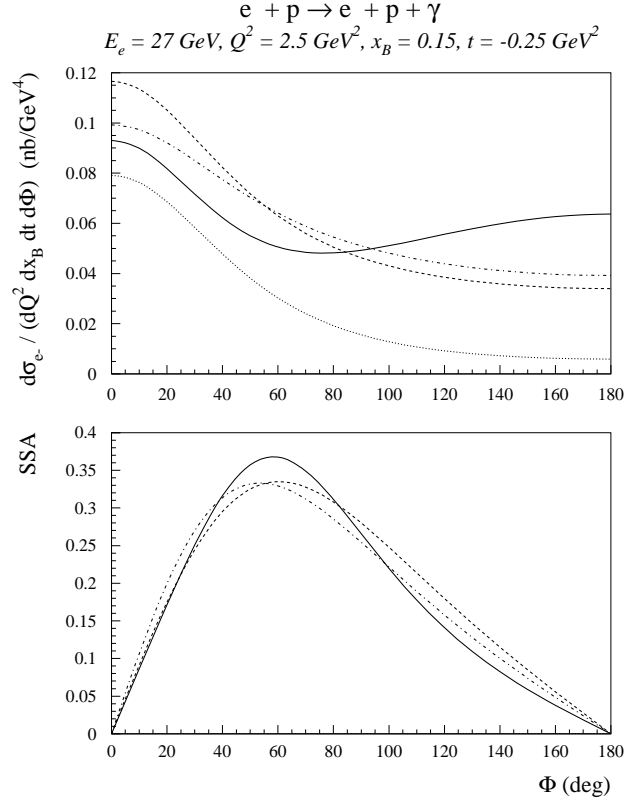


Figure 25: Invariant cross section for the $e^- p \rightarrow e^- p \gamma$ reaction (upper panel) and DVCS single spin asymmetry (lower panel) at $E_e = 27 \text{ GeV}$, for the kinematics as indicated in the figure. Curve conventions as in Fig. 23.

In Figs. 26 and 27 we investigate the sensitivity of the SSA to different parametrizations of the GPD H in kinematics of a HERMES experiment [Air01] and of a JLab experiment by the CLAS Collaboration [Step01, Bur01b, Guid01].

The calculations in the previous figures (Figs. 23 - 25) have been performed using the values $b_{val} = b_{sea} = 1$ for the parameters which enter in the profile function of Eq. (148) to reconstruct the GPD H . In Figs. 26 and 27, the SSA to twist-3 accuracy is shown for different values of b_{val} and b_{sea} . One sees that increasing the value of b_{val} and b_{sea} decreases the size of the SSA. It is seen from Fig. 15 that by increasing b_{val} and b_{sea} , one approaches the forward quark distribution (which corresponds to the limit $b_{val} = b_{sea} = \infty$). One may use this sensitivity to extract the parameters b_{val} and b_{sea} from accurate measurements of the SSA. For example, one sees from Fig. 27 that the maximum of the SSA is reduced to about 80 % of its value when increasing the values of b_{val} and b_{sea} over the indicated range.

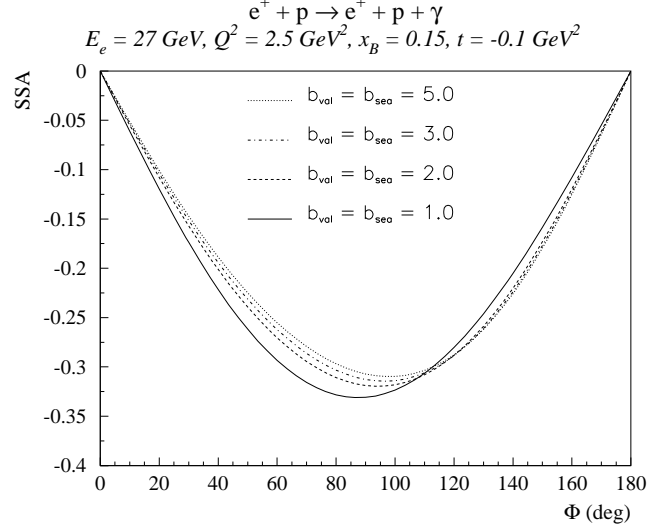


Figure 26: Sensitivity of the single spin asymmetry for the $e^+p \rightarrow e^+p\gamma$ reaction, in the HERMES kinematics [Air01], to different values of the parameters b_{val} and b_{sea} as indicated, which enter in the parameterization of the GPDs H^u and H^d (see Sec. 4.2.1). All calculations include the twist-3 effects to the DVCS amplitude.

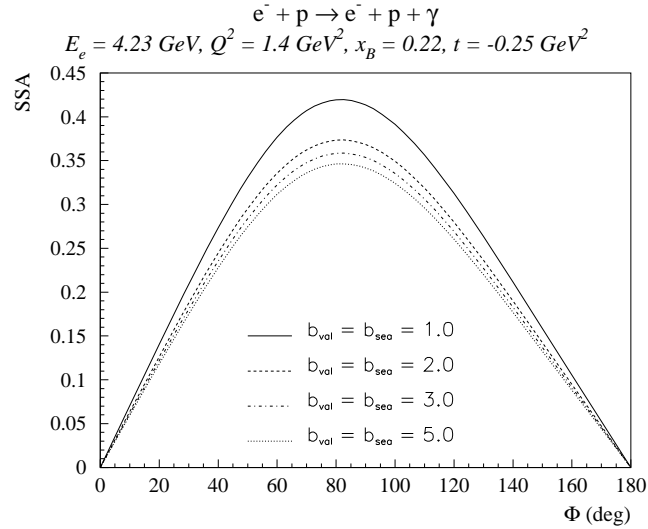


Figure 27: Sensitivity of the single spin asymmetry for the $e^-p \rightarrow e^-p\gamma$ reaction, in the CLAS kinematics [Step01], to different values of the parameters b_{val} and b_{sea} as indicated, which enter in the parameterization of the GPDs H^u and H^d (see Sec. 4.2.1). All calculations include the twist-3 effects to the DVCS amplitude.

The previous figures for DVCS observables have all been obtained by neglecting the GPD E (except for its D-term contribution of Eq. (153)). In Fig. 28, we investigate the effect of the GPD E on the DVCS SSA, using the three-component parametrization (D-term, valence contribution, and “vector-meson” (VM) contribution) of Eqs. (154, 174). This parametrization allows to see directly the sensitivity of observables to the total angular momentum contribution of the u -quark (J^u) and d -quark (J^d) to the proton spin.

In Fig. 28, we show the SSA in kinematics accessible at HERMES for different values of J^u (for a value $J^d = 0$) corresponding to the values shown in Fig. 20. Because the SSA is sensitive to the imaginary part of the DVCS amplitude (apart from a small contribution to the SSA due to the DVCS process alone, i.e. in absence of the BH process), it is mainly sensitive to the valence component of the GPD E^u (upper plot in Fig. 20). Indeed, the D-term and VM contributions to the GPD E give rise to a real amplitude. By comparing Fig. 20 (upper plot) and Fig. 28, one sees that neglecting the contribution of the GPD E^u , corresponds approximately to the value $J^u \sim 0.2$. Furthermore, one sees that varying the value of J^u from $J^u = 0.1$ to $J^u = 0.4$ changes the SSA by about 10% of its value. Since the sensitivity of the DVCS SSA to J^u (and J^d) is modest, it calls for precise measurements as well as detailed studies of higher-twist effects and NLO corrections. However, the physical importance of J^u and J^d warrants such dedicated efforts.

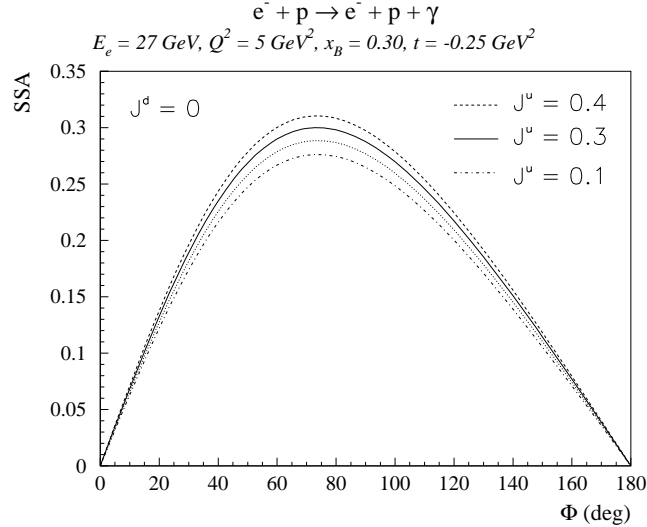


Figure 28: Sensitivity of the SSA for the $e^-p \rightarrow e^-p\gamma$ reaction, in HERMES kinematics, to different values of the quark contributions to the proton spin, J^u and J^d , which enter in the parametrization of the GPDs E^u and E^d (see Sec. 4.2.3). The dotted curve corresponds to the calculation when neglecting the contribution of the GPDs E^u and E^d . The calculations are performed for the BH + twist-2 DVCS amplitude.

In Fig. 29, we investigate the t -dependence of the DVCS cross section and SSA to twist-3 accuracy in CLAS kinematics. One sees from Fig. 29 that both cross section and SSA display a qualitative change with increasing values of $-t$ (note that the SSA vanishes at $t = t_{min}$). Furthermore, it is seen that when increasing the value of $-t$ at

fixed Q^2 and fixed x_B , the shape of the SSA changes from the “ $\sin \Phi$ ” dependence and adopts an increasingly larger “ $\sin(2\Phi)$ ” twist-3 component. This qualitative change in the t -dependence is important to investigate experimentally to have confidence in the extraction of GPDs from a fit to SSA data.

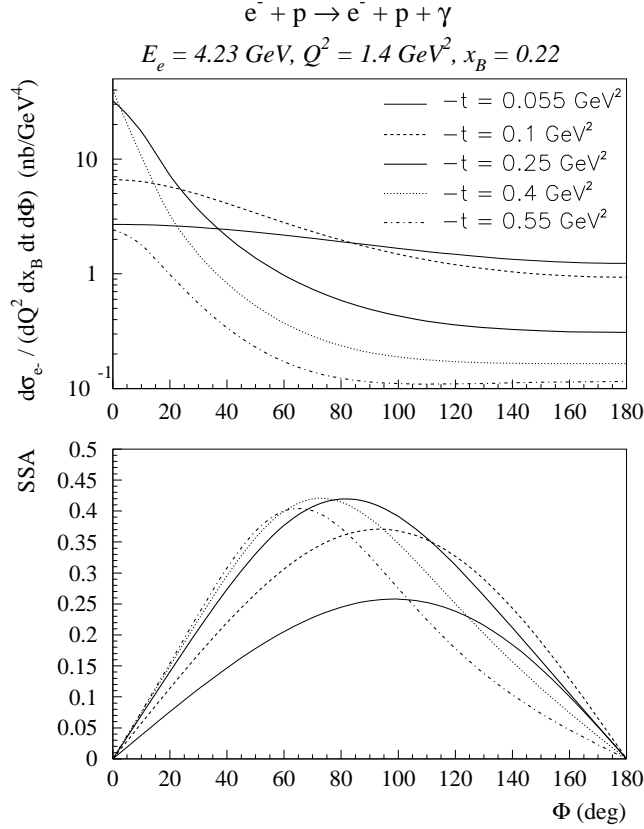


Figure 29: Effect of the twist-3 corrections on the Φ -dependence of the $e^- p \rightarrow e^- p \gamma$ invariant cross section (upper panel) and SSA (lower panel) in CLAS kinematics, for different values of the momentum transfer $-t$ as indicated in the figure. All calculations represent BH + twist-2 + twist-3 DVCS cross sections for $b_{val} = b_{sea} = 1.0$.

In Fig. 30, we investigate the sensitivity of the DVCS SSA to different models for the t -dependence of the GPD H (we perform this comparison for the twist-2 DVCS amplitude). We compare the factorized model of Eq. (149) which has been used in all calculations before with an unfactorized, Regge inspired model of Eqs. (135,152) (with $\alpha' = 0.8 \text{ GeV}^{-2}$), which has an exponential t -dependence and exhibits shrinkage at small values of ξ , as was shown in Fig. 17. One sees from Fig. 30 that at $-t = 0.25 \text{ GeV}^2$, the unfactorized form leads to a slightly reduced SSA compared to the factorized one. However, for a value of $-t = 0.55 \text{ GeV}^2$, one already sees a noticeable reduction of the unfactorized model over the factorized one, and the SSA gets reduced to about 65 % of its value when using an unfactorized ansatz.

Such important sensitivity clearly points out the need to map out experimentally the t -dependence of the SSA carefully in order to extract GPDs. It also stresses the need from the theoretical side to study the parametrization of the t -dependence of GPDs in more detail in the future.

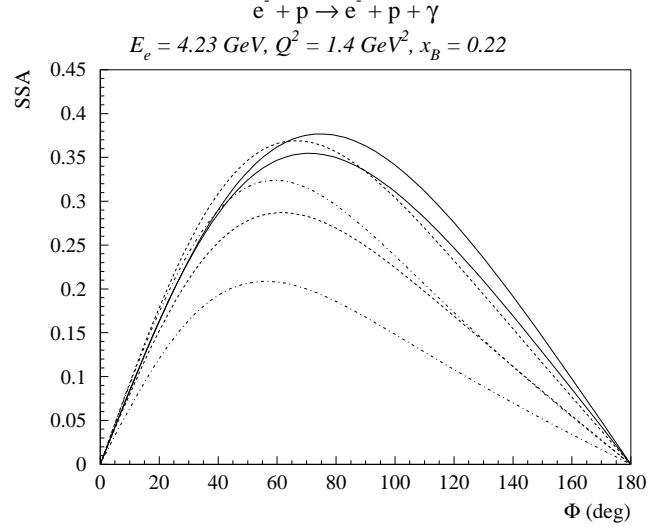


Figure 30: Single spin asymmetry for the $e^-p \rightarrow e^-p\gamma$ reaction in CLAS kinematics, for two models for the t -dependence of the GPD H . The factorized model of Eq. (149) (thick upper curves) is compared to the unfactorized (Regge inspired) model of Eqs. (135,152) (thin lower curves) for different values of $-t$: 0.25 GeV^2 (full curves), 0.4 GeV^2 (dashed curves), 0.55 GeV^2 (dashed-dotted curves). All calculations represent BH + twist-2 DVCS cross sections for $b_{val} = b_{sea} = 1.0$.

4.4 DVCS with $N \rightarrow \Delta$ transition

To derive the $N \rightarrow \Delta$ DVCS amplitudes, we use analogously as for $N \rightarrow N$ DVCS a frame where the virtual photon momentum q^μ and the average $N\Delta$ momentum \bar{P}^μ , defined in Eq. (85), are collinear along the z -axis and in opposite directions. By denoting the lightlike vector along the positive and negative z -directions as \tilde{p}^μ and n^μ respectively, we can decompose the physical momenta of the $N \rightarrow \Delta$ DVCS process as follows :

$$\bar{P}^\mu = \frac{1}{2} (p^\mu + p'^\mu) = \tilde{p}^\mu + \frac{\bar{m}_{N\Delta}^2}{2} n^\mu, \quad (207)$$

$$q^\mu = - \left(2\xi' \right) \tilde{p}^\mu + \left(\frac{Q^2}{4\xi'} \right) n^\mu, \quad (208)$$

$$\Delta^\mu \equiv p'^\mu - p^\mu = - (2\xi) \tilde{p}^\mu + \left[\xi \bar{m}_{N\Delta}^2 + \frac{1}{2} (m_\Delta^2 - m_N^2) \right] n^\mu + \Delta_\perp^\mu, \quad (209)$$

$$q'^\mu \equiv q^\mu - \Delta^\mu = -2 \left(\xi' - \xi \right) \tilde{p}^\mu + \left[\frac{Q^2}{4\xi'} - \xi \bar{m}_{N\Delta}^2 - \frac{1}{2} (m_\Delta^2 - m_N^2) \right] n^\mu - \Delta_\perp^\mu, \quad (210)$$

where the variables $\bar{m}_{N\Delta}^2$, ξ' and ξ are given by

$$\bar{m}_{N\Delta}^2 = \frac{1}{2} (m_N^2 + m_\Delta^2) - \frac{\Delta^2}{4}, \quad (211)$$

$$2\xi' = \frac{\bar{P} \cdot q}{\bar{m}_{N\Delta}^2} \left[-1 + \sqrt{1 + \frac{Q^2 \bar{m}_{N\Delta}^2}{(\bar{P} \cdot q)^2}} \right], \quad (212)$$

$$2\xi = 2\xi' \cdot \frac{Q^2 - \Delta^2 - (2\xi') (m_\Delta^2 - m_N^2)}{Q^2 + \bar{m}_{N\Delta}^2 (2\xi')^2}. \quad (213)$$

The leading order $N \rightarrow \Delta$ DVCS tensor follows from the handbag diagrams (Fig. 1 where the outgoing nucleon is replaced by a Δ^+). By parametrizing the $N \rightarrow \Delta$ matrix elements of the vector and axial vector bilocal quark operators as in Eqs. (84) and (90) respectively, the leading order $N \rightarrow \Delta$ DVCS tensor $H^{\mu\nu}$, defined in an analogous way as in Eq. (182), is given by :

$$\begin{aligned} H^{\mu\nu} (\gamma^* p \rightarrow \gamma \Delta^+) &= \frac{1}{2} [\tilde{p}^\mu n^\nu + \tilde{p}^\nu n^\mu - g^{\mu\nu}] \int_{-1}^{+1} dx C^+(x, \xi) \\ &\times \sqrt{\frac{2}{3}} \frac{1}{6} \bar{\psi}^\beta(p') \left\{ H_M(x, \xi, t) (-\mathcal{K}_{\beta\kappa}^M) n^\kappa \right. \\ &\quad + H_E(x, \xi, t) (-\mathcal{K}_{\beta\kappa}^E) n^\kappa \\ &\quad \left. + H_C(x, \xi, t) (-\mathcal{K}_{\beta\kappa}^C) n^\kappa \right\} N(p) \\ &+ \frac{1}{2} [i \varepsilon^{\nu\mu\kappa\lambda} n_\kappa \tilde{p}_\lambda] \int_{-1}^{+1} dx C^-(x, \xi) \\ &\times \frac{1}{6} \bar{\psi}^\beta(p') \left\{ C_1(x, \xi, t) n_\beta + C_2(x, \xi, t) \Delta_\beta \frac{\Delta \cdot n}{m_N^2} \right. \\ &\quad \left. + C_3(x, \xi, t) \frac{1}{m_N} (\not{\Delta} n_\beta - \not{n} \Delta_\beta) \right\} \end{aligned}$$

$$+ C_4(x, \xi, t) \frac{2}{m_N^2} (\Delta \cdot \bar{P} n_\beta - \Delta_\beta) \Big\} N(p) , \quad (214)$$

where the factor $1/6$ in Eq. (214) results from the quadratic quark charge combination $(e_u^2 - e_d^2)/2$.

To give estimates for the $N \rightarrow \Delta$ DVCS amplitudes, we need a model for the $N \rightarrow \Delta$ GPDs which appear in Eq. (214). Here we will be guided by the large N_c relations discussed in Sec. 2.7. These relations connect the $N \rightarrow \Delta$ GPDs H_M, C_1 and C_2 to the $N \rightarrow N$ isovector GPDs $E^u - E^d$, $\tilde{H}^u - \tilde{H}^d$ and $\tilde{E}^u - \tilde{E}^d$ respectively, as expressed by Eq. (93). All other (sub-dominant) GPDs, which vanish at leading order in the $1/N_c$ expansion, are set equal to zero in our estimates for the processes involving the $N \rightarrow \Delta$ GPDs. For the $N \rightarrow N$ GPDs, we use the phenomenological ξ -dependent ansatz as discussed in Sec. 4.2.

For the $N \rightarrow \Delta$ DVCS in the near forward direction, unlike the $N \rightarrow N$ DVCS case, the axial transitions (distributions C_1 and C_2) are numerically much more important than the vector transition (distribution H_M). This is because the H_M comes with a momentum transfer (Δ) in the tensor $\mathcal{K}_{\beta\kappa}^M$ as seen from Eq. (88). In contrast, the GPD C_1 , which is proportional to the polarized quark distribution in the forward limit ($\Delta \rightarrow 0$), enters with no momentum transfer in Eq. (192). Besides C_1 , the distribution C_2 is numerically most important as it contains a pion-pole contribution. The π^0 pole contribution to the $N \rightarrow \Delta$ DVCS amplitude can be evaluated analytically by using :

$$\int_{-1}^{+1} dx \left[\frac{1}{x - \xi + i\epsilon} - \frac{1}{x + \xi - i\epsilon} \right] \frac{1}{6} C_{2,\pi\text{-pole}}(x, \xi, t) = -\frac{1}{2\xi} \frac{\sqrt{3}}{4} h_A(t) , \quad (215)$$

with the pion-pole part of the pseudoscalar form factor $h_A(t)$ given by Eq. (41). This leads then for the π^0 pole contribution to the $N \rightarrow \Delta$ DVCS tensor

$$H_{\pi\text{-pole}}^{\mu\nu}(\gamma^* p \rightarrow \gamma \Delta^+) = \frac{1}{2} i \varepsilon^{\nu\mu\kappa\lambda} n_\kappa \tilde{p}_\lambda \frac{g_A \sqrt{3}}{-t + m_\pi^2} \bar{\psi}^\beta(p') \Delta_\beta N(p) . \quad (216)$$

The $N \rightarrow \Delta$ DVCS process can be accessed experimentally through the $ep \rightarrow e\Delta^+\gamma$ reaction. In Fig. 31, we show our predictions for the fivefold differential $ep \rightarrow e\Delta^+\gamma$ cross sections in the JLab energy range. As for the $ep \rightarrow ep\gamma$ reaction, there is also for the $ep \rightarrow e\Delta^+\gamma$ reaction an analog contribution when the photon is emitted from the electron line, which is the Bethe-Heitler (BH) process. In comparison with the BH for the $ep \rightarrow ep\gamma$ reaction, the BH process in the $ep \rightarrow e\Delta^+\gamma$ reaction is reduced by an order of magnitude in the near forward direction. Firstly, this is due to the photon propagator in the BH process, which goes like $1/t$, which is smaller for the $N \rightarrow \Delta$ case due to the larger value of t_{min} in the unequal mass case compared to the $N \rightarrow N$ transition. Secondly, the electromagnetic $N \rightarrow \Delta$ vertex in the BH process contains an additional momentum transfer (magnetic $N \rightarrow \Delta$ transition), which results in an additional suppression at the small angles.

Fig. 31 shows that if one stays away from the BH peaks by going in the opposite halfplane (negative angles on Fig. 31) as the electron lines, the $N \rightarrow \Delta$ DVCS process shows a fast increase with energy and starts to dominate over the BH already around 10 GeV.

As mentioned above, the $N \rightarrow \Delta$ DVCS in the near forward direction is dominated by the axial transitions C_1 and C_2 . The vector transitions, which dominate the $N \rightarrow N$ DVCS are suppressed here by a momentum transfer in the corresponding tensors. Among

the axial transitions, the pion pole contribution in C_2 dominates in the valence region. This is also seen in Fig. 31, where the C_1 contribution to the $N \rightarrow \Delta$ DVCS amplitude is shown separately (at 12 GeV).

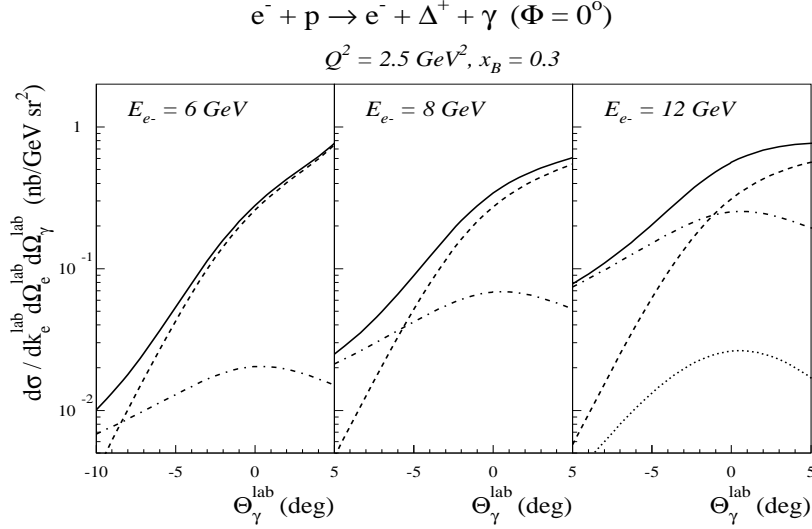


Figure 31: Angular distribution for the $N \rightarrow \Delta$ DVCS cross section at $Q^2 = 2.5 \text{ GeV}^2$, $x_B = 0.3$, and for different beam energies accessible at JLab. A comparison is shown between the BH (dashed curves), the $N \rightarrow \Delta$ DVCS (dashed-dotted curves) and their coherent sum (full curves). We also show the contribution of the C_1 GPD (dotted curve at 12 GeV).

Due to dominance of the pion pole in the valence region, our predictions for $N \rightarrow \Delta$ DVCS are relatively model independent. Therefore, they can be used to estimate the background for the DVCS on the proton as it may be difficult in an actual DVCS experiment to pin down the final state unambiguously. If one does not have the resolution to distinguish the $ep \rightarrow e\gamma\Delta^+ \rightarrow e\gamma\pi^0 p$ reaction from the $ep \rightarrow e\gamma p$ reaction, an estimate of the former process may be helpful to quantify the background from the $ep \rightarrow e\gamma\Delta^+$ contribution.

4.5 Hard meson electroproduction (HMP)

In the previous sections, we discussed how the GPDs enter into different DVCS observables. As discussed in Sec. 1, the GPDs reflect the structure of the nucleon independently of the reaction which probes the nucleon. In this sense, they are universal quantities and can also be accessed, in different flavor combinations, through the hard exclusive electroproduction of mesons - $\pi^{0,\pm}, \eta, \dots, \rho^{0,\pm}, \omega, \phi, \dots$ - (see Fig. 2) for which a QCD factorization proof was given in Refs. [Col97]. According to Ref. [Col97], the factorization applies when the virtual photon is longitudinally polarized, which corresponds to a small size configuration compared to a transversely polarized photon. More technically, for a longitudinally polarized photon the end-point contributions in the meson wave function are power suppressed. Furthermore, it was shown that the cross section for a transversely polarized photon is suppressed by $1/Q^2$ compared to a longitudinally polarized photon.

In the hard scattering regime, the leading order diagrams for meson production are shown in Fig. 32 (T_H part in Fig. 2)²¹. Because the quark helicity is conserved in the hard scattering process, the meson acts as a helicity filter. In particular, the leading order perturbative QCD predicts [Col97] that the longitudinally polarized vector meson channels ($\rho_L^{0,\pm}, \omega_L, \phi_L$) are sensitive only to the unpolarized GPDs (H and E) whereas the pseudo-scalar channels ($\pi^{0,\pm}, \eta, \dots$) are sensitive only to the polarized GPDs (\tilde{H} and \tilde{E}). In comparison to meson electroproduction reactions, we recall that DVCS depends at the same time on *both* the unpolarized (H and E) and polarized (\tilde{H} and \tilde{E}) GPDs. This property makes the hard meson electroproduction reactions complementary to the DVCS process, as it provides an additional tool to disentangle the different GPDs.

It was shown in Ref. [Die99] that the leading twist contribution to exclusive electroproduction of transversely polarized vectors mesons vanishes at all orders in perturbation theory.

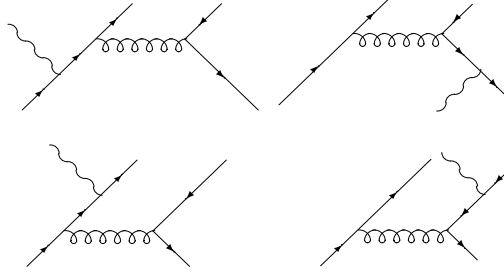


Figure 32: Leading order diagrams for the quark exchange contribution to hard meson electroproduction.

According to the above discussion, we give predictions only for the meson electroproduction observables which involve a longitudinal virtual photon. The longitudinal $\gamma_L^* + p \rightarrow M + p$ two-body cross section $d\sigma_L/dt$ is given by :

$$\frac{d\sigma_L}{dt} = \frac{1}{16\pi(s - m_N^2)\Lambda(s, -Q^2, m_N^2)} \frac{1}{2} \sum_{h_N} \sum_{h'_N} |\mathcal{M}^L(\lambda_M = 0, h'_N; h_N)|^2, \quad (217)$$

²¹For neutral isoscalar mesons with positive C-parity (e.g. f_0, f_2, \dots), besides the quark diagrams shown in Fig. 32, an additional diagram contributes with 2 collinear gluons projecting onto the meson wavefunction [Leh00].

where \mathcal{M}^L is the amplitude for the production of a meson with helicity $\lambda_M = 0$ by a longitudinal photon, and where h_N, h'_N are the initial and final nucleon helicities. Furthermore in Eq. (217), the standard kinematic function $\Lambda(x, y, z)$ is defined by

$$\Lambda(x, y, z) = \sqrt{x^2 + y^2 + z^2 - 2xy - 2xz - 2yz} . \quad (218)$$

which gives $\Lambda(s, -Q^2, m_N^2) = 2m_N |\vec{q}_L|$, where $|\vec{q}_L|$ is the virtual photon momentum in the *lab* system. As the way to extract $d\sigma_L/dt$ from the measured fivefold electroproduction cross section is a matter of convention, all results for $d\sigma_L/dt$ are given with the choice of the flux factor of Eq. (217).

4.5.1 Hard electroproduction of vector mesons

In this section, we consider the vector meson electroproduction processes $\gamma_L^* + N \rightarrow V_L + N$ at large Q^2 on the nucleon N , where V_L ($\rho_L^0, \rho_L^+, \omega_L, \dots$) denotes the produced vector meson with longitudinal polarization. The longitudinal polarization component of the vector meson is obtained experimentally through its decay angular distribution. ρ^0 electroproduction data both at high W ($30 < W < 140$ GeV) [Adl00] as well as at intermediate values of W ($3.8 < W < 6.5$ GeV) [Ack99, Tyt01] support the fact that s-channel helicity conservation (SCHC) holds to good accuracy. This implies that a longitudinally polarized vector meson originates from a longitudinally polarized photon. Therefore, when SCHC holds, one can access the leading order longitudinal photon cross section for vector meson production solely by measuring the decay angular distribution of the vector meson, i.e. without performing a Rosenbluth separation of longitudinal and transverse photon cross sections.

In the valence region, the vector meson amplitude in leading order in Q is obtained from the hard scattering diagrams of Fig. 32. At small x_B , ρ^0 and ω electroproduction can also proceed through a two gluon exchange mechanism, as discussed in [Bro94, Fra96, Rad96b] to which we refer for details. We restrict ourselves in the following discussion to the quark exchange contribution, and will mostly show results in the valence region.

The resulting amplitudes \mathcal{M}^L for electroproduction of longitudinally polarized vector mesons were calculated in Refs. [Man98a, Vdh98], yielding the following expression :

$$\begin{aligned} \mathcal{M}_{V_L}^L &= -ie \frac{4}{9} \frac{1}{Q} \left[\int_0^1 dz \frac{\Phi_{V_L}(z)}{z} \right] \frac{1}{2} (4\pi\alpha_s) \\ &\times \left\{ A_{V_L N} \bar{N}(p') \not{n} N(p) + B_{V_L N} \bar{N}(p') i\sigma^{\kappa\lambda} \frac{n_\kappa \Delta_\lambda}{2m_N} N(p) \right\} , \end{aligned} \quad (219)$$

where $\Phi_{V_L}(z)$ is the distribution amplitude (DA) for a longitudinally polarized vector meson, and where α_s is the strong coupling constant.

For $\rho_L^0 p$ electroproduction on the proton, the amplitudes A and B in Eq. (219) are given by [Man98a, Vdh98] :

$$A_{\rho_L^0 p} = \int_{-1}^1 dx \frac{1}{\sqrt{2}} (e_u H^u - e_d H^d) \left\{ \frac{1}{x - \xi + i\epsilon} + \frac{1}{x + \xi - i\epsilon} \right\} , \quad (220)$$

$$B_{\rho_L^0 p} = \int_{-1}^1 dx \frac{1}{\sqrt{2}} (e_u E^u - e_d E^d) \left\{ \frac{1}{x - \xi + i\epsilon} + \frac{1}{x + \xi - i\epsilon} \right\} , \quad (221)$$

where $e_u = +2/3$ ($e_d = -1/3$) are the u (d) quark charges respectively.

For $\rho_L^+ n$ electroproduction on the proton, the amplitudes A and B are given by [Man99a, Vdh99] :

$$A_{\rho_L^+ n} = - \int_{-1}^1 dx (H^u - H^d) \left\{ \frac{e_u}{x - \xi + i\epsilon} + \frac{e_d}{x + \xi - i\epsilon} \right\}, \quad (222)$$

$$B_{\rho_L^+ n} = - \int_{-1}^1 dx (E^u - E^d) \left\{ \frac{e_u}{x - \xi + i\epsilon} + \frac{e_d}{x + \xi - i\epsilon} \right\}. \quad (223)$$

For $\omega_L p$ electroproduction on the proton, the amplitudes A and B are given by [Man98a, Vdh98] :

$$A_{\omega_L p} = \int_{-1}^1 dx \frac{1}{\sqrt{2}} (e_u H^u + e_d H^d) \left\{ \frac{1}{x - \xi + i\epsilon} + \frac{1}{x + \xi - i\epsilon} \right\}, \quad (224)$$

$$B_{\omega_L p} = \int_{-1}^1 dx \frac{1}{\sqrt{2}} (e_u E^u + e_d E^d) \left\{ \frac{1}{x - \xi + i\epsilon} + \frac{1}{x + \xi - i\epsilon} \right\}. \quad (225)$$

One sees from Eqs. (220-225) that the amplitudes for the hard electroproduction of longitudinally polarized ρ^0 , ρ^+ and ω mesons involve different flavor combinations of the GPDs $H^u(x, \xi, t)$, $H^d(x, \xi, t)$, and analogously for $E^u(x, \xi, t)$, $E^d(x, \xi, t)$. Therefore, measuring those different channels allows to make a flavor decomposition of the GPDs H^q and E^q .

In order to extract the GPDs from cross sections of hard meson electroproduction, one needs to specify the meson distribution amplitude $\Phi_{V_L}(z)$ entering in Eq. (219). For the longitudinally polarized ρ^0 meson, an experimental estimate of the second Gegenbauer coefficient of its distribution amplitude has been given for the first time in Ref. [Cle00], and was found to be $a_2^{(\rho)} = -0.1 \pm 0.2$ at a scale $\langle \mu^2 \rangle = 21.2 \text{ GeV}^2$. Unfortunately the precision in the determination of $a_2^{(\rho)}$ is still too low to discriminate between different model predictions for this quantity (QCD sum rules: 0.18 ± 0.1 [Ball96], 0.08 ± 0.02 [Bak98] and instanton model: -0.14 [Pol99a] all at a scale around $\mu \approx 1 \text{ GeV}$). However all these analyses point to relatively small values for the second Gegenbauer coefficient and favor therefore a DA for the longitudinally polarized ρ meson that is rather close to its asymptotic form.

In view of these findings, we use in all calculations shown below, the asymptotic DA for longitudinally polarized vector mesons :

$$\Phi_{V_L}(z) = f_V 6 z (1 - z), \quad (226)$$

with $f_\rho \approx 0.216 \text{ GeV}$ and $f_\omega \approx 0.195 \text{ GeV}$, determined from the electromagnetic decay $V \rightarrow e^+ e^-$.

One sees from Eq. (219) that the leading order electroproduction amplitude for longitudinally polarized vector mesons is of order $1/Q$, in contrast to the leading order DVCS amplitude which is constant in Q . This difference is due to the additional gluon propagator in the hard scattering amplitude for the leading order meson electroproduction amplitude (see Fig. 32). This also leads to the dependence of the leading order amplitude on the strong coupling constant $\alpha_s(\sim Q^2)$. At large scales Q^2 , the running coupling constant is given by its expression from perturbative analyses. However, the average virtuality of

the exchanged gluon in the leading order meson electroproduction amplitudes can be considerably less than the external Q^2 , which is therefore not the “optimal” choice for the renormalization scale. This puts some caveats on the applicability of the leading order meson electroproduction amplitude to analyse absolute cross sections at accessible scales. The corrections to the leading order vector meson electroproduction amplitude (both in powers of $1/Q$ and in α_s) is still an open question to be addressed in future work.

We next compare the results for ρ_L^0 electroproduction cross sections to the available data. Because the leading order amplitude of Eq. (219) is of order $1/Q$, it predicts a $1/Q^6$ scaling behavior for the cross section $d\sigma_L/dt$. By measuring the Q^2 behavior of the meson electroproduction cross section, one may study how fast one approaches the scaling regime predicted by perturbative QCD. In particular, the measurement of hard electroproduction reactions in the region $Q^2 \approx 1 - 20 \text{ GeV}^2$, which is accessible experimentally, may provide information on the importance of power corrections to the leading order amplitudes. One source of power corrections is evident from the structure of the matrix element of Eq. (5) which defines the GPDs, where the quarks are taken at zero transverse separation. This amounts to neglect, at leading order, the quark’s transverse momentum compared to its large longitudinal (+ component) momentum. A first study of these corrections due to the quark’s intrinsic transverse momentum, assuming a gaussian dependence, has been performed in Ref. [Vdh99]. At virtualities Q^2 of a few GeV^2 , these corrections were found to lead to a sizeable reduction of the cross section [Vdh99], e.g. a factor 4 reduction at $x_B \approx 0.3$ and $Q^2 \approx 4 \text{ GeV}^2$ (see Ref. [Vdh99] for details). A comparison of these calculations to existing ρ_L^0 electroproduction data in the few GeV^2 range is shown in Fig. 33.

As the $\gamma_L^* p \rightarrow \rho_L^0 p$ reaction has mostly been measured at small values of x_B [Der95, Bre98, Adl00] (or equivalently large values of the c.m. energy W of the $\gamma^* p$ system ²²), the calculations in Fig. 33 for ρ_L^0 electroproduction can reveal how the valence region is approached, with decreasing value of W , where one is sensitive to the quark GPDs. For the purpose of this discussion, we call the mechanism proceeding through the quark GPDs of Fig. 2, the quark exchange mechanism (QEM). Besides the QEM, ρ^0 electroproduction at large Q^2 and small x_B proceeds predominantly through a perturbative two-gluon exchange mechanism (PTGEM) as studied in Ref. [Bro94, Fra96]. To compare to the data at intermediate Q^2 , the power corrections due to the parton’s intrinsic transverse momentum dependence were implemented in both mechanisms using the estimate of Ref. [Vdh99]. The comparison of the calculations with the data in Fig. 33 show that the PTGEM explains well the fast increase of the cross section at high c.m. energy (W), but substantially underestimates the data at the lower energies. This is where the QEM is expected to contribute since x_B is then in the valence region. The results including the QEM describe the change of behavior of the data at lower W quite nicely.

Recently, ρ_L^0 data have also been obtained by the HERMES Collaboration for Q^2 up to 5 GeV^2 and around $W \approx 5 \text{ GeV}$ [Air00]. The comparison of the calculations for ρ_L^0 with those data is shown in Fig. 34. One sees from Fig. 34 a clear dominance of the QEM in the intermediate W range as predicted in Refs. [Vdh98, Vdh99]. When including the model estimate for the power corrections, a fairly good agreement with these longitudinal ρ^0 electroproduction data [Air00] is obtained, as seen from Fig. 34.

A dedicated experiment to investigate the onset of the scaling behavior of ρ_L^0 electroproduction in the valence region ($Q^2 \approx 3.5 \text{ GeV}^2$ and $x_B \approx 0.3$) is also planned in the

²² W is expressed in terms of x_B as : $W^2 = m_N^2 + Q^2(1 - x_B)/x_B$.

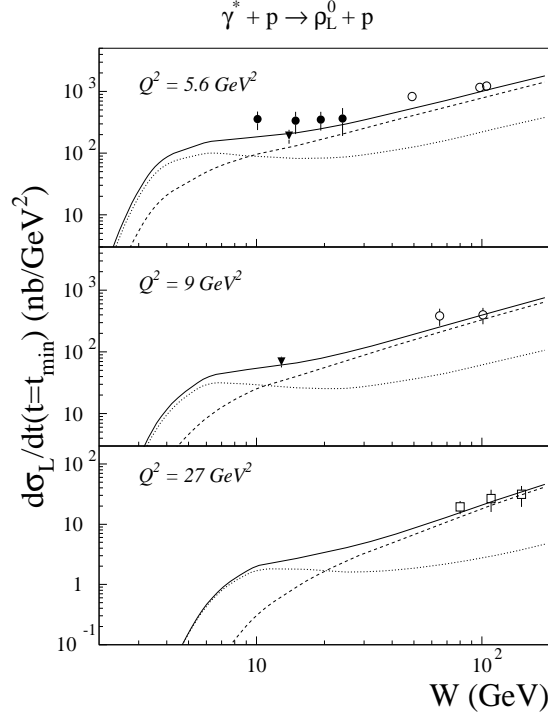


Figure 33: Longitudinal forward differential cross section for ρ_L^0 electroproduction. Calculations compare the quark exchange mechanism (dotted curves) with the two-gluon exchange mechanism (dashed curves) and the sum of both (full curves). The calculations include the corrections due to the intrinsic transverse momentum dependence for the quark exchange [Vdh99] as well as for the two-gluon exchange [Fra96]. The data are from NMC (triangles) [Arn94], E665 (solid circles) [Ada97], ZEUS 93 (open circles) [Der95] and ZEUS 95 (open squares) [Bre98]. Figure from Ref. [Vdh99].

very near future [Guid98] using the CLAS detector at JLab.

Besides the ρ_L^0 electroproduction cross section, the ω_L electroproduction cross section has also been measured recently by the HERMES Collaboration [Tyt01] at intermediate values of $W \approx 5$ GeV. The measurement of the ratio of ω_L/ρ_L^0 electroproduction cross sections at these lower values of W allows one to see the departure from the diffractive regime, at small x_B , where this cross section ratio is given by $\omega_L : \rho_L^0 = 1 : 9$. In the valence region, around $x_B \approx 0.3$, the quark exchange mechanism of Fig. 2 leads to a ratio $\omega_L : \rho_L^0 \approx 1 : 5$ [Col97, Vdh99], which is nearly twice as large as in the diffractive region. This larger ratio of around 0.2 for the ω_L/ρ_L^0 cross sections at larger values of x_B is in good agreement with the recent HERMES measurements [Tyt01], and also supports the dominance of the quark exchange process of Fig. 2.

It is also instructive to compare the t -dependences for vector meson electroproduction cross sections. In particular we found that a factorized ansatz in t for the GPD as in Eq. (149) gives a much less steep t -dependence around $x_B \simeq 0.1$ as the unfactorized (Regge motivated) form of Eq. (152). In particular, the unfactorized form of Eq. (152) leads, in the region $x_B \simeq 0.1$, to an exponential t dependence $d\sigma_L \sim e^{-B|t|}$ in the small $-t$ region.

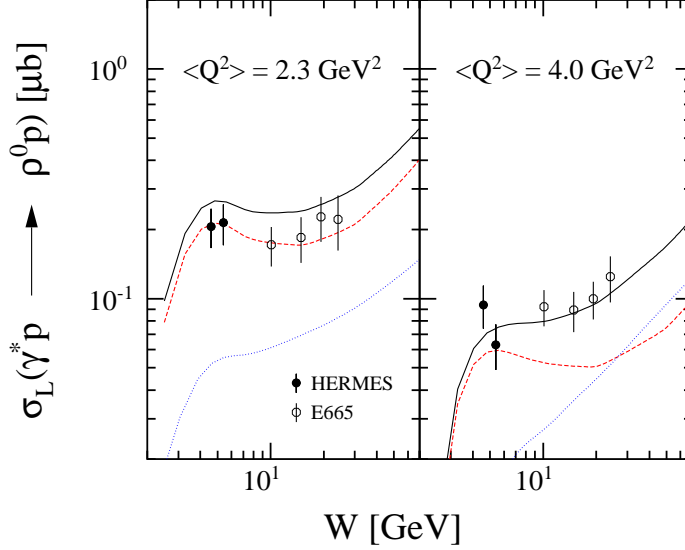


Figure 34: Longitudinal cross section for ρ_L^0 electroproduction. Calculations compare the quark exchange mechanism (dashed curves) with the two-gluon exchange mechanism (dotted curves) and the sum of both (full curves). The calculations include the corrections due to intrinsic transverse momentum dependence as calculated in Ref. [Vdh99]. The data are from E665 (open circles) [Ada97] and HERMES (solid circles) [Air00]. Figure from Ref. [Air00].

When using the value $\alpha' = 0.8 \text{ GeV}^{-2}$ for the Regge slope parameter in Eq. (152), we found for the t -slope of the (twist-2) cross section $d\sigma_L$ for ρ_L^0 electroproduction the value : $B_{\rho^0} \simeq 6.5 \text{ GeV}^{-2}$. This value is remarkably close to the experimentally extracted slope parameters for ρ^0 electroproduction on the proton which has been measured at HERMES [Tyt01] in the kinematic range $0.7 < Q^2 < 5.0 \text{ GeV}^2$ and $4.0 < W < 6.0 \text{ GeV}$, and which was found to be [Tyt01] :

$$B_{\rho^0} = 7.08 \pm 0.14 \text{ (stat.) } {}^{+0.58}_{-0.08} \text{ (syst.) } \text{ GeV}^{-2}. \quad (227)$$

This hints that a Regge type (unfactorized) form as in Eq. (152) might be a reasonable starting point for a more realistic parametrization of the t -dependence of GPDs. The t -slope of the vector meson electroproduction cross sections was also addressed in Ref. [Fra96] where it was shown that higher-twist contributions are able to explain the change of the t -slope with Q^2 . In particular the value of B_{ρ^0} decreases with increasing Q^2 .

Although the data for the vector meson electroproduction channels at intermediate values of x_B discussed above point towards the dominance of the quark exchange mechanism, it would be too premature at the present stage to try to extract quark GPDs from these vector meson electroproduction cross sections. To reach this goal, one first needs to get a better theoretical control over the power (higher-twist) corrections, which is an important topic for future work.

Besides the cross section σ_L , the second observable which involves only longitudinal amplitudes and which is therefore a leading order observable for hard exclusive meson electroproduction, is the transverse spin asymmetry, \mathcal{A}_{VLN} (TSA) for a proton target polarized

perpendicular to the reaction plane (or the equivalent recoil polarization observable). For definiteness let us consider the following (azimuthal) asymmetry :

$$\mathcal{A} = \frac{1}{|S_\perp|} \frac{\int_0^\pi d\beta \sigma(\beta) - \int_\pi^{2\pi} d\beta \sigma(\beta)}{\int_0^{2\pi} d\beta \sigma(\beta)}, \quad (228)$$

where β is the angle between the transverse proton spin S_\perp and the reaction plane (spanned by the virtual photon and the produced meson).

For the electroproduction of longitudinally polarized vector mesons, induced by a longitudinal virtual photon, we found this transverse spin asymmetry to be given by (compare with the corresponding Eq. (240) for the pion) :

$$\mathcal{A}_{V_L N} = - \frac{2 |\Delta_\perp|}{\pi} \frac{\text{Im}(AB^*)/m_N}{|A|^2 (1 - \xi^2) - |B|^2 (\xi^2 + t/(4m_N^2)) - \text{Re}(AB^*) 2\xi^2}, \quad (229)$$

which is proportional to the modulus $|\Delta_\perp|$ of the perpendicular component of the momentum transfer Δ of Eq. (186), and where A and B are given by Eqs. (220-225) for the different vector meson channels. One sees that the transverse spin asymmetry is proportional to the imaginary part of the *interference* of the amplitudes A and B , which contain the GPDs H and E respectively. Therefore, it depends *linearly* on the GPD E . Note that in contrast, both in the DVCS cross sections and SSA as well as in the longitudinal cross sections for (longitudinally polarized) vector mesons, the GPD E only enters besides a large contribution of the GPD H . In order to increase the sensitivity to the GPD E in those observables, one needs to increase the value of the momentum transfer Δ , because the function E is kinematically suppressed in the amplitudes when $\Delta \rightarrow 0$. Since the value of Δ should remain small however in comparison with the hard scale Q in order not to be totally dominated by higher twist effects, the DVCS cross sections, SSA and vector meson cross sections give only a limited handle in the extraction of the GPD E . In this context, the transverse spin asymmetry of Eq. (229) provides a unique observable to extract the GPD E .

Besides, also the theoretical uncertainties and open questions which we discussed for the meson electroproduction cross sections largely disappear for the transverse spin asymmetry. Indeed, because the transverse spin asymmetry involves a ratio of cross sections, the dependence on the distribution amplitude and the strong coupling constant in Eq. (219) drops out in this ratio. This also suggest that the transverse spin asymmetry is less sensitive to pre-asymptotic effects and that the leading order expression of Eq. (229) is already accurate at accessible values of Q^2 (in the range of a few GeV^2).

Due to its linear dependence on the GPD E , the transverse spin asymmetry for longitudinally polarized vector mesons opens up the perspective to extract from it the total angular momentum contributions J^u and J^d of the u - and d -quarks to the proton spin. Indeed, in the three-component parametrization for E^u and E^d presented in Eqs. (154, 174), the values of J^u and J^d enter as free parameters (see Figs. 20, 21). We therefore investigate in the following the dependence of the transverse spin asymmetry for ρ_L^0 , ω_L and ρ_L^\pm electroproduction on J^u and J^d . Due to the different u - and d -quark content of the vector mesons, the asymmetries for the ρ_L^0 , ω_L and ρ_L^\pm channels are sensitive to different combinations of J^u and J^d . From Eqs. (220-225), one finds that the ρ_L^0 production is mainly sensitive to the combination $2J^u + J^d$, ω_L to the combination $2J^u - J^d$, and ρ_L^\pm to the isovector combination $J^u - J^d$.

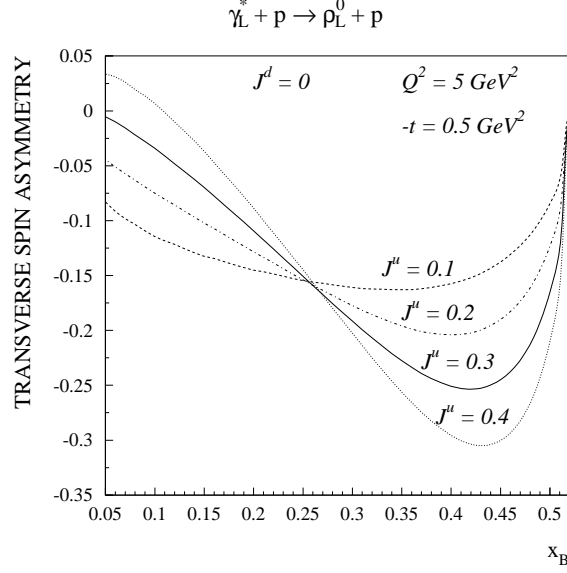


Figure 35: Transverse spin asymmetry for the $\gamma_L^* \vec{p} \rightarrow \rho_L^0 p$ reaction at $t = -0.5 \text{ GeV}^2$ and $Q^2 = 5 \text{ GeV}^2$. The estimates are given using the three-component model for E^u and E^d as described in Sec. 4.2.3, where J^d was fixed to the value $J^d = 0$. The curves show the sensitivity to the value of J^u as indicated on the curves, which enters in the model for the GPD E^u , shown in Fig. 20. For the GPDs H^u , H^d and for the valence part of E^u , E^d , the values $b_{val} = b_{sea} = 1$ have been used.

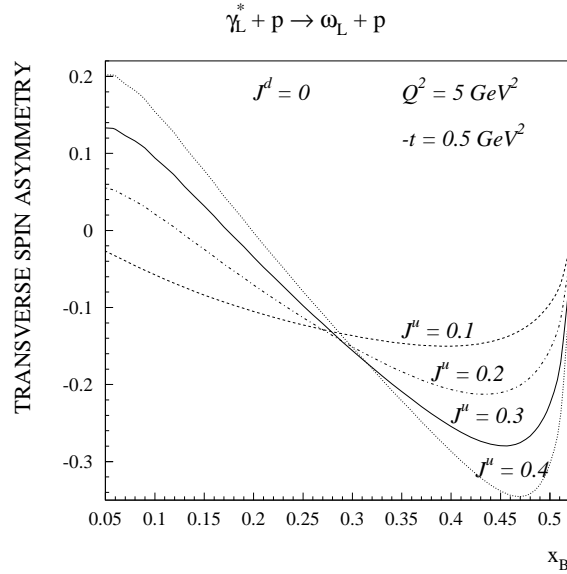


Figure 36: Same as Fig. 35 but for the $\gamma_L^* \vec{p} \rightarrow \omega_L p$ reaction.

In Figs. 35 and 36 we firstly show the x_B dependence of the transverse spin asymmetry for ρ_L^0 and ω_L production at $Q^2 = 5 \text{ GeV}^2$ and $-t = 0.5 \text{ GeV}^2$. In these figures, we fixed the value of $J^d = 0$, which is close to the valence estimate of Eq. (162), for which the VM part of E^d vanishes (see Fig. 21). For this value of J^d , we then demonstrate in Figs. 35,36 the sensitivity of the ρ_L^0 and ω_L transverse spin asymmetries to different values of J^u . Note that the value $J^u \approx 0.3$ would correspond to the valence estimate of Eq. (161), as is also seen from the vanishing of the VM part of E^u in Fig. 20 for this value.

From Figs. 35,36, one sees that the transverse spin asymmetries for ρ_L^0 and ω_L electroproduction display a pronounced sensitivity to J^u around $x_B \approx 0.4$, where asymmetries are predicted in the -15 % to -30 % range according to the value of J^u . This transverse spin asymmetry for ρ_L^0 and ω_L at large x_B gets enhanced by the (isoscalar) D-term, which contributes to both processes. In particular, it gives a large real part to the amplitude B in Eq. (229) which is then multiplied by the imaginary part of the amplitude A , proportional to $H(\xi, \xi, t)$. At these larger values of x_B a precise extraction of the values of J_u and J_d from the ρ_L^0 and ω_L asymmetries requires a good knowledge of the D-term which can be measured e.g. through the charge asymmetry for DVCS as discussed in Sec. 4.3.4. At smaller values of x_B , where the D-term contribution shrinks away, the sensitivity to J^u and J^d arises through both the real and imaginary parts of B , which depend on J^u through the VM contribution to E^u (giving a purely real part to B) and the valence contribution to E^u (giving predominantly an imaginary contribution to B).

For comparison, we show in Fig. 37 the transverse spin asymmetry for ρ_L^0 at the smaller value of $-t = 0.25 \text{ GeV}^2$ (the asymmetry of Eq. (229) is proportional to $|\Delta_\perp|$) and $Q^2 = 2.5 \text{ GeV}^2$. Those values are at present already accessible at HERMES. It will therefore be very interesting to provide a first measurement of this asymmetry in the near future for a transversely polarized target.

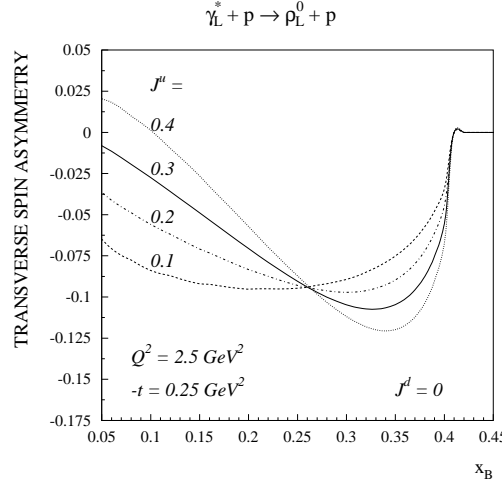


Figure 37: Same as Fig. 35, but for $t = -0.25 \text{ GeV}^2$ and $Q^2 = 2.5 \text{ GeV}^2$.

Although we showed the transverse spin asymmetries in Figs. 35,36, for the value $J^d = 0$, one can vary this value and exploit the different dependence of the ρ_L^0 (sensitive to $2J^u + J^d$) and ω_L (sensitive to $2J^u - J^d$) transverse spin asymmetries to extract information on the different flavor contributions.

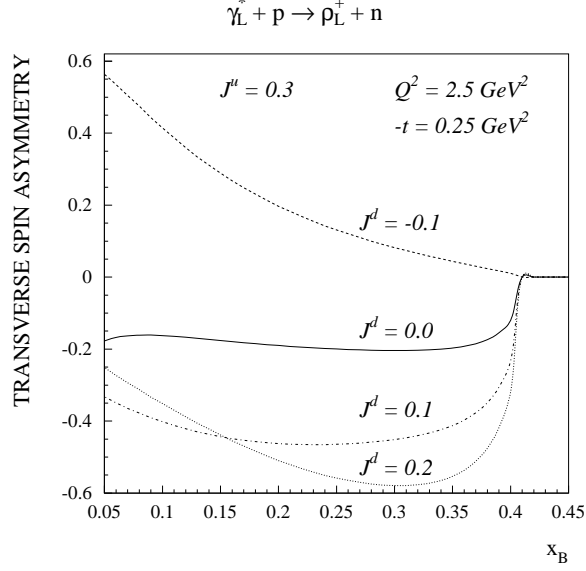


Figure 38: Transverse spin asymmetry for the $\gamma_L^* \vec{p} \rightarrow \rho_L^+ n$ reaction at $t = -0.25 \text{ GeV}^2$ and $Q^2 = 2.5 \text{ GeV}^2$. The estimates are given using the three-component model for E^u and E^d , where J^u was fixed to the value $J^u = 0.3$. The curves show the sensitivity to the value of J^d as indicated on the curves, which enters in the model for the GPD E^d , shown in Fig. 21.

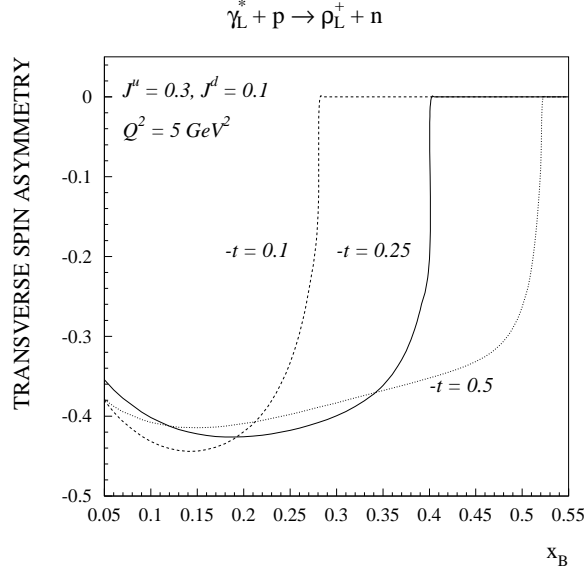


Figure 39: Transverse spin asymmetry for the $\gamma_L^* \vec{p} \rightarrow \rho_L^+ n$ reaction at $Q^2 = 5 \text{ GeV}^2$ for different values of t , as indicated on the curves (in GeV^2). The estimates are given using the three-component model for E^u and E^d , where J^u and J^d were fixed as indicated on the figure.

One is directly sensitive to the difference $J^u - J^d$ by measuring the transverse spin asymmetry for ρ_L^+ production. The corresponding asymmetry is shown in Fig. 38 for a value of $J^u = 0.3$ and for different values of J^d . One observes that this asymmetry can be very large over a wide range in x_B . Because for ρ_L^+ , the isoscalar D-term contribution is absent, this large value for the asymmetry mainly originates from the product of the imaginary part of the amplitude A (proportional to $H(\xi, \xi, t)$) with the real part of the amplitude B (mainly proportional to the VM part of $E^u - E^d$ which contains the sensitivity to $J^u - J^d$).

In Fig. 39, we also show the t -dependence of the ρ_L^+ transverse spin asymmetry. One observes how by increasing the value of $-t$, the kinematical accessible region over which one can access this asymmetry gets larger.

Summarizing this section, we have identified the transverse spin asymmetry for longitudinally polarized vector mesons as a unique observable which depends *linearly* on the GPD E . These asymmetries for ρ_L^0 , ω_L and ρ_L^+ display a large sensitivity to the total angular momentum contributions J^u and J^d of the u - and d -quarks to the proton spin. As these asymmetries represent a ratio of cross sections, several theoretical uncertainties drop out. Also from the experimental point of view, such ratios are much easier to measure than absolute cross sections. A first measurement of these asymmetries will therefore be of high interest in the quest of our understanding of the quark contributions to the proton spin.

4.5.2 Hard electroproduction of pions

In this section, we discuss the hard pion electroproduction processes $\gamma_L^* + p \rightarrow \pi^+ + n$ and $\gamma_L^* + p \rightarrow \pi^0 + p$.

The pion electroproduction amplitude \mathcal{M}_π^L for a longitudinal virtual photon is also obtained in leading order in Q from the hard scattering diagrams of Fig. 32. This leads to the amplitude :

$$\begin{aligned} \mathcal{M}_\pi^L &= -ie \frac{4}{9} \frac{1}{Q} \left[\int_0^1 dz \frac{\Phi_\pi(z)}{z} \right] \frac{1}{2} (4\pi\alpha_s) \\ &\times \left\{ A_{\pi N} \bar{N}(p') \not{\epsilon} \gamma_5 N(p) + B_{\pi N} \bar{N}(p') \gamma_5 \frac{\Delta \cdot n}{2m_N} N(p) \right\}, \end{aligned} \quad (230)$$

where $\Phi_\pi(z)$ is the pion distribution amplitude, and where α_s is the strong coupling constant.

For $\pi^0 p$, the amplitudes A and B in Eq. (230) are given by [Man98a, Vdh98] :

$$A_{\pi^0 p} = \int_{-1}^1 dx \frac{1}{\sqrt{2}} \left(e_u \tilde{H}^u - e_d \tilde{H}^d \right) \left\{ \frac{1}{x - \xi + i\epsilon} + \frac{1}{x + \xi - i\epsilon} \right\}, \quad (231)$$

$$B_{\pi^0 p} = \int_{-1}^1 dx \frac{1}{\sqrt{2}} \left(e_u \tilde{E}^u - e_d \tilde{E}^d \right) \left\{ \frac{1}{x - \xi + i\epsilon} + \frac{1}{x + \xi - i\epsilon} \right\}. \quad (232)$$

For $\pi^+ n$ electroproduction on the proton, the amplitudes A and B are given by [Man99b, Fra99a] :

$$A_{\pi^+ n} = - \int_{-1}^1 dx \left(\tilde{H}^u - \tilde{H}^d \right) \left\{ \frac{e_u}{x - \xi + i\epsilon} + \frac{e_d}{x + \xi - i\epsilon} \right\}, \quad (233)$$

$$B_{\pi^+ n} = - \int_{-1}^1 dx \left(\tilde{E}^u - \tilde{E}^d \right) \left\{ \frac{e_u}{x - \xi + i\epsilon} + \frac{e_d}{x + \xi - i\epsilon} \right\}. \quad (234)$$

In the amplitudes for pion electroproduction of Eq. (230), the pion distribution amplitude Φ_π enters. Recent data [Gro98] for the $\pi^0 \gamma^* \gamma$ transition form factor up to $Q^2 = 9 \text{ GeV}^2$ are in agreement²³ with the asymptotic form of the distribution amplitude, given by :

$$\Phi_\pi(z) = \sqrt{2} f_\pi 6z(1-z), \quad (235)$$

with $f_\pi = 0.0924 \text{ GeV}$ from the pion weak decay.

As discussed in Sec. 2.4.2, the function $\tilde{E}^u - \tilde{E}^d$ contains a strong pion pole singularity in the limit $t \rightarrow m_\pi^2$. The pion pole gives a dominant contribution to the hard π^+ electroproduction amplitude $\mathcal{M}_{\pi^+}^L$ in the valence region, which can be worked out explicitly. Using the pion pole formula of Eq. (41) for the induced pseudoscalar form factor $h_A(t)$, and by using the PCAC relation $g_A/f_\pi = g_{\pi NN}/m_N$, where $g_{\pi NN}$ is the πNN coupling constant, one obtains for the pion pole part of the amplitude $\mathcal{M}_{\pi^\pm}^L$:

$$\mathcal{M}_{\pi^+}^L (\pi^+ - \text{pole}) = ie \sqrt{2} Q F_\pi (Q^2) \frac{g_{\pi NN}}{-t + m_\pi^2} \bar{N}(p') \gamma_5 N(p), \quad (236)$$

where F_π represents the pion electromagnetic form factor. When using an asymptotic distribution amplitude for the pion, the leading order pion pole amplitude is obtained by using in Eq. (236) the asymptotic pion form factor F_π^{as} , which is given by :

$$F_\pi^{as} (Q^2) = \frac{16\pi\alpha_s f_\pi^2}{Q^2}. \quad (237)$$

Besides the π hard electroproduction, one can also study the η and η' hard electroproduction. For the η electroproduction, when neglecting the effects of the QCD axial anomaly, the corresponding amplitudes A and B as in Eq. (230) are given by [Man98a] :

$$A_{\eta p} = \int_{-1}^1 dx \frac{1}{\sqrt{6}} \left(e_u \tilde{H}^u + e_d \tilde{H}^d - 2e_s \tilde{H}^s \right) \left\{ \frac{1}{x - \xi + i\epsilon} + \frac{1}{x + \xi - i\epsilon} \right\}, \quad (238)$$

$$B_{\eta p} = \int_{-1}^1 dx \frac{1}{\sqrt{6}} \left(e_u \tilde{E}^u + e_d \tilde{E}^d - 2e_s \tilde{E}^s \right) \left\{ \frac{1}{x - \xi + i\epsilon} + \frac{1}{x + \xi - i\epsilon} \right\}. \quad (239)$$

The effects of the QCD axial anomaly have been studied in Ref. [Eid99].

We show in Fig. 40 the leading order cross sections for various pseudoscalar meson production channels. As discussed before for the absolute cross sections for vector meson electroproduction, also for pseudoscalar meson production the (higher-twist) power corrections to the cross section have not yet been worked out systematically. Therefore, these leading order results could receive sizeable corrections (see e.g. Ref. [Vdh99] for a first estimate of such corrections). To be on the safe side, we therefore show in Fig. 40 the leading order predictions at a relatively large scale ($Q^2 = 10 \text{ GeV}^2$), where we use for the running coupling constant α_s its expression from perturbative analysis at a scale $Q^2 = 10 \text{ GeV}^2$.

²³See however Ref. [Bak01] for a recent discussion of the deviations from the asymptotic distribution amplitude for the pion.

By comparing in Fig. 40, the π^+n and π^0p channels, one immediately sees the prominent contribution of the charged pion pole to the π^+ cross section. The cross section for the π^0 channel, where this pion pole is absent, is more than a decade lower for $x_B \geq 0.15$. Going to smaller values of x_B , on the other hand, one finds an increasing ratio $\pi^0 : \pi^+$, due to the amplitudes A of Eqs. (231,233). This was also noticed in Ref. [Man99b]. One can also understand the ratio $\pi^0 : \pi^+$ at smaller x_B by comparing the amplitude of Eqs. (231) and (233). One sees that in the π^0p channel, the GPDs \tilde{H}^u and \tilde{H}^d enter with the same sign, whereas in the π^+n channel, they enter with opposite signs. These GPDs \tilde{H}^u and \tilde{H}^d are constructed starting from the polarized quark distributions Δu and Δd as discussed in Sec. 4.2.4. Because Δu and Δd have opposite signs, this leads to a partial cancellation for the π^0p channel compared to the π^+n channel, yielding a ratio $\pi^0 : \pi^+ \approx 1 : 5$ for the non-pole part of the π^+ channel [Vdh99].

For the ηp channel, using the ansatz for the GPDs \tilde{H}^q discussed in Sec. 4.2.4 in Eqs. (238,239), a slightly smaller cross section was found as for π^0 , i.e. $\eta : \pi^0 \approx 4 : 5$ [Vdh99], comparable with the ratio $\eta : \pi^0 \approx 2 : 3$ found in Ref. [Man98a]. This ratio is also very sensitive to the x -dependence of the polarized u - and d -quark distributions, giving a possibility to cross-check various parametrizations for those polarized quark distributions. Besides, when including the effects of the axial anomaly and $SU(3)$ breaking, markedly different results were obtained in Ref. [Eid99], i.e. $\pi^0 : \eta : \eta' = 27 : 1.6 : 1.4$, which will be interesting to check experimentally.

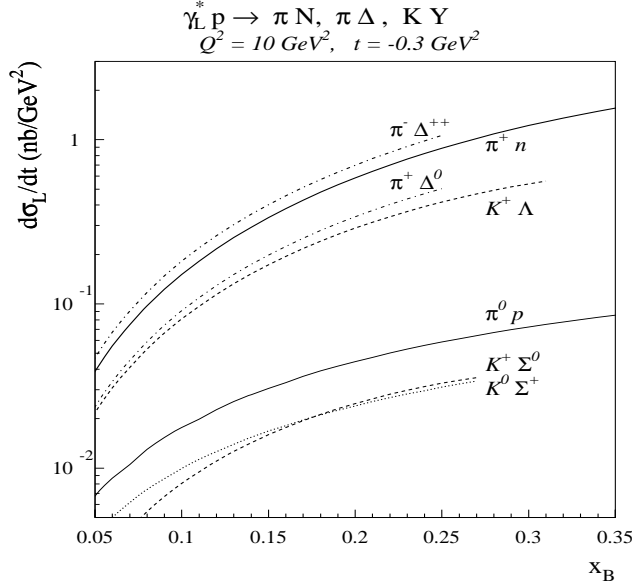


Figure 40: Leading order predictions for the πN , $\pi \Delta$ and KY longitudinal electroproduction cross sections at $t = -0.3 \text{ GeV}^2$, as function of x_B (plotted up to the x_B value for which $t = t_{min}$). Results for pion and charged kaon channels are given using an asymptotic distribution amplitude. For $K^0 \Sigma^+$, predictions are shown using the Chernyak-Zhitnitsky [Cher84] distribution amplitude with antisymmetric part : $\eta_K^a = 0.25$. Figure from Ref. [Fra00a].

As we discussed already for the hard electroproduction of longitudinally polarized

vector mesons there is, besides the cross section σ_L , a second relevant observable, which involves only longitudinal amplitudes and which is of leading order. This is the transverse spin asymmetry for a proton target polarized perpendicular to the reaction plane, see Eq. (228).

For the hard electroproduction of πN final states, the transverse spin asymmetry $\mathcal{A}_{\pi N}$ is given by [Fra99a] :

$$\mathcal{A}_{\pi N} = \frac{2|\Delta_\perp|}{\pi} \frac{\text{Im}(AB^*) 4\xi m_N}{|A|^2 4m_N^2 (1-\xi^2) - |B|^2 \xi^2 t - \text{Re}(AB^*) 8\xi^2 m_N^2}, \quad (240)$$

where A and B are defined as in Eqs. (231-234).

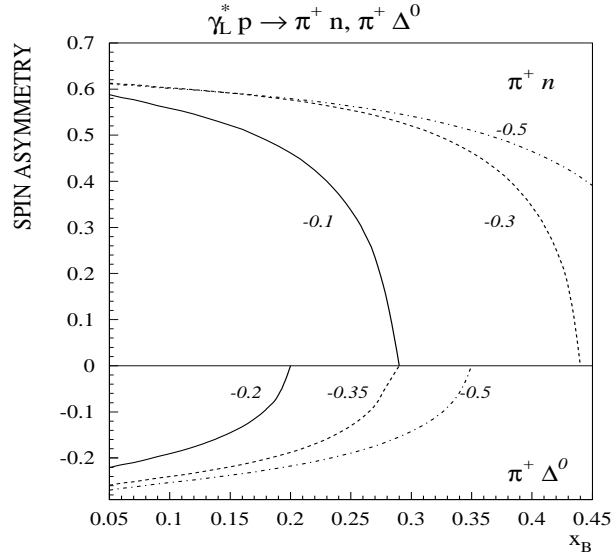


Figure 41: Transverse spin asymmetry $\mathcal{A}_{\pi N}$ for the longitudinal electroproduction of $\pi^+ n$ and $\pi^+ \Delta^0$, at different values of t (indicated on the curves in GeV^2). Figure from Ref. [Fra00a].

In Fig. 41 (upper plot), we display the transverse spin asymmetry $\mathcal{A}_{\pi^+ n}$ for $\pi^+ n$ electroproduction at several values of $-t$, as a function of x_B . For the GPDs \tilde{H}^u and \tilde{H}^d , we use the phenomenological parametrization as discussed in Sec. 4.2.4. It is obvious from Fig. 41 that the predicted $\mathcal{A}_{\pi^+ n}$ is large and comparable with the results of [Fra99a] in which the GPDs computed in the chiral quark soliton model [Pen00a] were used. As a consequence, the investigation of these processes can provide unique tests of the soliton type approach to baryon structure.

The transverse spin asymmetries are likely to be less sensitive to higher twist effects and to NLO (in α_s) corrections. The latter corrections have been calculated recently in Ref. [Bel01d] and were found to be sizeable as well as strongly scheme dependent for absolute cross sections, but nearly drop out of the transverse spin asymmetries. Hence these asymmetries can be explored already at presently accessible scales at HERMES and JLab, using a transversely polarized target.

The HERMES collaboration reported already preliminary a rather large asymmetry for π^+ electroproduction in case of a longitudinally polarized target along the beam

direction [Tho01]. As was noted in Ref. [Pol00], such a measurement includes a small target polarization component transverse to the virtual photon direction S_\perp , leading to the following form for the polarized cross section σ_P :

$$\sigma_P \sim \sin \Phi \left[S_\perp \sigma'_L + S_L \sigma'_{LT} \right], \quad (241)$$

where σ'_L receives only contributions from the longitudinal amplitude which dominates in the hard regime for the exclusive channel. The cross section σ'_{LT} contains the interference of longitudinal and transverse amplitudes, which is suppressed by a power of the hard scale ($1/Q$) relative to σ'_L . Note, however that the transverse spin component S_\perp drops as $1/Q$ relative to the longitudinal spin component S_L for a target polarized along the beam direction, so that in this case both terms in Eq. (241) are of the same order in $1/Q$. Therefore, to extract the transverse spin asymmetry unambiguously, an experiment using a transversely polarized target is really needed.

A measurement of $\mathcal{A}_{\pi N}$ can also provide an important help in the extraction of the pion electromagnetic form factor. For $x_B \leq 0.15$ where one reaches values $t_{min} \sim 2m_\pi^2$, we find that the pion pole constitutes about 70 % to the longitudinal cross section. Measurement of the transverse spin asymmetry, which is an interference between the amplitudes A and B in Eq. 230, would help to constrain the non-pole term, and in this way help to get a more reliable extraction of the pion form factor.

4.5.3 Hard electroproduction of strangeness

In this section, we turn to strangeness hard electroproduction reactions $\gamma_L^* + p \rightarrow K + Y$. In leading order, the kaon electroproduction amplitude is given by an expression analogous as Eq. (230).

For the charged kaon electroproduction channels, the amplitudes A and B are given by [Fra99a, Fra00a] :

$$A_{K+Y} = \int_{-1}^1 dx \tilde{H}^{p \rightarrow Y} \left\{ \frac{e_u}{x - \xi + i\epsilon} + \frac{e_s}{x + \xi - i\epsilon} \right\}, \quad (242)$$

$$B_{K+Y} = \int_{-1}^1 dx \tilde{E}^{p \rightarrow Y} \left\{ \frac{e_u}{x - \xi + i\epsilon} + \frac{e_s}{x + \xi - i\epsilon} \right\}, \quad (243)$$

where e_s is the s -quark charge, and Y is the produced hyperon ($Y = \Lambda, \Sigma^0$). To estimate the GPD $\tilde{H}^{p \rightarrow Y}$, we use the $SU(3)$ relations as discussed in Sec. 2.6. The SPD $\tilde{E}^{p \rightarrow Y}$ contains a charged kaon pole contribution, given by :

$$B_{K+Y}^{pole} = -3/(2\xi) \eta_K^s f_K g_{KNY} (2m_N)/(-t + m_K^2), \quad (244)$$

where $f_K \simeq 159$ MeV is the kaon decay constant, and where g_{KNY} are the KNY coupling constants. In line with our use of $SU(3)$ relations to estimate \tilde{H} , we use also $SU(3)$ predictions for the coupling constants : $g_{KN\Lambda}/\sqrt{4\pi} \approx -3.75$ and $g_{KN\Sigma}/\sqrt{4\pi} \approx 1.09$, which are compatible with those obtained from a Regge fit to high energy kaon photoproduction data [Guid97]. In Eq. (244), η_K^s is defined as :

$$\left\{ \begin{array}{c} \eta_K^s \\ \eta_K^a \end{array} \right\} \equiv \frac{2}{3} \int_{-1}^{+1} d\zeta \left\{ \begin{array}{c} \Phi_K^s(\zeta) \\ \zeta \Phi_K^a(\zeta) \end{array} \right\} \frac{1}{1 - \zeta^2}, \quad (245)$$

where $\Phi_K^s(\zeta)$ is the symmetric (in ζ) part of the distribution amplitude (DA) of the kaon, which runs over the range -1 to +1 in the notation of Eq. (245). One has $\eta_K^s = 1$ for an asymptotic DA ($\Phi^s(\zeta) = 3/4(1 - \zeta^2)$), and $\eta_K^s = 7/5$ for the Chernyak-Zhitnitsky (CZ) kaon DA [Cher84]. Furthermore, in Eq. (245) we have also defined - for further use - η_K^a for the antisymmetric part $\Phi_K^a(\zeta)$ of the kaon DA. The latter is due to $SU(3)_f$ symmetry breaking effects.

For the $K^0\Sigma^+$ electroproduction, the expressions for A and B , allowing for both a symmetric and antisymmetric component in the kaon DA, are given by [Fra00a] :

$$\begin{Bmatrix} A_{K^0\Sigma^+} \\ B_{K^0\Sigma^+} \end{Bmatrix} = \int_{-1}^1 dx \begin{Bmatrix} \tilde{H}^{p \rightarrow \Sigma^+} \\ \tilde{E}^{p \rightarrow \Sigma^+} \end{Bmatrix} \left[\frac{(1 - \eta_K^a/\eta_K^s) e_d}{x - \xi + i\epsilon} + \frac{(1 + \eta_K^a/\eta_K^s) e_s}{x + \xi - i\epsilon} \right]. \quad (246)$$

In contrast to π^0 electroproduction, K^0 electroproduction can contain a pole contribution, which is given by :

$$B_{K^0\Sigma^+}^{pole} = \frac{4}{3} \eta_K^a \left(\frac{3}{2\xi} \right) \frac{f_K g_{KN\Sigma}(2m_N)}{-t + m_K^2}, \quad (247)$$

and which vanishes when the kaon DA is symmetric (i.e. when $\eta_K^a = 0$). Therefore, the K^0 pole contribution to $B_{K^0\Sigma^+}$, provides a direct measure of the antisymmetric component of the kaon DA.

In Fig. 40, we show besides the leading order predictions for the pion electroproduction cross sections also the leading order predictions for kaon hard electroproduction cross sections at $Q^2 = 10 \text{ GeV}^2$. The charged pion and kaon channels obtain a large contribution in the range $x_B \gtrsim 0.1$ from the pion (kaon) pole. This largely determines the ratio between these channels at larger x_B . For values of $-t$ in the range $0.1 \rightarrow 0.5 \text{ GeV}^2$, this yields $\pi^+ n : K^+ \Lambda \approx 7 : 1 \rightarrow 1.8 : 1$, using an asymptotic DA for both π and K . The kaon DA is not well known however, and the results with a CZ kaon DA yield K^+ cross sections, for the pole contribution, larger by a factor $(7/5)^4 \approx 3.8$. The ratio $K^+ \Lambda : K^+ \Sigma^0$ at large x_B is determined from the ratio of the couplings : $g_{KN\Lambda}^2/g_{KN\Sigma}^2 \approx 12$. For the $K^0\Sigma^+$ channel, the pole contribution is absent if $\eta_K^a = 0$ (as for π^0). In this case, the ratio $\pi^0 p : K^0\Sigma^+$ is determined by the amplitude A and is very sensitive to the input valence quark distribution into \tilde{H} . For $\Delta u_V \approx -\Delta d_V$ expected in the large N_c limit, $\pi^0 : K^0 \approx 1 : 3$, while for $\Delta u_V \approx -2\Delta d_V$ preferred by the global fit to DIS of Ref. [Lea98], $\pi^0 : K^0 \approx 3 : 1$. The sensitivity of this ratio to the polarized quark distributions might be interesting to provide cross-checks on such global fits from DIS. In Fig. 40, we show the results for $K^0\Sigma^+$ by using the polarized distributions of [Lea98] as input for \tilde{H} (as discussed in Sec. 4.2.4).

Besides the contribution of the amplitude A , $K^0\Sigma^+$ electroproduction has also a pole contribution, given by Eq. (247), which is nonzero if $\eta_K^a \neq 0$. In the estimates shown here, we include the pole contribution of Eq. (247), and use the CZ kaon DA with $\eta_K^a = 0.25$. The resulting K^0 pole contribution provides a sizeable enhancement of the $K^0\Sigma^+$ cross section (it gives roughly half the value of the amplitude A at the largest x_B).

After the cross section, we next discuss the transverse spin asymmetry \mathcal{A}_{KY} for the strangeness channels, which is given by [Fra00a] :

$$\begin{aligned} \mathcal{A}_{KY} &= \frac{2|\Delta_\perp|}{\pi} \frac{\text{Im}(AB^*) 4\xi m_N}{D_{KY}}, & \text{with,} & \\ D_{KY} &= |A|^2 4m_N^2(1 - \xi^2) + |B|^2 \xi^2 [-t + (m_Y - m_N)^2] \\ &\quad - \text{Re}(AB^*) 4\xi m_N [\xi(m_Y + m_N) + m_Y - m_N], \end{aligned} \quad (248)$$

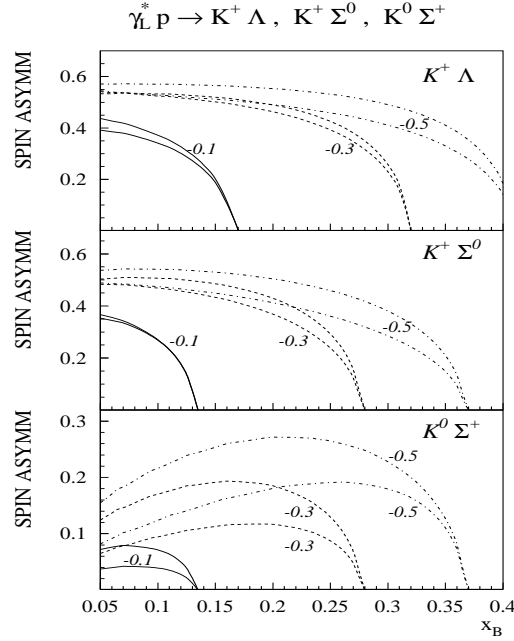


Figure 42: Transverse spin asymmetry, for $K^+\Lambda$, $K^+\Sigma^0$ and $K^0\Sigma^+$ longitudinal electroproduction for different values of t (indicated on the curves in GeV^2). For $K^+\Lambda$ and $K^+\Sigma^0$, the thick (thin) lines are the predictions with the asymptotic (Chernyak-Zhitnitsky) kaon distribution amplitude respectively. For $K^0\Sigma^+$, the thick (thin) lines are the predictions with Chernyak-Zhitnitsky type kaon DA, with antisymmetric part : $\eta_K^a = 0.25$ (0.1).

where A and B are as defined before. It is interesting to note that in the case of hyperon production, the same transverse spin asymmetry can be measured on an *unpolarized* target by measuring the polarization of the recoiling hyperon through its decay angular distribution. The transverse spin asymmetries $\mathcal{A}_{K^+\Lambda}$, $\mathcal{A}_{K^+\Sigma^0}$ and $\mathcal{A}_{K^0\Sigma^+}$ are shown in Fig. 42. A comparison with Fig. 41 for the π^+n channel shows that the transverse spin asymmetries for the charged kaon channels are as large as for π^+n . One also sees that $\mathcal{A}_{K^+\Sigma^0} \sim \mathcal{A}_{K^+\Lambda}$. For K^0 production, the sensitivity to the $SU(3)_f$ symmetry breaking effects in the kaon DA is illustrated (lower panel of Fig. 42), by plotting $\mathcal{A}_{K^0\Sigma^+}$ for two values of η_K^a . Because $\mathcal{A}_{K^0\Sigma^+}$ is directly proportional to η_K^a , it provides a very sensitive observable to extract the K^0 form factor.

As we discussed before, the hard electroproduction of strangeness also gives an unique access to the second class currents (e.g. weak electricity), for a first estimate see Sec. 2.6.

To summarize this section, we have shown that the yields for hard exclusive electroproduction reactions of decuplet and octet baryons are similar. Strange and nonstrange channels can be comparable and in some cases the strange channels can even dominate (depending on the distribution amplitude and polarized parton distributions), in contrast to low-energy strangeness production. Large transverse spin asymmetries are also predicted for these reactions.

4.5.4 Hard electroproduction of $\pi\Delta$ final states

In this section, we discuss the hard electroproduction of $\pi\Delta$ final states : $\gamma_L^* + p \rightarrow \pi + \Delta$.

In Sec. 2.7, we introduced the GPDs for the $N \rightarrow \Delta$ transition, and have seen how they can be expressed in terms of $N \rightarrow N$ GPDs through Eq. (93), using large N_c relations. The large N_c relations make definite predictions for the ratios between the different cross sections for charged pion production as [Fra00a] : $\sigma_L^{\gamma^* p \rightarrow \pi^+ n} : \sigma_L^{\gamma^* p \rightarrow \pi^+ \Delta^0} : \sigma_L^{\gamma^* p \rightarrow \pi^- \Delta^{++}} : \sigma_L^{\gamma^* n \rightarrow \pi^- p} \approx 1 : 0.5 : 1.25 : 0.8$, see also Fig. 40. For the production of neutral pseudoscalar mesons these estimates give : $\sigma_L^{\gamma^* p \rightarrow \eta(\eta') \Delta^+} \ll \sigma_L^{\gamma^* p \rightarrow \eta(\eta') p}$, and $\sigma_L^{\gamma^* p \rightarrow \pi^0 \Delta^+} \approx 0.1 \sigma_L^{\gamma^* p \rightarrow \pi^0 p}$.

In the $N \rightarrow \Delta$ DVCS process considered above, both unpolarized and polarized skewed quark distributions enter, as shown in Eq. (192). The longitudinal electroproduction of pions in the reaction $\gamma_L^* N \rightarrow \pi\Delta$ at large Q^2 allows to select out the polarized quark distributions in the $N \rightarrow \Delta$ transition.

For *charged* pions, the leading order amplitudes for longitudinal $\pi\Delta$ electroproduction on the proton are given by [Fra00a]

$$\begin{aligned} \left\{ \begin{array}{l} \mathcal{M}^L(\gamma^* p \rightarrow \pi^- \Delta^{++}) \\ \mathcal{M}^L(\gamma^* p \rightarrow \pi^+ \Delta^0) \end{array} \right\} &= -ie \frac{4}{9} \frac{1}{Q} \left[\int_0^1 dz \frac{\Phi_\pi(z)}{z} \right] \left\{ \begin{array}{l} -\sqrt{3}/2 \\ -1/2 \end{array} \right\} \\ &\times \frac{1}{2} \int_{-1}^{+1} dx \left[\left\{ \begin{array}{l} e_d \\ e_u \end{array} \right\} \frac{1}{x - \xi + i\epsilon} + \left\{ \begin{array}{l} e_u \\ e_d \end{array} \right\} \frac{1}{x + \xi - i\epsilon} \right] (4\pi\alpha_s) \\ &\times \bar{\psi}^\beta(p') \left\{ C_1(x, \xi, t) n_\beta + C_2(x, \xi, t) \Delta_\beta \frac{\Delta \cdot n}{m_N^2} \right. \\ &\quad + C_3(x, \xi, t) \frac{1}{m_N} (\not{\Delta} n_\beta - \not{p} \Delta_\beta) \\ &\quad \left. + C_4(x, \xi, t) \frac{2}{m_N^2} (\Delta \cdot \bar{P} n_\beta - \Delta_\beta) \right\} N(p). \quad (249) \end{aligned}$$

For *neutral* pions, the leading order amplitude for longitudinal $\pi\Delta$ electroproduction on the proton is given by

$$\begin{aligned} \mathcal{M}^L(\gamma^* p \rightarrow \pi^0 \Delta^+) &= -ie \frac{4}{9} \frac{1}{Q} \left[\int_0^1 dz \frac{\Phi_\pi(z)}{z} \right] \left(\frac{1}{\sqrt{2}} \frac{e_u + e_d}{2} \right) \\ &\times \frac{1}{2} \int_{-1}^{+1} dx \left[\frac{1}{x - \xi + i\epsilon} + \frac{1}{x + \xi - i\epsilon} \right] (4\pi\alpha_s) \\ &\times \bar{\psi}^\beta(p') \left\{ C_1(x, \xi, t) n_\beta + C_2(x, \xi, t) \Delta_\beta \frac{\Delta \cdot n}{m_N^2} \right. \\ &\quad + C_3(x, \xi, t) \frac{1}{m_N} (\not{\Delta} n_\beta - \not{p} \Delta_\beta) \\ &\quad \left. + C_4(x, \xi, t) \frac{2}{m_N^2} (\Delta \cdot \bar{P} n_\beta - \Delta_\beta) \right\} N(p). \quad (250) \end{aligned}$$

The charged pion production amplitudes (Eq. (249)) receive an important contribution from the pion pole contained in the function $C_2(x, \xi, t)$, which can again be evaluated analytically. Using the asymptotic distribution amplitude for the pion, and the pion-pole

part of $h_A(t)$ given by Eq. (41), the pion-pole contribution to the $\pi^- \Delta^{++}$ amplitude of Eq. (249) is given by

$$\mathcal{M}_{\pi^- \Delta^{++}}^L (\pi - \text{pole}) = -ie Q F_\pi(Q^2) \frac{1}{-t + m_\pi^2} \frac{f_{\pi N \Delta}}{m_\pi} \psi^\beta(p') \Delta_\beta N(p), \quad (251)$$

where $F_\pi(Q^2)$ represents the pion electromagnetic form factor as given by Eq. (237). In Eq. (251), we have introduced the $\pi N \Delta$ coupling $f_{\pi N \Delta}$ by using the ‘‘flavor-skewed’’ Goldberger-Treiman relation

$$\frac{g_A}{f_\pi} = 2 \frac{\sqrt{2}}{3} \frac{f_{\pi N \Delta}}{m_\pi}, \quad (252)$$

which is equivalent to the ordinary Goldberger-Treiman relation through $f_{\pi N \Delta} = 3/\sqrt{2} f_{\pi N N}$. Using the phenomenological value $f_{\pi N N}^2/4\pi \approx 0.08$, this yields $f_{\pi N \Delta} \approx 2.13$.

The leading order $\pi \Delta$ electroproduction cross sections are also shown in Fig. 40. One sees that those $\pi \Delta$ channels which contain a charged pion pole exchange give again large cross sections, e.g. the $\pi^- \Delta^{++}$ cross sections are comparable with the $\pi^+ n$ cross sections. Comparing the $\pi^- \Delta^{++}$ and $\pi^+ \Delta^0$ channels, their ratio is around 2.25 in our calculations, close to the ratio 3 which one would obtain if there was only charged pion pole exchange. We found the non-pole contribution to $\pi^- \Delta^{++}$ to be roughly about one-tenth of the total $\pi^- \Delta^{++}$ cross section. Also the small $\pi^0 \Delta^+$ cross section, which receives no contribution from pion exchange confirms the smallness of the non-pole contributions to the forward $\pi \Delta$ cross sections in the valence region.

Similar as for the electroproduction of πN final states, one can also define a transverse spin asymmetry $\mathcal{A}_{\pi \Delta}$ for $\pi \Delta$ electroproduction, which is given by [Fra00a] :

$$\begin{aligned} \mathcal{A}_{\pi \Delta} &= - \frac{2 |\Delta_\perp|}{\pi} \frac{\text{Im}(AB^*) 2 \xi m_N^2 m_\Delta}{D_{\pi \Delta}}, \quad \text{with,} \quad (253) \\ D_{\pi \Delta} &= |A|^2 m_N^4 (1 - \xi)^2 + |B|^2 \xi^2 [t^2 - 2t(m_\Delta^2 + m_N^2) + (m_\Delta^2 - m_N^2)^2] \\ &+ \text{Re}(AB^*) 2 \xi m_N^2 [\xi t - \xi(3m_\Delta^2 + m_N^2) - t - m_\Delta^2 + m_N^2]. \end{aligned}$$

For $\pi^+ \Delta^0$ electroproduction, A and B are given by :

$$A_{\pi^+ \Delta^0} = \int_{-1}^1 dx C_1 \left\{ \frac{e_u}{x - \xi + i\epsilon} + \frac{e_d}{x + \xi - i\epsilon} \right\}, \quad (254)$$

$$B_{\pi^+ \Delta^0} = \int_{-1}^1 dx C_2 \left\{ \frac{e_u}{x - \xi + i\epsilon} + \frac{e_d}{x + \xi - i\epsilon} \right\}, \quad (255)$$

where the functions C_1, C_2 are as defined in Eq. (90). Eq. (255) implies that the pion pole contribution to $B_{\pi^+ \Delta^0}$ is given by $B_{\pi^+ \Delta^0}^{\text{pole}} = \sqrt{3}/4 B_{\pi^+ n}^{\text{pole}}$. We use an asymptotic pion distribution amplitude (DA), for which $B_{\pi^+ n}^{\text{pole}}$ is given by :

$$B_{\pi^+ n}^{\text{pole}} = -3/(2\xi) g_A (2m_N)^2 / (-t + m_\pi^2). \quad (256)$$

For the electroproduction of $\pi^- \Delta^{++}$ one has - up to a global isospin factor - analogous expressions as Eqs. (254,255), by making the replacement $e_u \leftrightarrow e_d$.

In Fig. 41 (lower plot), we also show the transverse spin asymmetry $\mathcal{A}_{\pi^+ \Delta^0}$ for $\pi^+ \Delta$ production at several values of $-t$, as a function of x_B . We use the large N_c relations Eqs. (93) for the $N \rightarrow \Delta$ GPDs. Fig. 41 shows that $\mathcal{A}_{\pi^+ \Delta^0}$ has the opposite sign compared with $\mathcal{A}_{\pi^+ n}$. Although the magnitude of $\mathcal{A}_{\pi^+ \Delta^0}$ is smaller than $\mathcal{A}_{\pi^+ n}$, as anticipated in [Fra99a], it is still sizeable. Similarly, we find $\mathcal{A}_{\pi^- \Delta^{++}} \approx 0.5 \mathcal{A}_{\pi^+ \Delta^0}$.

5 CONCLUSIONS, PERSPECTIVES AND KEY EXPERIMENTS

In this work, we outlined in detail the structure of generalized parton distributions (GPDs), which are universal non-perturbative objects entering the description of hard exclusive electroproduction processes. We focussed mostly on the physics of the internal quark-gluon structure of hadrons encoded in the GPDs. For this we presented calculations of the GPDs within the context of the chiral quark-soliton model. Guided by this physics we constructed a parametrization of the GPDs H , E , \tilde{H} and \tilde{E} , all depending on the variable x , the skewedness ξ , and the momentum transfer to the target nucleon, t . The parameters entering this parametrization can be related in a rather general way to such (not yet measured) quantities as the contribution of the nucleon spin carried by the quark total angular momentum (J^u, J^d , etc.), $\bar{q}q$ components of the nucleon wave function (in particular the D-term and the “vector meson” (VM) part of the GPD E), the strength of the skewedness effects in the GPDs (b_{val} and b_{sea}), the weak electricity GPD in nucleon to hyperon transitions (E_{WE}), flavor $SU(3)$ breaking effects, and others.

Below we give a list of promising observables which we studied in this work and indicate their sensitivity to the different physics aspects of the GPDs. We also discuss for each of them the present experimental status and perspectives. We concentrate on deeply virtual Compton scattering (DVCS) and hard meson electroproduction (HMP).

- DVCS : single spin asymmetry (SSA) (see Sec. 4.3.5)

The DVCS SSA, using a polarized lepton beam, accesses (in leading order) directly (i.e. without convolution) the GPDs along the line $x = \xi$, e.g. $H^q(\xi, \xi, t)$. We found that the DVCS SSA displays :

- a sensitivity to the strength of the skewedness effects in GPDs (parametrized by b_{val} and b_{sea})
- a modest sensitivity to the total angular momentum contributions of the u -quark (J^u) and d -quark (J^d) to the proton spin
- an important sensitivity to the t -dependence of the GPDs. In particular in kinematics where the Bethe-Heitler (BH) contribution dominates, the SSA is basically given by a ratio of the imaginary part of the DVCS amplitude to the BH amplitude. Therefore it depends linearly on the GPDs and therefore the parametrization of the t -dependence directly influences the size of the SSA.

On the experimental side, the first data for the DVCS SSA have been obtained very recently, and several projects both by the HERMES Collaboration and at JLab are already planned in the near future.

- First measurements of the SSA were performed by HERMES [Air01] (27 GeV beam energy), and at Jlab by the CLAS Collaboration [Step01, Guid01] (around 4.2 GeV beam energy) and display already a clear “sin Φ ” structure of the DVCS SSA, indicating that the higher twist effects are modest for this observable at the presently accessible scales.

- Further measurements of the DVCS SSA are planned at JLab (at 6 - 11 GeV beam energy), both in Hall-A [Ber00], and by the CLAS Collaboration [Bur01b, Bur01a].
- At HERMES a dedicated large acceptance recoil detector project has been proposed [Kai01]. This will allow a substantial improvement over existing measurements of the DVCS SSA [Air01], in particular regarding the exclusivity of the reaction by detecting the recoiling proton.

• DVCS : cross section and charge asymmetry (see Sec. 4.3.4)

One accesses the real part of the DVCS amplitude by detecting the DVCS cross sections or the DVCS charge asymmetry (i.e. the difference between the reactions induced by an electron and a positron). The real part of the DVCS amplitude contains (in a convolution) the information on the GPDs away from the line $x = \xi$. In particular we have demonstrated the followings points.

- The DVCS charge asymmetry displays an important sensitivity to the D-term, which is required by the polynomiality condition of GPDs. The D-term leads to a DVCS charge asymmetry with opposite sign as compared to the charge asymmetry when this D-term would be absent.
- It was discussed how this D-term is a consequence of the spontaneous breaking of the chiral symmetry and an estimate of the D-term in the chiral quark-soliton model has been given.
- More generally, the GPDs in the region $-\xi < x < \xi$ contain totally new information on nucleon structure compared to the forward quark distribution. In particular, in this region the GPDs behave like a meson distribution amplitude and one accesses $q\bar{q}$ (mesonic) components in the proton state.
- We have shown that the real part of the DVCS amplitude displays quite some sensitivity to the twist-3 effects, which were estimated in the Wandzura-Wilczek approximation.

On the experimental side, different facilities are complementary in the measurement of the DVCS charge asymmetry and DVCS cross sections.

- The measurement of the DVCS charge asymmetry provides a unique opportunity for HERMES where both e^+ and e^- beams are available. A dedicated measurement of the DVCS charge asymmetry is planned in the near future [Kai01].
- The measurement of the DVCS cross section is favorable in a regime where the DVCS dominates over the Bethe-Heitler process. This is the case at high beam energy. An experiment to measure the DVCS cross section at COMPASS (in the 100 - 200 GeV beam energy range) has been proposed [d’Ho99].
- At small x_B , first data for DVCS cross sections have been obtained by the H1 [Adl01] and ZEUS [Sau99] Collaborations, and can map out the behavior

of GPDs in the small x_B region. These first DVCS data at small x_B are in agreement with theoretical predictions [Fra98b, Fra99a], implying that higher-twist effects are rather small for $Q^2 \geq 4 \text{ GeV}^2$.

- HMP : Transverse spin asymmetries for longitudinal vector meson production
(see Sec. 4.5.1)

We showed that in the electroproduction of longitudinally polarized vector mesons on a transversely polarized proton target, the GPD E enters *linearly* in the spin asymmetry. Therefore, this transverse spin asymmetry provides a unique observable to extract the GPD E and the quark total angular momentum contribution J^q to the proton spin.

- We found large asymmetries for longitudinally polarized vector meson electroproduction, which display a clear sensitivity to the quark total angular momentum contribution J^u and J^d to the proton spin. Specifically, ρ^0 electroproduction is mainly sensitive to the combination $2J^u + J^d$, ρ^+ electroproduction to the combination $J^u - J^d$ and ω electroproduction to the combination $2J^u - J^d$.
- To control the model dependence in the extraction of the values J^u and J^d , the measurement of the transverse spin asymmetries for ρ_L^0 , ω_L and ρ_L^+ electroproduction over a large kinematic range may be helpful as an additional cross check on the modeling of the functions E^u and E^d .
- Because the transverse spin asymmetry involves a ratio of cross sections, it is expected to be a clean observable already at accessible values of Q^2 (in the few GeV^2 range), where the precise form of the t -dependence of the GPDs, the NLO corrections and higher twist effects drop out to a large extent.

These transverse spin asymmetries for longitudinally polarized vector meson electroproduction have not yet been addressed experimentally until now. At HERMES, an experimental program with a transversely polarized target is just starting [Now01]. In view of their large sensitivity to J^u and J^d , we strongly encourage dedicated experiments, at different facilities, to access these transverse spin asymmetries.

- HMP : Transverse spin asymmetries for pseudoscalar meson production
(see Secs. 4.5.2, 4.5.3, 4.5.4)

- The electroproduction of charged pseudoscalar mesons π^+ , K^+ on a transversely polarized proton target also leads to large asymmetries due to the pion (kaon) pole contribution to the GPD \tilde{E} .
- Given the knowledge of this pion (kaon) pole contributions, this asymmetry is mainly sensitive to the GPD $\tilde{H}(\xi, \xi, t)$, i.e. along the line $x = \xi$. With the help of the flavor $SU(3)$ relations for the $N \rightarrow Y$ GPDs one accesses in this way polarized strange quark and antiquark distributions in the nucleon.

- Transverse asymmetries for kaon production can teach us about $SU(3)$ symmetry breaking effects. In particular, the K^0 production gives an access to the antisymmetric part of the kaon distribution amplitude which is due to the flavor $SU(3)$ breaking effects. Also the transverse spin asymmetry for kaon production is sensitive to the effects of second class currents, especially to the weak electricity.

Besides these observables which have been discussed above, other observables can be valuable in the study of the onset of the scaling regime, such as e.g. cross section measurements for meson electroproduction (for experimental plans at JLab, see Ref. [Guid98], and projects at COMPASS, see Ref. [Poc99]) and double spin asymmetries (DVCS with polarized beam and target).

For a more detailed extraction of the physics content of the GPDs from observables further theoretical work is definitely needed. Let us just give an (incomplete) list of theoretical problems which, in our opinion, need further clarification.

- Calculations of NLO perturbative corrections to hard meson production amplitudes. For DVCS this work is largely done. Apart from a more accurate access to the GPDs, a NLO analysis of the data would allow to perform a global analysis of various data on hard reactions from small to large x_B .
- A major open theoretical issue is to get a better understanding of the power (higher twist) corrections to meson production which are expected to be sizeable. For DVCS observables the immediate task is to quantify the contributions of the target mass corrections and the genuine twist-3 operators related to quark-gluon correlations in the nucleon.
- The analysis of the higher twist effects can be useful in identifying observables for which higher twist effects tend to cancel, such as expected in transverse spin asymmetries for meson production.
- A further effort is required in modeling the t -dependence of the GPDs. In this respect the emerging chiral theory of hard processes can be of a big help.
- Studying hard exclusive processes such as DVCS in the presence of an additional soft pion.
- Developing the theory and phenomenology of a new resonance spectroscopy with light-cone probes can be complementary to traditional low energy probes and bring us a breakthrough in the understanding of hadrons as bound states of quark and gluons.
- Establishing links between GPDs and other nucleon structure quantities, such as generalized form factors, polarizabilities, etc.
- Studying the transition from exclusive \rightarrow semi-exclusive \rightarrow semi-inclusive \rightarrow inclusive processes.

Summarizing, one may say that the study of hard exclusive processes has generated a lot of activity and excitement over the last few years, bringing together several fields investigating low and high energy strong interaction phenomena. One may expect new discoveries in the near future both on the theoretical and experimental side. We hope that the underlying work can stimulate such further efforts.

Acknowledgements

This work was supported by the Deutsche Forschungsgemeinschaft (SFB 443, Schwerpunktprogramm), the Russian Foundation for Basic Researches (RFBR 00-15-96610), BMBF, COSY (Jülich).

We would like to express our gratitude to I. Börnig, L.L. Frankfurt, P.A.M. Guichon, M. Guidal, N. Kivel, M. Penttinen, V. Petrov, P. Pobylitsa, A. Schäfer, A. Shuvaev, M. Strikman, O. Teryaev, C. Weiss in collaboration with whom some of the results, which are reviewed in this work, were obtained.

Furthermore we would like to thank M. Amarian, A. Belitsky, P.Y. Bertin, V. Burkert, N. d'Hose, D. Diakonov, M. Diehl, R. Kaiser, P. Kroll, L. Mankiewicz, L. Mossé, D. Müller, A. Radyushkin, D. Ryckbosch, F. Sabatié, N. Stefanis, M. Tytgat, G. Van der Steenhoven, D. von Harrach for many useful and stimulating discussions.

We also would like to thank Dima Kiptily for his assistance in checking the references.

References

- [Abr97] Abramowicz H., Frankfurt L.L., and Strikman M., in Proceedings of SLAC 1994 Summer School (SLAC Report 484), p.539; *Survey High Energy Physics* **11**, 51 (1997), [hep-ph/9503437](#).
- [Ack99] Ackerstaff K., et al. (HERMES Collaboration), *Phys. Lett. B* **464**, 123 (1999).
- [Ack00] Ackerstaff K., et al. (HERMES Collaboration), *Eur. Phys. J. C* **18**, 303 (2000).
- [Ada97] Adams M.R. et al. (E665 Collaboration), *Z. Phys. C* **74**, 237 (1997).
- [Ade98] Adeva B., et al. (Spin Muon Collaboration), *Phys. Lett. B* **420**, 180 (1998).
- [Adk83] Adkins G., C. Nappi, and E. Witten, *Nucl. Phys.* **B228**, 552 (1983).
- [Adl68] Adler S., R. Dashen, “Current algebras”, Benjamin, New York, 1968.
- [Adl75] Adler S., *Ann. Phys. (N.Y.)* **50**, 189 (1968); *Phys. Rev. D* **12**, 2644 (1975).
- [Adl00] Adloff, C. *et al.* (H1 Collaboration), *Eur. Phys. J. C* **13**, 371 (2000).
- [Adl01] Adloff, C. *et al.* (H1 Collaboration), [hep-ex/0107005](#).
- [Air00] Airapetian A., et al. (HERMES Collaboration), *Eur. Phys. J. C* **17**, 389 (2000).
- [Air01] Airapetian A., et al. (HERMES Collaboration), [hep-ex/0106068](#).
- [Alk96] Alkofer R., H. Reinhardt, and H. Weigel, *Phys. Rep.* **265**, 139 (1996).
- [Ani00] Anikin I.V., B. Pire, and O.V. Teryaev, *Phys. Rev. D* **62**, 071501 (2000).
- [Ani01] Anikin I.V., and O.V. Teryaev, [hep-ph/0102209](#).
- [Arn94] Arneodo M. *et al.* (NMC Collaboration), *Nucl. Phys.* **B429**, 503 (1994).
- [Arn01] Arndt D. and M. J. Savage, [nucl-th/0105045](#).
- [Bak98] Bakulev, A.P., and S. V. Mikhailov, *Phys. Lett. B* **436**, 351 (1998).
- [Bak01] Bakulev A.P., S. V. Mikhailov and N. G. Stefanis, [hep-ph/0103119](#).
- [Bal89] Balitsky I.I. and V.M. Braun, *Nucl. Phys.* **B311**, 541 (1989).
- [Bal97] Balitsky I., and X. Ji, *Phys. Rev. Lett.* **79**, 1225 (1997).
- [Ball96] Ball P., and V.M. Braun, *Phys. Rev. D* **54**, 2182 (1996).
- [Ball98] Ball, P., V.M. Braun, Y. Koike and K. Tanaka, *Nucl. Phys.* **B529**, 323 (1998).
- [Balla98] Balla J., M.V. Polyakov and C. Weiss, *Nucl. Phys.* **B510**, 327 (1998).
- [Bar82] Bartels J., and M. Loewe, *Z. Phys. C* **12**, 263 (1982).
- [Bel98a] Belitsky A.V., D. Müller, L. Niedermeier, and A. Schäfer, *Phys. Lett. B* **437**, 160 (1998); *Nucl. Phys.* **B546**, 279 (1999).

- [Bel98b] Belitsky A.V., and D. Müller, Phys. Lett. B **417**, 129 (1998).
- [Bel99] Belitsky A.V., D. Müller, Nucl. Phys. **B537**, 397 (1999).
- [Bel00a] Belitsky A.V., D. Müller, L. Niedermeier, and A. Schäfer, Phys. Lett. B **474**, 163 (2000).
- [Bel00b] Belitsky A.V., and D. Müller, Nucl. Phys. **B589**, 611 (2000).
- [Bel00c] Belitsky A.V., D. Müller, A. Kirchner and A. Schäfer, hep-ph/0011314.
- [Bel00d] Belitsky A.V., D. Müller, Phys. Lett. **B486**, 369 (2000).
- [Bel00e] Belitsky A.V., A. Freund, D. Müller, Nucl. Phys. **B 574**, 347 (2000).
- [Bel01a] Belitsky A.V., D. Müller, L. Niedermeier, and A. Schäfer, Nucl. Phys. **B593**, 289 (2001).
- [Bel01b] Belitsky A.V., and D. Müller, Phys. Lett. B **507**, 173 (2001).
- [Bel01c] Belitsky A.V., A. Kirchner, D. Müller, and A. Schäfer, Phys. Lett. B **510**, 117 (2001).
- [Bel01d] Belitsky A.V., and D. Müller, hep-ph/0105046.
- [Ber94] Bernard V., N. Kaiser, T. S. Lee and U. Meissner, Phys. Rept. **246**, 315 (1994)
- [Ber00] Bertin P.Y., C.E. Hyde-Wright, and F. Sabatié, spokespersons JLab experiment, E-00-110.
- [Blu00] Blümlein, J. and D. Robaschik, Nucl. Phys. **B581**, 449 (2000).
- [Bos00] Bosted P. (E155x Collaboration), Nucl. Phys. **A663**, 297 (2000).
- [Bra87] Braun V.M., and A.V. Kolesnichenko, Nucl. Phys. **B283**, 723 (1987).
- [Bra01] Braun V.M., D.Y. Ivanov, A. Schäfer and L. Szymanowski, Phys. Lett. B **509**, 43 (2001).
- [Bre98] Breitweg J. *et al.* (ZEUS Collaboration), Eur. Phys. J. C **6**, 603 (1999).
- [Bro72] Brodsky S.J., F. E. Close and J. F. Gunion, Phys. Rev. D **6**, 177 (1972).
- [Bro94] Brodsky S.J., L. Frankfurt, J. F. Gunion, A. H. Mueller and M. Strikman, Phys. Rev. D **50**, 3134 (1994).
- [Bro01] Brodsky S.J., M. Diehl and D. S. Hwang, Nucl. Phys. **B596**, 99 (2001).
- [Burk01] Burkardt M., hep-ph/0105324.
- [Bur01a] Burkert V. *et al.*, in JLab 12 GeV upgrade “White Book”, 2001.
- [Bur01b] Burkert V., L. Elouadrhiri, M. Garcon, S. Stepanyan, spokespersons of the “Deeply Virtual Compton Scattering with CLAS at 6 GeV” Proposal to the JLab PAC 20 (June 2001).

- [BurC70] Burkhardt H. and W.N. Cottingham, *Annals Phys.* **56**, 453 (1970).
- [Che01] Chen J. and X. Ji, hep-ph/0105197.
- [Cher84] Chernyak V.L., and A.R. Zhitnitsky, *Phys. Rep.* **112**, 173 (1984).
- [Cher01] Chernyak V., hep-ph/0103295.
- [Cho01] Choi H.-M., C.R. Ji, and L.S. Kisslinger, hep-ph/0104117.
- [Chr96] Christov Chr.V., A. Blotz, H.-C. Kim, P. Pobylitsa, T. Watabe, Th. Meissner, E. Ruiz Arriola, and K. Goeke, *Prog. Part. Nucl. Phys.* **37**, 91 (1996).
- [Cle00] Clerbaux B., and M. V. Polyakov, *Nucl. Phys. A* **679**, 185 (2000).
- [Col97] Collins J.C., L.L. Frankfurt, and M. Strikman, *Phys. Rev. D* **56**, 2982 (1997).
- [Col99] Collins J.C., and A. Freund, *Phys. Rev. D* **59**, 074009 (1999).
- [Das95] Dashen R.F., E. Jenkins and A. V. Manohar, *Phys. Rev. D* **51**, 3697 (1995).
- [Der95] Derrick M. *et al.* (ZEUS Collaboration), *Phys. Lett. B* **356**, 601 (1995).
- [d’Ho99] d’Hose N. *et al.*, Letter of Intent for COMPASS experiment (1999).
- [Dia83] Diakonov D.I., and M. Eides, *Sov. Phys. JETP Lett.* **38**, 433 (1983).
- [Dia86] Diakonov D.I., and V. Petrov, *Nucl. Phys.* **B272**, 457 (1986).
- [Dia88] Diakonov D.I., V. Petrov, and P. Pobylitsa, *Nucl. Phys.* **B306**, 809 (1988).
- [Dia96] Diakonov D.I., V. Petrov, P. Pobylitsa, M.V. Polyakov, and C. Weiss, *Nucl. Phys.* **B480**, 341 (1996).
- [Dia97] Diakonov D.I., V. Petrov, P. Pobylitsa, M.V. Polyakov, and C. Weiss, *Phys. Rev. D* **56**, 4069 (1997).
- [Dia98] Diakonov D., hep-ph/9802298.
- [Dia00] Diakonov D. and V.Y. Petrov, hep-ph/0009006.
- [Die97] Diehl M., T. Gousset, B. Pire, and J.P. Ralston, *Phys. Lett. B* **411**, 193 (1997).
- [Die99] Diehl M., T. Feldmann, R. Jakob, and P. Kroll, *Eur. Phys. J.* **C8**, 409 (1999).
- [Die01a] Diehl M., T. Feldmann, R. Jakob and P. Kroll, *Nucl. Phys.* **B596**, 33 (2001) 33.
- [Die01b] Diehl M., *Eur. Phys. J. C* **19**, 485 (2001).
- [Dit88] Dittes F.M., D. Müller, D. Robaschik, B. Geyer, and J. Horejsi, *Phys. Lett. B* **209**, 325 (1988).
- [Dre00] Drechsel D., in *Proceedings of the Symposium on GDH Sum Rule and the Nucleon Spin Structure (GDH2000)* June 14-17, 2000, Mainz, Germany; Eds. D. Drechsel and L. Tiator (World Scientific, Singapore, 2000).

- [Dres00a] Dressler B., and M.V. Polyakov, Phys. Rev. D **61**, 097501 (2000).
- [Dres00b] Dressler B., K. Goeke, M.V. Polyakov, and C. Weiss, Eur. Phys. J. C **14**, 147 (2000).
- [Efr80] Efremov A.V., and A.V. Radyushkin, Phys. Lett. B **94**, 245 (1980).
- [Efr97] Efremov A.V., O.V. Teryaev, E. Leader, Phys. Rev. D **55**, 4307 (1997).
- [Eid99] Eides M.I., L. L. Frankfurt and M. I. Strikman, Phys. Rev. D **59**, 114025 (1999).
- [Fra93] Frankfurt L.L., G. A. Miller and M. Strikman, Phys. Lett. B **304**, 1 (1993).
- [Fra96] Frankfurt L.L., W. Koepf and M. Strikman, Phys. Rev. D **54**, 3194 (1996).
- [Fra98a] Frankfurt L.L., M.V. Polyakov and M. Strikman, hep-ph/9808449.
- [Fra98b] Frankfurt L.L., A. Freund and M. Strikman, Phys. Rev. D **58**, 114001 (1998)
[Erratum-ibid. D **59**, 119901 (1999)]
- [Fra98c] Frankfurt L., W. Koepf and M. Strikman, Phys. Rev. D **57**, 512 (1998).
- [Fra99a] Frankfurt L.L., A. Freund and M. Strikman, Phys. Lett. B **460**, 417 (1999)
- [Fra99b] Frankfurt L.L., P.V. Pobylitsa, M.V. Polyakov, and M. Strikman, Phys. Rev. D **60**, 014010 (1999).
- [Fra99c] Frankfurt L.L., M.F. McDermott and M. Strikman, JHEP **9902**, 002 (1999).
- [Fra00a] Frankfurt L.L., M. V. Polyakov, M. Strikman, and M. Vanderhaeghen, Phys. Rev. Lett. **84**, 2589 (2000).
- [Fra00b] Frankfurt L.L., G.A. Miller and M. Strikman, Found. Phys. **30**, 533 (2000).
- [Fra01] Frankfurt, L.L., P.V. Pobylitsa, M. Strikman, and M.V. Polyakov, “Handbook of hard exclusive amplitudes”, preprint RUB-TP2-02/01, unpublished.
- [Fri33] Frisch R., O. Stern, Z. Phys. **85**, 4 (1933); I. Estermann, O. Stern, *ibid*, 17.
- [Gam98] Gamberg L., H. Reinhardt, and H. Weigel, Int. J. Mod. Phys. **A13**, 5519 (1998).
- [Gar85] Garcia A., P. Kielanowsk, “The Beta Decay Of Hyperons,” *Berlin, Germany: Springer (1985) 173 P. (Lecture Notes In Physics, 222).*
- [Glu98] Glück M., E. Reya, and A. Vogt, Eur. Phys. J. C **5**, 461 (1998).
- [Goc01] Gockeler M. *et al.*, Phys. Rev. D **63**, 074506 (2001).
- [Gol98] Golec-Biernat K., J. Kwiecinski and A. D. Martin, Phys. Rev. D **58**, 094001 (1998).
- [Gro98] Gronberg J. *et al.* (CLEO Collaboration), Phys. Rev. D **57**, 33 (1998).
- [Gui98] Guichon P.A.M., and M. Vanderhaeghen, Prog. Part. Nucl. Phys. **41**, 125 (1998).
- [Guid97] Guidal M., J.-M. Laget and M. Vanderhaeghen, Nucl. Phys. **A627**, 645 (1997).

- [Guid98] Guidal M., C. Marchand, and E. Smith, spokespersons JLab experiment E-98-107/E-99-105.
- [Guid01] Guidal M., in *Proceedings of the 3rd International Conference on Perspectives in Hadronic Physics*, Trieste, May 7-11, 2001, Nucl. Phys. **A** (to be published).
- [Hoo98] Hoodbhoy P., and X. Ji, Phys. Rev. D **58**, 054006 (1998)
- [’tHo74] ’t Hooft G., Nucl. Phys. **B72**, 461 (1974).
- [Jaf91] Jaffe R.L., and X. Ji, Phys. Rev. Lett. **67**, 552 (1991); Nucl. Phys. B **375**, 527 (1992).
- [Ji96] Ji, X., J. Tang, and P. Hoodbhoy, Phys. Rev. Lett. **76**, 740 (1996).
- [Ji97a] Ji, X., W. Melnitchouk, and X. Song, Phys. Rev. D **56**, 1 (1997).
- [Ji97b] Ji X., Phys. Rev. Lett. **78**, 610 (1997); Phys. Rev. D **55**, 7114 (1997).
- [Ji98a] Ji X., and J. Osborne, Phys. Rev. D **58**, 094018 (1998).
- [Ji98b] Ji X., J. Phys. G **24**, 1181 (1998).
- [Ji01] Ji X., and R. F. Lebed, Phys. Rev. D **63**, 076005 (2001).
- [Jon73] Jones H.F., M.D. Scadron, Ann. of Phys. **81**, 1 (1973).
- [Iva98] Ivanov, D. and R. Kirschner, Phys. Rev. D **58**, 114026 (1998).
- [Iva99] Ivanov I. and N. N. Nikolaev, JETP Lett. **69**, 294 (1999).
- [Kai01] Kaiser R., Contact Person (HERMES Collaboration) for “A Large Acceptance Recoil Detector for HERMES”, Addendum to the Proposal DESY PRC 97-07, HERMES 97-032.
- [Kim98] Kim H., M.V. Polyakov, M. Praszalowicz and K. Goeke, Phys. Rev. D **57**, 299 (1998).
- [Kiv01a] Kivel N., and M.V. Polyakov, Nucl. Phys. **B600**, 334 (2001).
- [Kiv01b] Kivel N., M.V. Polyakov, and M. Vanderhaeghen, Phys. Rev. D **63**, 114014 (2001).
- [Kiv01c] Kivel N., M.V. Polyakov, A. Schäfer and O.V. Teryaev, Phys. Lett. B, **497**, 73 (2001).
- [Kro96] Kroll P., M. Schürmann and P.A.M. Guichon, Nucl. Phys. **A598**, 435 (1996).
- [Lai00] Lai, H.L. *et al.*, Eur. Phys. J. C **12**, 375 (2000).
- [Lea98] Leader E., A.V. Sidorov and D.B. Stamenov, Phys. Rev. D **58**, 114028 (1998).
- [Leh00] Lehmann-Dronke B., P. V. Pobylitsa, M. V. Polyakov, A. Schäfer and K. Goeke, Phys. Lett. B **475**, 147 (2000).

- [Leh01] Lehmann-Dronke B., A. Schaefer, M. V. Polyakov and K. Goeke, Phys. Rev. D **63**, 114001 (2001).
- [Lep79] Lepage G.P., and S.J. Brodsky, Phys. Lett. B **87**, 359 (1979).
- [Man98a] Mankiewicz L., G. Piller, and T. Weigl, Eur. Phys. J. C **5**, 119 (1998).
- [Man98b] Mankiewicz L., G. Piller, E. Stein, M. Vantinnen, and T. Weigl, Phys. Lett. B **425**, 186 (1998).
- [Man99a] Mankiewicz L., G. Piller, and T. Weigl, Phys. Rev. D **59**, 017501 (1999).
- [Man99b] Mankiewicz L., G. Piller, and A. V. Radyushkin, Eur. Phys. J. C **10**, 307 (1999).
- [Mano98] Manohar A.V., hep-ph/9802419.
- [Mar98a] Martin A.D., R.G. Roberts, W.J. Stirling, and R.S. Thorne, Eur. Phys. J. C **4**, 463 (1998).
- [Mar98b] Martin A.D., and M. G. Ryskin, Phys. Rev. D **57**, 6692 (1998).
- [Mar99] Martin A.D., M. G. Ryskin and T. Teubner, Phys. Lett. B **454**, 339 (1999).
- [Mat00] Mathur N., S.J. Dong, K.F. Liu, L. Mankiewicz, and N.C. Mukhopadhyay, Phys. Rev. D **62**, 114504 (2000).
- [Mit99] Mitchell G.S., (on behalf of the E155 Collaboration), hep-ex/9903055.
- [Mos01] Mosse L. *et al.*, in preparation.
- [Mul94] Muller D., D. Robaschik, B. Geyer B., F.-M. Dittes, and J. Horejsi, Fortschr. Phys. **42**, 101 (1994).
- [Now01] Nowak W. D. (on behalf of the HERMES Collaboration), Talk given at the *Workshop on Deep Inelastic Scattering (DIS 2001)*, Apr 27 - May 1, 2001, Bologna, Italy.
- [Pen00a] Penttinen M., M.V. Polyakov, and K. Goeke, Phys. Rev. D **62**, 014024 (2000).
- [Pen00b] Penttinen M., M.V. Polyakov, A.G. Shuvaev, and M. Strikman, Phys. Lett. B **491**, 96 (2000).
- [Pet98] Petrov V., P. Pobylitsa, M.V. Polyakov, I. Bornig, K. Goeke, and C. Weiss, Phys. Rev. D **57**, 4325 (1998).
- [Pet99] Petrov V.Yu., et al., Phys. Rev. D **59**, 114018 (1999).
- [Pob96] Pobylitsa P.V. and M. V. Polyakov, Phys. Lett. B **389**, 350 (1996).
- [Pob99] Pobylitsa P.V., M.V. Polyakov, K. Goeke, T. Watabe and C. Weiss, Phys. Rev. D **59**, 034024 (1999).
- [Pob00] Pobylitsa P.V., M. V. Polyakov, Phys. Rev. D **62**, 097502 (2000).

- [Pob01] Pobylytsa P.V., M. V. Polyakov and M. Strikman, Phys. Rev. Lett. **87**, 022001 (2001).
- [Poc99] Pochodzalla J., L. Mankiewicz, M. Moinester, G. Piller, A. Sandacz, and M. Vanderhaeghen; in Proceedings of the joint INT/JLab workshop *Exclusive and Semi-Exclusive Processes at High Momentum Transfer*, May 19-22, 1999, Jefferson Lab, Newport News, VA, USA; Eds. C. Carlson and A. Radyushkin (World Scientific, Singapore, 2000), hep-ph/9909534.
- [Pol98] Polyakov M.V., in Proceedings of the *8th International Conference on the Structure of Baryons (Baryons 98)*, September 22-26, 1998, Bonn, Germany; Eds. D.W. Menze and B. Metsch, (World Scientific, Singapore, 1999).
- [Pol99a] Polyakov M.V., Nucl. Phys. **B555**, 231 (1999).
- [Pol99b] Polyakov M.V., and C. Weiss, Phys. Rev. D **60**, 114017 (1999).
- [Pol00] Polyakov M.V., and M. Vanderhaeghen, in Proceedings of the *8th International Workshop on Deep Inelastic Scattering (DIS 2000)*, April 25-30, 2000, University of Liverpool, Liverpool, UK; Eds. J.A. Gracey and T. Greenshaw (World Scientific, Singapore, 2001).
- [Rad96a] Radyushkin A.V., Phys. Lett. B **380**, 417 (1996).
- [Rad96b] Radyushkin A.V., Phys. Lett. B **385**, 333 (1996).
- [Rad97] Radyushkin A.V., Phys. Rev. D **56**, 5524 (1997).
- [Rad98] Radyushkin A.V., Phys. Rev. D **58**, 114008 (1998).
- [Rad99] Radyushkin A.V., Phys. Rev. D **59**, 014030 (1999); Phys. Lett. B **449**, 81 (1999).
- [Rad00] Radyushkin A.V., and C. Weiss, Phys. Lett. B **493**, 332 (2000).
- [Rad01a] Radyushkin A.V., and C. Weiss, Phys. Rev. D **63**, 114012 (2001).
- [Rad01b] Radyushkin A.V., hep-ph/0101225.
- [Rys97] Ryskin M.G., R. G. Roberts, A. D. Martin and E. M. Levin, Z. Phys. C **76**, 231 (1997).
- [Sau99] Saull P.R., (ZEUS Collaboration), hep-ex/0003030.
- [Shu99] Shuvaev A.G., K. J. Golec-Biernat, A. D. Martin and M. G. Ryskin, Phys. Rev. D **60**, 014015 (1999).
- [Ste95] Stein E., P. Gornicki, L. Mankiewicz, A. Schäfer and W. Greiner, Phys. Lett. B **343**, 369 (1995).
- [Step01] Stepanyan S., V.D. Burkert, L. Elouadrhiri, *et al.* (CLAS Collaboration), submitted to Phys. Rev. Lett.
- [Str01] Stratmann S. *et al.*, in preparation.

- [Ter01] Teryaev O.V., Phys. Lett. B **510**, 125 (2001).
- [Tho00] Thomas A.W., W. Melnitchouk and F. M. Steffens, Phys. Rev. Lett. **85**, 2892 (2000).
- [Tho01] Thomas E. (on behalf of the HERMES Collaboration), Talk given at the *Workshop on Deep Inelastic Scattering (DIS 2001)*, Apr 27 - May 1, 2001, Bologna, Italy.
- [Tib01] Tiburzi B.C. and G.A. Miller, hep-ph/0104198.
- [Tyt01] Tytgat M., PhD Thesis, University Gent, Belgium (2001).
- [Vdh98] Vanderhaeghen M., P.A.M. Guichon, and M. Guidal, Phys. Rev. Lett. **80**, 5064 (1998).
- [Vdh99] Vanderhaeghen M., P.A.M. Guichon, and M. Guidal, Phys. Rev. D **60**, 094017 (1999).
- [Vdh00a] Vanderhaeghen M., J.M. Friedrich, D. Lhuillier, D. Marchand, L. Van Hoorebeke, and J. Van de Wiele, Phys. Rev. C **62**, 025501 (2000).
- [Vdh00b] Vanderhaeghen M., Eur. Phys. J. A **8**, 455 (2000).
- [Wak98] Wakamatsu M. and T. Kubota, Phys. Rev. D **57**, 5755 (1998).
- [Wak99] Wakamatsu M. and T. Kubota, Phys. Rev. D **60**, 034020 (1999).
- [Wan77] Wandzura S. and F. Wilczek, Phys. Lett. B **72**, 195 (1977).
- [Wei97] Weigel H., L. Gamberg and H. Reinhardt, Phys. Rev. D **55**, 6910 (1997).
- [Wit79] Witten E., Nucl. Phys. **B160**, 57 (1979).